AD NUMBER

AD885270

LIMITATION CHANGES

TO:

Approved for public release; distribution is unlimited.

FROM:

**Distribution authorized to U.S. Gov't. agencies and their contractors;
Administrative/Operational Use; MAR 1971. Other requests shall be referred to Air Force Aero Propulsion Lab., Wright-Patterson AFB, OH 45433.**

AUTHORITY

AFAL ltr 24 Sep 1973

AFAL-TR-71-111

SUDAAR No. 418

12

STANFORD UNIVERSITY

CENTER FOR SYSTEMS RESEARCH

The Homicidal Chauffeur - A Differential Game

by

Antony W. Merz

March 1971

Guidance and Control Laboratory

Air Force Aero Propulsion Laboratory
Air Force Systems Command
Wright-Patterson Air Force Base, Ohio

116

NOTICE

When Government drawings, specifications, or other data are used for any purpose other than in connection with a definitely related Government procurement operation, the United States Government thereby incurs no responsibility nor any obligation whatsoever; and the fact that the government may have formulated, furnished, or in any way supplied the said drawings, specifications, or other data, is not to be regarded by implication or otherwise as in any manner licensing the holder or any other person or corporation, or conveying any rights or permission to manufacture, use, or sell any patented invention that may in any way be related thereto.

Copies of this report should not be returned unless return is required by security considerations, contractual obligations, or notice on a specific document.

AFAL-TR-71-111

Department of Aeronautics and Astronautics
Stanford University
Stanford, California

THE HOMICIDAL CHAUFFEUR - A DIFFERENTIAL GAME

by

Antony W. Merz

SUDAAR No. 418

March 1971

This work was performed in association with research sponsored by the Air Force under Contract F33615-67-C-1245 and Contract F33615-70-C-1637

ACKNOWLEDGMENTS

I express my most profound gratitude to Professor Breakwell for his direction, patience, and unflagging enthusiasm during the course of this research. Many of the results of the work would certainly not have come to light without his extraordinary mathematical perception. I also thank Professor Bryson and Professor Franklin for agreeing to serve as readers and for the interest and understanding they have shown in this work. Fellow doctoral candidates Pierre Bernhard and John Dixon were frequently helpful during the study, and I thank them both. Further, I wish to record my gratitude to my wife, Peggy, who typed several versions of the manuscript, and who provided encouragement and solace when they were needed. Mrs. Diana Shull typed the final version of this document with perseverance and skill, for which I am grateful.

Financial support was provided under Air Force Contract No. F33615-67-C-1245 and F33615-70-C-1637.

BLANK PAGE

UNCLASSIFIED

Security Classification

DOCUMENT CONTROL DATA - R & D

Security classification of title, body of abstract and indexing annotation must be entered when the overall report is classified

Stanford University
Department of Aeronautics and Astronautics
Stanford, California 94305

2a. REPORT SECURITY CLASSIFICATION
UNCLASSIFIED

2b. GROUP

THE HOMICIDAL CHAUFFEUR - A DIFFERENTIAL GAME

March 1971 Scientific Interim

Antony W. Merz

March 1971	7a. TOTAL NO. OF PAGES: 113	7b. NO. OF REFS: 2
F33615-67-C-1245 & F33615-70-C-1637 5102 Task No. 510215	9a. ORIGINATOR'S REPORT NUMBER(S): SUDAAR No. 418 9b. OTHER REPORT NO(S) (Any other numbers that may be assigned this report): AFAL-TR-71-111	

This document is subject to special export controls and each transmittal to foreign governments or foreign nationals may be made only with the prior approval of AFAL(AVNE).

12. SPONSORING MILITARY ACTIVITY
Air Force Avionics Lab
Wright-Patterson Air Force Base
Dayton, Ohio 45433

"The homicidal chauffeur" is the name of a pursuit-evasion differential game originated by Isaacs in his book, Differential Games. In this game, the chauffeur chases a slower pedestrian in an unbounded parking lot. The chauffeur's control is his turn rate, bounded in magnitude, and the pedestrian's control is his velocity direction, which can be changed at will. The pursuer and evader seek respectively to minimize and maximize the capture time, when the radial separation becomes less than a known capture radius. The two equations of relative motion and the terminal conditions can then be written in terms of the two constant parameters of the game: i) the speed ratio, ii) the ratio of capture radius to pursuer's minimum turn radius. The solution to the problem consists in finding the optimizing strategies of both players as functions of the position relative to the pursuer. These "min-max" strategies are specified in terms of the local position variables and the local components of the gradient in the optimal time-to-go, values of which are known at the termination of the game. The equations of relative motion and the gradient equations are then integrated retrogressively from termination, so as to fill the relative space with optimal paths which satisfy all of the necessary conditions for the solution. The retrogressive solution is made difficult by the presence of certain "exceptional" lines in the relative space. These lines border the various regular regions in the relative space, and in each of these regions the optimal paths take a specific form. The exceptional lines themselves may or may not be trajectories, and they are often characterized by discontinuities in the gradient vector and in one or both of the controls. In addition to the exceptional lines discovered by Isaacs (e.g., the "barrier", across which the time-to-go is discontinuous, the "universal line", and the "equivocal line"), two new types of lines are found to exist. These have been given the names "switch envelope" and "focal line".

DD FORM 1473

continued

UNCLASSIFIED

Security Classification

13. Abstract (continued)

Furthermore, "safe-contact" motion, for which the evader maneuvers so as to touch but not penetrate the capture circle, is found to be sometimes optimal, and "dispersal lines" for both pursuer and evader are encountered, as is a new barrier. Also, certain details in the preliminary results reported at the 1st International Differential Game Conference in 1969 have been corrected. Each type of exceptional line (e.g., focal line, evader's dispersal line, etc.) occurs only for parameters in certain regions of the parameter space. More than twenty such regions are found to exist, each of which corresponds to a different configuration of exceptional lines. The results obtained are believed to provide a complete solution to the game for all combinations of the two parameters.

14 KEY WORDS	LINK A		LINK B		LINK C	
	ROLE	WT	ROLE	WT	ROLE	WT
differential games						
pursuit-evasion						

TABLE OF CONTENTS

LIST OF SYMBOLS

A	E's dispersal point from which a range of strategies are optimal
B	far end of barrier or of EDL and PDL
$\mathfrak{B}$	barrier
C	conjugate point
$C_1,\ldots,C_{10}$	parameter space loci shown in Fig. 4.10
D	inverse magnitude of adjoint vector; also junction of SE and PDL or of SE and FL
E	evader
EDL	E's dispersal line from which two of E's strategies are optimal
EL	equivocal line
F	focal point
FL	focal line
G	lower end of SE
H	Hamiltonian; the "main equation" of Isaacs (Ref. 1)
h	$\sqrt{r^2-2x}$, function of position on the EL
ℓ	capture circle radius
P	pursuer
PDL	P's dispersal line from which two of P's strategies are optimal
r	polar coordinate giving E's radial distance from P
R	P's minimum turn radius
S	$V_x y - V_y x$, switch function determining P's turn rate
SE	switch envelope, on which S passes discontinuously through zero

SL	switch line, on which S passes continuously through zero
t	time
UL	universal line, or singular arc, on which $S = \dot{S} = 0$
V	value of the game, or optimal time-to-go from any (x,y)
V_x, V_y	cartesian components of ∇V , the vector gradient of V
V_r, V_θ	polar components of ∇V
x,y	cartesian components of $\underline{x}$, the position vector of E relative to P
x_e, y_e	location of E in fixed coordinates
x_p, y_p	location of P in fixed coordinates
β	ℓ/R , dimensionless capture radius
γ	E's dimensionless velocity, when P's velocity is 1
θ	polar coordinate giving E's relative position, measured clockwise from y-axis
θ_e	E's velocity direction in real space
θ_{eq}	equilibrium angle given by (2) of Sec. 4.1
θ_p	P's velocity direction in real space; also, the angular location of the PDL on capture circle
θ_T	angular location of point-tangential trajectory
θ_{up}	$\cos^{-1}\gamma$, half angle denoting usable part of capture circle
ζ	$-\ell n(\theta_{eq}-\theta)$, auxiliary variable
ν_x, ν_y	normalized gradient vector components for motion on $\mathcal{B}$
τ	retrogressive time
τ'	retrogressive time from tangency

τ_B	$2(\pi-\cos^{-1}\gamma)$, retrogressive time to traverse the open barrier
φ	P's turn-rate strategy, $\lvert\varphi\rvert \leq 1$
ψ	E's direction strategy, positive clockwise from y-axis

Subscripts

o	initial value or terminal value
A	"dispersal" point
B	end of barrier or junction of EDL and PDL
C	conjugate point
EL	equivocal line
eq	equilibrium value
f	focal line
s	switch envelope or switch line
T	tangency (safe-contact)
θ	partial derivative with respect to an angular coordinate
τ	partial derivative with respect to retrogressive time

Superscripts

+,-	distinguishing opposite sides of a PDL, EDL, EL, etc.
$\circ$	retrogressive time derivative
$\cdot$	time derivative

LIST OF FIGURES

LIST OF TABLES

Chapter I

INTRODUCTION

"The homicidal chauffeur" is a pursuit-evasion differential game, first described by Isaacs in his epochal book, Differential Games (Ref. 1). As one of the first physically motivated problems in this emerging field of optimization, it has both historical and mathematical interest. The game is easily described and visualized, pitting a chauffeur (the pursuer, P) with a finite minimum-turn radius, R , against a slower pedestrian (the evader, E) with unrestricted turn radius. The pursuer's speed advantage is partially offset by the evader's agility; these features provide the game with its competitive aspects.

As suggested by the name of the game, P wishes to minimize the "capture time," defined as the time when the mutual separation becomes less than the capture radius, ℓ . Simultaneously, E understandably seeks to maximize this time or, if possible, to avoid capture forever. The differential game thus represents a generalization of the minimum-time optimization problem in that there are two opposing controls, both of which influence the relative motion and the resulting optimal or "min-max" capture time. Much of the interest and difficulty of the game lies in the fact that the optimal controls are not always unique, and that the form taken by the optimal solution to the game depends very strongly upon the speeds of the players and the maneuverability of P . More than 20 qualitatively different forms of the solution will be found to be possible, these forms depending on the relative capabilities of the players. The unexpected variety and complexity of the solutions to the problem support and justify certain generalizations regarding differential games made by Isaacs in Ref. 1.

1.1 Assumptions and Definitions

The game is visualized as taking place on a horizontal plane. When suitably normalized, the differential equations giving the relative position of the players depend on two parameters which are the speed ratio, γ , and the ratio of capture radius to P's minimum turn radius,

β . This latter parameter is used in defining the terminal conditions of the game.

An important problem in a pursuit-evasion game is the determination of those parameters for which capture is possible only from starting points inside a certain boundary, the evader otherwise avoiding capture forever. A subsidiary problem arises when capture is known to be possible from all starting points, but for which there exist loci of discontinuity in the optimal time-to-go. In Chapters II and III, these "barriers" are shown to exist for certain ranges of the parameters.

When the parameters and relative position are such that capture is possible, a solution to the game consists in specifying the optimal strategy of each player as a function of E's position (x,y) relative to P . These "min-max" strategies are:

i) For P , the rate of turn, $\varphi(x,y)$, with $|\varphi| \leq 1$,

ii) For E , the velocity direction, $\psi(x,y)$,

and when capture is possible, each relative position is associated with an optimal positive time-to-go, $V(x,y)$. The optimal strategies (which are not necessarily unique) are such that, e.g., if only E deviates from his optimal strategy for a finite time, capture occurs sooner than $V(x,y)$. Likewise, if only P deviates from optimality, capture must occur later than $V(x,y)$. This is the source of the "saddle-point" terminology used in differential-game theory.

The important assumptions of the game are:

i) Both P and E know the relative position exactly.

ii) Both players know the speeds, the capture radius, and P's minimum turn radius.

Other assumptions which represent departures from "reality" (as in, say, air-to-air combat games) are evident from the previous discussion. Treating the speeds as constant, forcing the motion to occur in a plane, and ignoring any response-time lags in the dynamics of P and E are the most obvious of these.

It is appropriate to state here that the complexity and variety of the solutions to this differential game were underestimated for some time. In fact, early in the study of this game, it was mistakenly believed that little remained to be learned from it. Attention was consequently directed to generalizing the dynamical model, the third-order "game of two cars" being the most natural generalization. Certain difficulties in this third-order problem raised doubts about our understanding of the simpler homicidal chauffeur game. These doubts proved to be well founded, and led to the decision to find the complete solution to the present game for all values of the parameters.

The pioneering work by Isaacs describes a treatment of the problem which is complete only for certain rather narrow ranges of the two parameters. In the course of his researches into this problem, various loci in the relative space were found, across which either or both of the strategies change. Specifically, a barrier and an equivocal line were found to enclose "turn-away" regions in the relative space, and the y-axis was found to be either a universal line or a pursuer's dispersal line. Loci of this type, which separate two qualitatively distinct families of relative trajectories, and which may or may not be trajectories themselves, will be termed "exceptional" lines. As will be made clear by later results, Isaacs' terminology "singular line" has an undesirable connotation to most control theoreticians, and is not sufficiently broad in meaning. The present choice is made to accommodate as large a class of such arcs as possible, and its definition is therefore intentionally general.

In the effort to extend the parameter space to its limits, several new types of exceptional line were found to be necessary. Two of these lines are apparently new, not only to the specific game at hand, but to the theory of differential games. The others are found to occur in other games described in Ref. 1. Each type of exceptional line occurs only for parameters in certain areas of the parameter space, but all such areas appear to have been found. Consequently, a complete solution to the game is believed known, for all values of the parameters. The startling discoveries made at intervals during this study, on the other

hand, discourage presumptions of this type. That is, there may yet be novel types of trajectories or strategies which might occur for certain isolated ranges of the parameters. So many cases have been analyzed numerically in the course of this work, however, that this is considered unlikely. That is, the deformations in the trajectory configurations are found to be smooth and continuous with changes in the parameters, so that smooth qualitative changes in the configurations can be observed whenever a parameter locus is crossed. These loci are actually the end result of the study, but there is no proof that the loci are complete.

1.2 Equations of Motion and General Solutions

The pursuer's location in the playing field is given (Fig. 1.1) by solving

$$\begin{aligned} \dot{x}_p &= \sin\theta_p = s\theta_p \\ \dot{y}_p &= \cos\theta_p = c\theta_p \\ \dot{\theta}_p &= \varphi\ , \quad |\varphi| \le 1\ . \end{aligned} \tag{1}$$

These equations effectively normalize the dimensions of length and time, as P has been given unit speed and a maximum turn rate of unity. The position of the slower evader is given by solving

$$\begin{aligned} \dot{x}_e &= \gamma s\theta_e \\ \dot{y}_e &= \gamma c\theta_e\ , \end{aligned} \tag{2}$$

where $0 \le \gamma < 1$. If E's control is taken as $\psi = \theta_e - \theta_p$, and the relative coordinates defined as in Fig. 1.1 by

$$\begin{aligned} x &= (x_e - x_p)c\theta_p - (y_e - y_p)s\theta_p \\ y &= (x_e - x_p)s\theta_p + (y_e - y_p)c\theta_p\ , \end{aligned}$$

the relative position (x,y) is given by the solutions to:

*Here, as throughout the thesis, s and c are used as abbreviations for sine and cosine.

$$\dot{x} = -\varphi y + \gamma s\psi$$
$$\dot{y} = -1 + \varphi x + \gamma c\psi \ . \tag{3}$$

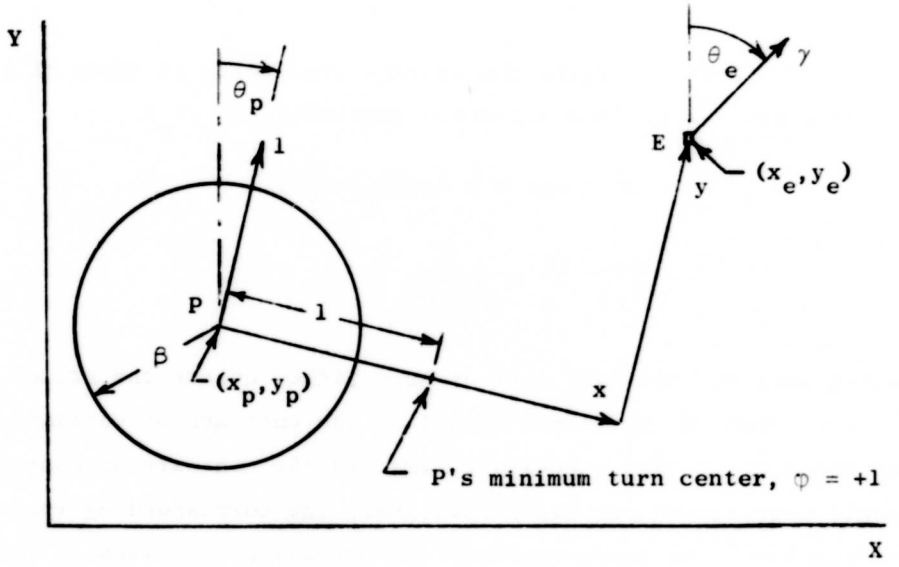

FIGURE 1.1. P and E in Fixed and Relative Coordinate Systems

In retrogressive time, $d\tau = -dt$, and the equations become

$$\overset{\circ}{x} = \varphi y - \gamma s\psi$$
$$\overset{\circ}{y} = 1 - \varphi x - \gamma c\psi \ , \tag{4}$$

where the superscript circle denotes the derivative with respect to the dimensionless time-to-go, τ .

When capture is possible, each relative position (x,y) has associated with it a positive constant, the optimal time-to-go, $V(x,y)$, which is to be found by postulating optimal play from that point on. Its total time rate of change can be written in terms of its gradients,

as

$$\frac{dV}{dt} = \min_{\varphi} \max_{\psi} \left[V_x\dot{x} + V_y\dot{y}\right] = -1 \ . \tag{5}$$

This is the "main equation" of Ref. 1, and using (3) it may be expressed as the "Hamiltonian," or

$$H = \min_{\varphi} \max_{\psi} \left[-V_y - \varphi(V_x y - V_y x) + \gamma(V_x s\psi + V_y c\psi)\right] + 1 = 0 \ . \tag{6}$$

This "min-max" operation gives the optimal strategies in terms of the (known) position (x,y) and (unknown) gradients (V_x,V_y) ,

$$\begin{aligned} \varphi &= \operatorname{sgn} S \triangleq \operatorname{sgn}(V_x y - V_y x) \\ \frac{s\psi}{V_x} &= \frac{c\psi}{V_y} = \frac{1}{\sqrt{V_x^2+V_y^2}} \ . \end{aligned} \tag{7}$$

P is thus to turn hard left or hard right, unless the switch function $S = 0$, and E is to run normal to the contours of constant time-to-go. Whenever S has a constant sign and the contours of constant V have continuous second partial derivatives, the corresponding region is termed "regular." In these regions, the partial derivatives of the main equation with respect to x and y must vanish. Thus, for example,

$$\frac{\partial}{\partial x}\left[V_x\dot{x}+V_y\dot{y}\right] = V_{xx}\dot{x} + V_{xy}\dot{y} + V_x\dot{x}_x + V_y\dot{y}_x = 0 \ .$$

The first two terms on the right equal the time derivative of V_x , and the last two can be evaluated by reference to (3). Repeating this operation with respect to y gives the gradient equations as

$$\begin{aligned} \dot{V}_x &= -\partial H/\partial x = -\varphi V_y \\ \dot{V}_y &= -\partial H/\partial y = \varphi V_x \ , \end{aligned} \tag{8}$$

where $\varphi = \pm 1$. Note that since H is stationary with respect to ψ , the partial derivatives are most easily obtained by treating ψ , as well as φ and (V_x,V_y) , as fixed.

In retrogressive time, and for general initial conditions, the solutions to (8) are

$$V_x = \sqrt{V_{x_o}^2 + V_{y_o}^2}\, s(\psi_o + \varphi\tau)$$
$$V_y = \sqrt{V_{x_o}^2 + V_{y_o}^2}\, c(\psi_o + \varphi\tau) \quad . \tag{9}$$

We have found that, when $S > 0$ or $S < 0$, E's optimal direction in relative space varies linearly with time, $\psi = \psi_o + \varphi\tau$. Since P's rate of turn is φ, this means that E's motion is rectilinear in real space, and that the linear time variation is due to P's turn strategy.

The retrogressive solutions to the state equations (4), over any time interval during which φ is constant (S of constant sign) are

$$x = \varphi(1-c\tau) + x_o c\tau + \varphi y_o s\tau - \gamma\tau s(\psi_o + \varphi\tau)$$
$$y = (1-\varphi x_o)s\tau + y_o c\tau - \gamma\tau c(\psi_o + \varphi\tau) \quad , \tag{10}$$

where the controls ψ_o and φ are given by (7) in terms of the gradients (V_{x_o}, V_{y_o}). Determination of the gradients, as functions of the relative position (x,y), is the most important source of theoretical difficulties in the problem, since these functions used in (7) essentially yield the feedback-solution to the problem.

The approach taken in the investigation of the game is the same as that used by Isaacs in Ref. 1. That is, terminal conditions for $\underline{x}$ and W are found, in terms of the parameters λ and γ, which lead to terminal values for the controls ψ and φ. Then the retrograde solutions (10) are used to find where these terminal points must have come from. Since any point outside the capture circle is a possible initial condition, the intention is simply that of filling the entire space with retrogressive paths. We will find, however, that for any choice of parameters, the space is subdivided by exceptional lines into various regular regions, in <u>each</u> of which (10) is satisfied. The exceptional lines which border the regular regions have one or more of the following distinguishing features:

i) The time-to-go is discontinuous across the line;

ii) The gradient in the time-to-go is discontinuous across the line (as is therefore E's strategy);

iii) The switch function on the line has the value $S = 0$;

iv) The line is the capture circle itself.

These lines may or may not be optimal paths themselves. Certain additional necessary conditions must be satisfied by the exceptional lines which, together with the main equation, will guarantee global optimality.

Chapter II

CLASSICAL RESULTS

Isaacs' analysis of this game, as given in Ref. 1, begins with the determination of the "usable part" of the capture circle. This allows the specification of the strategies (φ,ψ_o) and the terminal conditions (x_o,y_o) in the solutions given by (10) of the previous section. Working retrogressively from termination, he then shows how to fill the (x,y) space with trajectories, using the main equation and its derivatives. Implicit in this analysis is the restriction of parameters to certain regions in the parameter space, which will be specified below. But these "classical" results, apart from their many interesting features, provide a foundation of conclusions which will ultimately lead to solutions in adjacent areas of parameter space.

2.1 One-Stage Game

The "usable part" of the capture circle, on which the optimally played game must end, is easily determined by writing the main equation in polar coordinates,

$$\min_{\varphi}\max_{\psi}[V_r\dot{r} + V_\theta\dot{\theta}] = -1 \tag{1}$$

where

$$\dot{r} = -c\theta + \gamma c(\psi-\theta)$$

$$\dot{\theta} = -\psi + [s\theta + \gamma s(\psi-\theta)]/r$$

Since termination is defined independent of the terminal angle θ_o, the terminal value of the angular adjoint V_θ must be zero, while the radial adjoint at this time is given by substituting for $\dot{r}$ in (1) and performing the indicated maximization:

$$\max_{\psi} V_r[-c\theta_o + \gamma c(\psi-\theta_o)] = V_r(\gamma-c\theta_o) = -1 \ . \tag{2}$$

This brief analysis has provided three important results:

i) At termination, when $r = \beta$, P's control (turn rate) is irrelevant, and E's control (direction) is radially outward, $\psi = \theta_o$, as suggested by intuition;

ii) The terminal adjoints are $V_\theta = 0$, $V_r = \frac{1}{c\theta_o - \gamma} > 0$;

iii) The terminal value of the angular coordinate must satisfy $|\theta_o| < \theta_{up}$, where the "usable part" is defined by the half-angle $\theta_{up} \triangleq \cos^{-1}\gamma$.

At the terminal location $r = \beta$, $\theta = \theta_o$, we first find the switch function which determines P's strategy, according to (7) of Sec. 1.2. The cartesian adjoints are

$$V_x = V_r s\theta + (V_\theta/r)c\theta = \frac{s\theta_o}{c\theta_o - \gamma}$$

$$V_y = V_r c\theta - (V_\theta/r)s\theta = \frac{c\theta_o}{c\theta_o - \gamma} . \tag{3}$$

With these terminal values for the gradients, it is easy to verify that the switch function is the angular gradient, and therefore it vanishes. The retrogressive time-derivative, however, is

$$\dot{S} = V_x = \frac{s\theta_o}{c\theta_o - \gamma} , \tag{4}$$

which means that $\varphi = \operatorname{sgn} \dot{S} = 1$, for $\theta_o > 0$; hence P is turning toward E just before termination. This result has an obvious intuitive interpretation. More generally, we note that, according to (7) of Sec. 1.2, whenever $S = 0$, E's velocity is radial; E is running directly toward or away from P.

For right half-plane terminal conditions, $x_o = \beta s\theta_o \geq 0$, the solution (10) of Sec. 1.2 is, with $\varphi = 1$,

$$x = 1 - c\tau + (\beta - \gamma\tau)s(\theta_o + \tau)$$

$$y = s\tau + (\beta - \gamma\tau)c(\theta_o + \tau) . \tag{5}$$

Here it is noted that, when $\tau = \beta/\gamma$, the point (x,y) is independent of the arrival angle θ_o , and that this point, A , has coordinates

$$x_A = 1 - c\tau_A$$
$$y_A = s\tau_A \ , \tag{6}$$

where

$$\tau_A = \beta/\gamma \ .$$

These equations imply that the point A is located on a unit circle in the x,y plane according to the value taken by the ratio β/γ , as shown in Fig. 2.1.

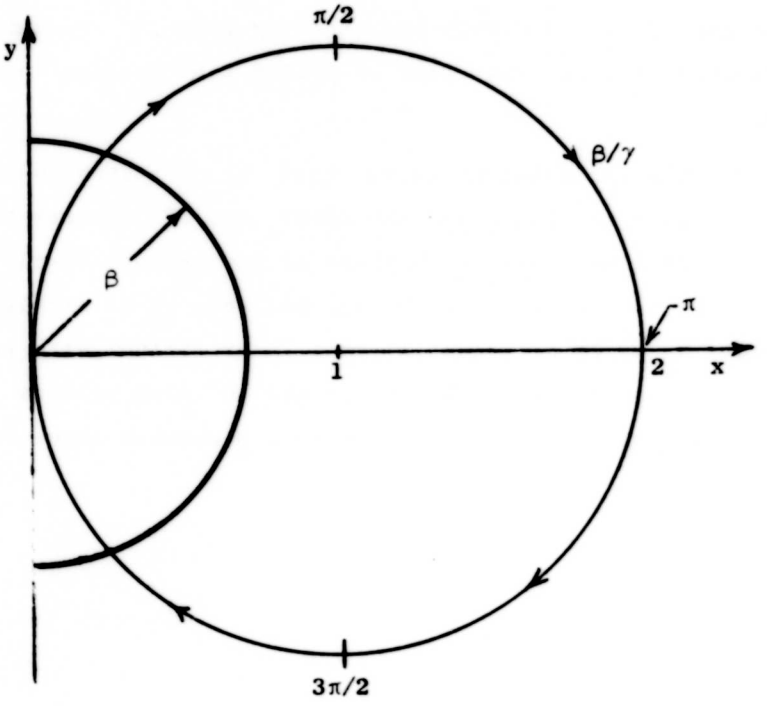

FIGURE 2.1. Locus of Point A for $\varphi = +1$

We note here that all optimal trajectories terminating at $\theta_o \leq \theta_{up}$ can be considered as emanating from this point A , which is then a "dispersal point" for E . This is, in fact, the convention adopted by Isaacs, and according to the arrival angle "preferred" by E , his optimal strategy ψ_A at the dispersal point need not be unique. This strategy need only satisfy the inequality,

$$\beta/\gamma \leq \psi_A \leq \beta/\gamma + \cos^{-1}\gamma \ , \tag{7}$$

any one of which leads to $r = \beta$ in the time β/γ .

As shown in (1) when $r = \beta$, the radial velocity is $\dot{r} = \gamma - c\theta_o$ for the paths (c), and hence $\dot{r} = 0$ when $\theta_o = \theta_{up}$. The sidemost path from A , as shown in Fig. 2.2(a), touches but does not penetrate the capture circle. Accordingly, this path is here considered as distinct from its neighbors, in that it leads to "safe-contact" for E , rather than capture. Thus, our convention differs from that of Isaacs in that we consider E to have only one strategy from A , assuming that P turns toward E , and this will be called the "barrier" or "safe-contact" strategy.

It is also interesting to see that, if P turns toward E when he is initially on $\mathcal{B}$ but above the point A , E chooses the barrier strategy. This path arrives earlier at the capture circle than does the two-stage trajectory via the y-axis, but here it is simply evident that E prefers an early safe-contact to a later arrival with penetration, and he runs accordingly. Whether or not P also prefers the barrier strategy will be determined by a certain parameter inequality, to be derived in Sec. 2.3.

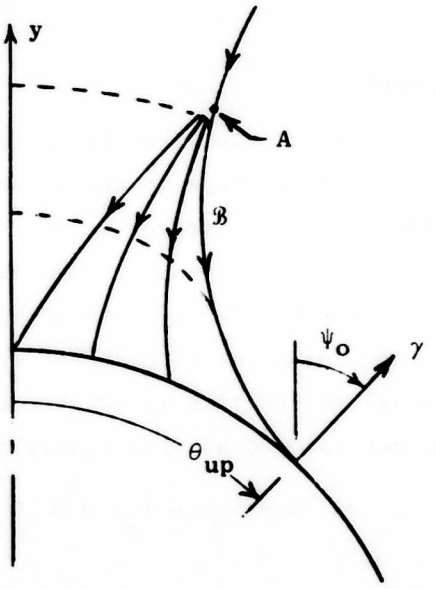

(a) Relative Space

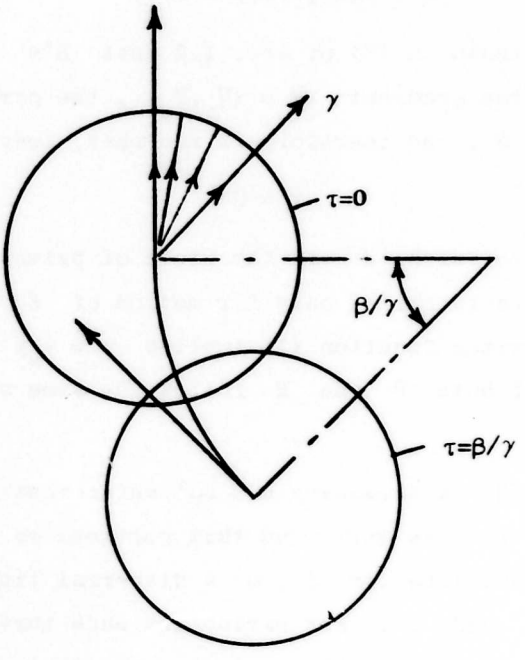

(b) Real Space

FIGURE 2.2. Trajectories from Near Point A

2.2 Universal Line

In Fig. 2.2, trajectories from the neighborhood of A terminate on the capture circle over a range of angles for $\varphi = 1$. A symmetric group of paths for which $\varphi = -1$ arrives at the capture circle from the left. One's curiosity is therefore aroused regarding the conditions under which $\varphi = 0$ is optimal. We have shown that $\varphi = \text{sgn } S$, and the classical definition of universal line (UL) or "singular arc," is a path along which the switch function is identically zero. Thus, using the equations of motion (3) and adjoint equations (8) of Sec. 1.2, we find

$$S = V_x y - V_y x = 0$$

$$\dot{S} = V_x(1-\gamma c\psi) + V_y \gamma s\psi = 0 \ . \tag{1}$$

In order for V_x and V_y not to be both zero, these equations imply that the determinant of their coefficients is zero, or

$$x - \gamma(xc\psi - ys\psi) = 0 \ . \tag{2}$$

But, since we have shown in (7) of Sec. 1.2 that E's control $(s\psi, c\psi)$ is proportional to the gradient $\nabla V = (V_x, V_y)$, the parenthesis in (2) is proportional to S , and therefore it vanishes, leaving

$$x = 0 \tag{3}$$

as the only candidate for a UL in the field of primaries. Thus, the hypotheses in (1) are fulfilled only for motion of E down the y-axis. On this line, the switch function (1) implies $\varphi = V_x y = 0$, and hence $V_x = \psi = 0$, so that both P and E follow the same straight path in real space.

The condition (3) is necessary but not sufficient for the existence of the UL , and in fact we will find that portions of the y-axis can instead be a dispersal line for P , or a dispersal line for E , depending again on β and γ . For parameters such that a barrier exists (to be specified in Sec. 2.3), the trajectory configuration near the positive y-axis resembles the upper paths of Fig. 2.2. As shown in Ref. 1 (p. 194), these tributary paths correspond to sharp turns by P ,

with E running tangent to P's turn circle. The contours of time-to-go, shown as dashed lines in the figure, are smooth at the y-axis, which implies that E's strategy is continuous here, being the same straight-line motion before and after P stops turning.

Specifically, for a trajectory which encounters the y-axis at the ordinate y_1, the retrogressive continuous solutions to the adjoint equations are, with $\varphi = +1$,

$$V_x = \frac{1}{1-\gamma}\, s\tau$$
$$V_y = \frac{1}{1-\gamma}\, c\tau \tag{4}$$

and the path equations are

$$x = 1 - c\tau + (y_1 - \gamma\tau)s\tau$$
$$y = s\tau + (y_1 - \gamma\tau)c\tau \tag{5}$$

where τ is measured on the path back from the ordinate y_1. The magnitude of the gradient vector along and adjacent to the UL is given by the main equation when $x = \psi = 0$, so $|\nabla W| = V_y = 1/\beta = 1/(1-\gamma)$. For the rectilinear chase to which this result applies, the interpretation of the gradient is particularly simple; i.e., the change in optimal time-to-go resulting from a change in relative (y-axis) position is the inverse of the difference in speeds.

2.3 Barrier

When the trajectories derived in (5) of Sec. 2.1 have the boundary value $\theta = \theta_{up}$, the resulting locus defines the "barrier," $\mathfrak{B}$. There is here an infinite discontinuity in the radial adjoint, as shown by putting $\theta_o = \theta_{up} = \cos^{-1}\gamma$ in (2) of Sec. 2.1. At the barrier, then, according to (3) of Sec. 2.1, both V_x and V_y are infinite in magnitude. Accordingly, as the barrier is approached, the main equation may be divided by the magnitude of the adjoint, so that, with $V_\theta = 0$,

$$\lim_{V_r \to \infty} \left\{ \min_{\varphi} \max_{\psi} \frac{[V_x\dot{x}+V_y\dot{y}]}{V_r} \right\} = \lim_{V_r \to \infty} \frac{-1}{V_r} = 0 \ . \tag{1}$$

Hence, defining a normalized adjoint vector,

$$\nabla\nu = (\nu_x,\nu_y) = \frac{1}{\sqrt{V_x^2+V_y^2}} (V_x,V_y) \ ,$$

the main equation becomes

$$\min_{\varphi} \max_{\psi} [\nu_x\dot{x}+\nu_y\dot{y}] = 0 \ . \tag{2}$$

The adjoint vector $\nabla\nu$ is therefore normal to the barrier trajectory, as is E's optimal velocity direction, ψ .

Thus, for $r = \beta$, $\theta_o = \theta_{up}$, (2) becomes, with $(\nu_x,\nu_y) = (s\theta_{up},c\theta_{up})$ and $\varphi = +1$,

$$\max_{\psi_o} [s\theta_{up}(\beta c\theta_{up}-\gamma s\psi_o) + c\theta_{up}(1-\beta s\theta_{up}-\gamma c\psi_o)] = 0 \tag{3}$$

which implies $\psi_o = \theta_{up}$.

The retrogressive adjoint equations are, with their boundary conditions,

$$\begin{aligned} \mathring{\nu}_x &= \nu_y & \nu_x(0) &= s\theta_{up} \\ \mathring{\nu}_y &= -\nu_x & \nu_y(0) &= c\theta_{up} \ , \end{aligned} \tag{4}$$

and the solutions give E's barrier strategy for $\varphi = +1$,

$$\begin{aligned} \nu_x &= s(\theta_{up}+\tau) \\ \nu_y &= c(\theta_{up}+\tau) \ , \end{aligned} \tag{5}$$

so that

$$\psi(\tau) = \theta_{up} + \tau \ . \tag{6}$$

The equations of the barrier are then given by (5) of Sec. 2.1,

$$x = 1 - c\tau + (\beta-\gamma\tau)s(\theta_{up}+\tau)$$

$$y = s\tau + (\beta-\gamma\tau)c(\theta_{up}+\tau) \ . \tag{7}$$

The barrier is termed a semipermeable surface by Isaacs (p. 70) since, if $\varphi = +1$, no strategy of E allows $\underline{x}$ to penetrate the barrier in the "E-direction," and if ψ is given by (6), no strategy of P allows penetration in the P-direction. Here the P-direction refers to the side of smaller time-to-go, and in general the optimal time-to-go is discontinuous at the barrier. Thus, for $\underline{x}$ on the barrier, a departure from the strategy $\psi = \theta_{up} + \tau$ by E results in motion away from the barrier in the P-direction, to a region of small V . Likewise, a departure by P from $\varphi = +1$, if E is paying attention, moves E across the barrier to a region of large (perhaps infinite) V . The discontinuity in V decreases to zero at the end B of $\mathfrak{B}$, which is indicated by the vanishing of P's switch function. Combining (5) and (7), this function is

$$S = v_x y - v_y x = \gamma - c(\theta_{up}+\tau) \ . \tag{8}$$

P's barrier strategy is thus $\varphi = +1$ for $S > 0$, or for

$$0 < \tau < 2(\pi-\theta_{up}) \triangleq \tau_B \ , \tag{9}$$

and unless the barriers intersect on the positive y-axis, τ_B is the time required to traverse the barrier.

The right and left barriers intersect tangentially, on the y-axis, for given values of β and γ , if τ exists such that $x(\beta,\gamma,\tau) = \dot{x}(\beta,\gamma,\tau) = 0$. Using (5) of Sec. 2.1, and eliminating τ from these equations, gives the condition for tangential closing as

$$\beta = \gamma \sin^{-1}\gamma + \sqrt{1-\gamma^2} - 1 \ . \tag{10}$$

Implicit in this derivation is an important parameter inequality, necessary for the existence of the barrier. This inequality can be derived by calculating the velocity components when $\varphi = +1$ and $\psi = \cos^{-1}\gamma$ at $r = \beta$. In polar coordinates, these velocities are, in

general,

$$\dot{r} = -c\theta + \gamma c(\psi-\theta)$$
$$\dot{\theta} = -\varphi + \frac{1}{r}[s\theta + \gamma s(\psi-\theta)] \tag{11}$$

and for the given terminal conditions, the retrogressive velocity components are found to be

$$\overset{\circ}{r} = 0$$
$$\overset{\circ}{\theta} = -1 + \frac{\sqrt{1-\gamma^2}}{\beta} . \tag{12}$$

The retrogressive radial acceleration, however, is

$$\overset{\circ\circ}{r} = -\sqrt{1-\gamma^2}\ \overset{\circ}{\theta}$$

and will be positive only so long as $\overset{\circ}{\theta} \leq 0$ or, by (12), when

$$\beta^2 + \gamma^2 \leq 1 . \tag{13}$$

This is the parameter space inequality necessary for the existence of the barrier which terminates at $\theta = \theta_{up}$ with tangential velocity.

For β larger than the value given in (10), the barriers do not contact the y-axis but instead curve away to the rear, according to the parametric equations (7). In this case, the end of the barrier is reached at $\tau_B = 2(\pi-\cos^{-1}\gamma)$, and this point has coordinates given by (7); i.e.,

$$x_B = \sqrt{1-\gamma^2}\ [2\sqrt{1-\gamma^2} - \beta + \gamma\tau_B]$$
$$y_B = -\gamma[2\sqrt{1-\gamma^2} - \beta + \gamma\tau_B] . \tag{14}$$

Note that the bracket in (14) is the radial distance, r_B , and that

$$\tfrac{1}{2}(r_B-\beta) = \sqrt{1-\gamma^2} + \gamma(\pi-\cos^{-1}\gamma) - \beta > 0 .$$

This inequality is implied by (13), and it means that the end of the barrier, B , is always outside the capture circle.

It is possible for parameters to be such that the point A is not on the barrier; i.e., $\tau_A \geq \tau_B$. Substituting for these retrogressive times from (9) and from (6) of Sec. 2.1, this inequality can be reduced to

$$c(\beta/2\gamma) + \gamma \geq 0 \ . \tag{15}$$

2.4 Equivocal Line and Pursuer's Dispersal Line

For parameters such that the barriers are open, the equivocal line (EL) joins the end of the barrier to the y-axis or to the capture circle, and the y-axis below the EL is a dispersal line for P . The EL is a locus of points along which E's strategy is locally the same as his incoming strategy, which is such as to cause P's switch function to be zero; i.e.,

$$S^- = V_x^- y - V_y^- x = 0 \ . \tag{1}$$

This implies that $\tan \psi^- = x/y$, and that E is running directly toward P . Though the minimization through the main equation yields $\varphi = \text{sgn } S$, the signum operator is indeterminate at $S = 0$, and so we require the intermediate value of turn rate by other means. Continuity of the components of the gradients along the EL , and requiring unit rate of decrease of the time-to-go thereon together gives

$$V_x^- \dot{x}_{EL} + V_y^- \dot{y}_{EL} = V_y^+ \dot{x}_{EL} + V_y^+ \dot{y}_{EL} = -1 \ . \tag{2}$$

These equations are interpreted vectorially in Fig. 2.3, where it is seen that the adjoint vectors before and after arrival at the EL have equal components along the EL , and that the main equation is satisfied both above and below the EL .

Thus, the EL is a locus along which E can choose between two strategies, and P's strategy depends on this choice. If E chooses ψ^- , P is forced to mix* his strategies, for a resultant intermediate control, $\breve{\varphi}(x,y)$, depending on E's position. This "chatter" strategy

*The "mix" is accomplished at infinite frequency, such that $\breve{\varphi} = 2p-1$, where p = proportion of time spent at $\varphi = +1$.

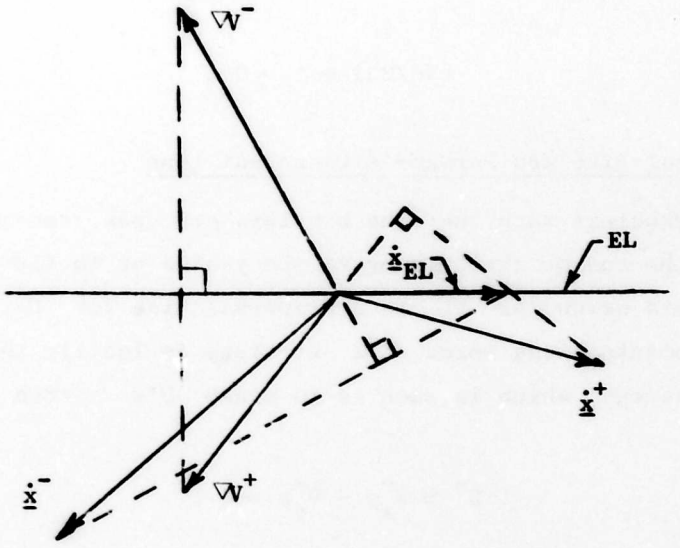

FIGURE 2.3. Velocities and Gradients Near the EL

produces a path for P of time-varying curvature in real space. When E chooses ψ^+, he flees along the tangent to P's minimum turn circle, and P's optimal strategy jumps to $\varphi = +1$. For EL motion, the retrogressive equations read

$$\begin{aligned} \mathring{x} &= \breve{\varphi} y - \gamma s\psi^- \\ \mathring{y} &= 1 - \breve{\varphi} x - \gamma c\psi^- \end{aligned} \tag{3}$$

where

$$\frac{s\psi^-}{c\psi^-} = \frac{x}{y} = \frac{V_x^-}{V_y^-} . \tag{4}$$

The main equation on the prior side then gives the magnitude of the adjoint vector, so that, with (4),

$$V_x^- = \frac{x}{y+\gamma r}$$

$$V_y^- = \frac{y}{y+\gamma r} \ . \tag{5}$$

To evaluate $\breve{\varphi}$, (4) is used to give E's control in (2), which then becomes

$$V_x^+(\breve{\varphi}y+\gamma x/r) + V_y^+(1-\breve{\varphi}x+\gamma y/r) = 1 \ , \tag{6}$$

where the gradients are to be found as functions of (x,y) on the EL . Specifically, the adjoints and position are given by

$$V_x^+ = \frac{s\tau_1}{1-\gamma}$$

$$V_y^+ = \frac{c\tau_1}{1-\gamma} \tag{7}$$

$$x = 1 - c\tau_1 + (y_1-\gamma\tau_1)s\tau_1$$

$$y = s\tau_1 + (y_1-\gamma\tau_1)c\tau_1 \ , \tag{8}$$

where τ_1 is measured back from the position $(0,y_1)$. Eliminating $(y_1-\gamma\tau_1)$ from (8) and solving the resulting quadratic equation give the time from EL to y-axis as a function of position on the EL :

$$c\tau_1 = \frac{1-x+hy}{h^2+1}$$

$$s\tau_1 = \frac{y-h(1-x)}{h^2+1} \ ,$$

where $h^2 = x^2+y^2-2x$. Substituting these relations into (7) and this result into (6) give P's intermediate control as

$$\breve{\varphi} = 1 - \gamma\,\frac{r^2-x+hr}{r(r-y)} \ . \tag{9}$$

It is easy to prove that $\breve{\varphi} \neq 1$, since the numerator in (9) cannot vanish except at $x = y = 0$. At the left end of the EL , $x = 0$, and the chatter strategy here is $\breve{\varphi} = 1-\gamma$. Typical numerical examples pro-

duce deviations of $\breve{\varphi}$ over the EL of only a few percent from this initial value. The point B, where the EL joins the barrier, has coordinates given by (14) of Sec. 2.3. These are the initial conditions for the retrogressive integration of the EL, which then proceeds by using (4) and (9) in the equations (3).

It can readily be shown that the slopes of EL and barrier are equal at B. The reason is that $y + \gamma r = 0$ at the point B, because $\dot{r} = 0$ on both arcs and therefore the slope at B is <u>independent</u> of φ; $dy/dx = \sqrt{1-\gamma^2}/\gamma$. This also implies, according to (5), that the gradient becomes unbounded at B, since the sensitivity of capture time to a change in position is infinite at this point.

Our convention regarding the barrier has been briefly discussed in Sec. 2.1. While this topic is discussed completely in Chapter III, special consideration must be given here to its end-point, B. For those trajectories which begin above the EL, we have found that E can choose to remain on the EL to the point B, if P plays optimally. But, since E can avoid termination by playing the barrier strategy, P must <u>prevent</u> E from reaching B. As mentioned by Isaacs (p. 300), P can postpone his switch to $\breve{\phi}$ by an infinitesimal time. The ensuing equivocal path is then imagined as occurring slightly <u>below</u> the EL, such that B cannot be reached by E.

As shown in Fig. 2.5(b), a portion of the negative y-axis may be a UL for P, with $\varphi = 0$. That is, if the EL encounters the negative y-axis (instead of the capture circle), the trajectories leading to the EL from the "turn-away" region arrive also at the negative y-axis just under the capture circle. This segment will then be a UL as discussed in Sec. 2.2, and this "reverse chase" strategy of E's is continuous with the strategies on either side of the y-axis, as E strives to delay P's turn maneuver.

The intersection of the UL and EL is a multiple-choice point in the relative space. That is, both P and E must choose strategies, and trajectories can depart from this point in four different directions. If E chooses to continue his reverse chase policy at the EL, the

switch function remains at zero while P executes a slow turn at the intermediate rate, $\breve{\varphi}(x,y)$. If he does not so choose, E runs tangent to the minimum turn circle chosen by P . On arrival at this four-way junction, then, P "first" chooses a turn direction (or the sign of φ), and E , by his choice of strategies, simultaneously forces P to turn at one of two specific magnitudes ($|\varphi| = \breve{\varphi}$ or 1) .

Immediately below the intersection of the EL with the y-axis (where y is given by numerical solution of the EL equations), we find the value of the switch function to be $S^+ = V_x y$. Using (7) and (8), this reduces to $S^+ = (1-c\tau_1)/(1-\gamma)$. Substituting for $c\tau_1$ in terms of the position (0,y) then yields

$$S^+ = \frac{2y^2}{(1-\gamma)(1+y^2)} > 0 \ . \tag{10}$$

A similar analysis for trajectories in the left half plane ($\varphi = -1$) shows that $S^- < 0$, and since this analysis can hold for all retrograde paths not intersecting the EL , we conclude that the switch function is discontinuous across the negative y-axis at all points below the EL .

A dispersal line is defined in Ref. 1 as a locus of initial conditions along which either or both of the strategies are not unique. They are often found as the retrograde intersection of two distinct families of optimal paths, for each of which the main equation is satisfied. At the intersection, the optimal time-to-go is the same for either pair of strategies, and the dispersal line condition is expressed in terms of the two fields of trajectories, as follows:

$$\nabla W^- \cdot \dot{\underline{x}}^- = \nabla W^+ \cdot \dot{\underline{x}}^+ \ . \tag{11}$$

This reduces to a differential equation for the slope of the dispersal line,

$$\frac{dy}{dx} = - \frac{V_x^- - V_x^+}{V_y^- - V_y^+} \ , \tag{12}$$

where the superscripts refer to opposite sides of the line.

The discontinuity of S across this portion of the negative y-axis, as derived in (10), coupled with the symmetry of strategies and paths across it, is a special case of (12), as here we have $V_x^- = -V_x^+$ and $V_y^- = V_y^+$. This portion of the y-axis is then a dispersal line along which the sign of S is undefined.* A diagram of the velocity vector components for $\underline{x}$ on the negative y-axis below the EL shows that P's contribution to the x-velocity $(-\varphi y)$ exceeds E's contribution $(\gamma s\psi)$, and hence P determines the departure direction. The line is therefore called a "pursuer's dispersal line" (PDL). The present case has a geometrically obvious interpretation (when E is directly behind P, P can turn sharp right or sharp left, and E's strategy depends on P's choice) but we will find other more general circumstances in which (12) holds. In these other situations, the discontinuity $\nabla V^+ \neq \nabla V^-$ implies a discontinuity in E's control $(\psi^+ \neq \psi^-)$, but it need not imply a change in P's control. That is, the switch function can be discontinuous across the line, while retaining the same sign on either side.

2.5 Parameter Space and Trajectories

To summarize the developments of this chapter, it has been shown that the "usable part" of the capture circle is an angular sector on which the game must end. If the parameters are such that a trajectory arrives tangentially at the boundary of this region, such a trajectory is a "barrier," across which the time-to-go is discontinuous, and along which the gradient is infinite. These parameters satisfy the relation $\beta^2 + \gamma^2 \leq 1$, the equality being shown as C_1 in Fig. 2.4. If the parameters fall above this curve, a tangential trajectory cannot arrive at the boundary of the usable part. It has also been shown that if β is sufficiently small, the capture region is a finite curvilinear triangle. If E is initially outside of this region, he can avoid capture indefinitely, using the sidestep tactic of the bullfighter. This finite capture region exists (for $\beta^2 + \gamma^2 \leq 1$) if $\beta \leq \gamma \sin^{-1}\gamma + \sqrt{1-\gamma^2} - 1$.

*By contrast, we have seen in Sec. 2.2 that the y-axis above the EL is a UL, since there $S^+ = S^- = 0$.

The latter function appears as C_2 in Fig. 2.4. It has also been shown that the point A occurs on the barrier (as assumed in Ref. 1) only if $c(\beta/2\gamma) + \gamma \geq 0$; C_3 is the corresponding locus in Fig. 2.4.

These three loci determine two regions in the parameter space, but optimal trajectories which fill the playing space have been found in this chapter only for parameters in Region I. A typical set of trajectories for parameters in this region is shown in Fig. 2.5(a). Because the time-to-go is discontinuous (and infinite) at the barrier, where the point A is located, paths "from" A must instead be regarded as starting from points infinitesimally close to A . From this range of initial points, trajectories depart to terminate at angles in the half-open interval, $0 \leq \theta < \theta_{up}$. We follow the convention that when the

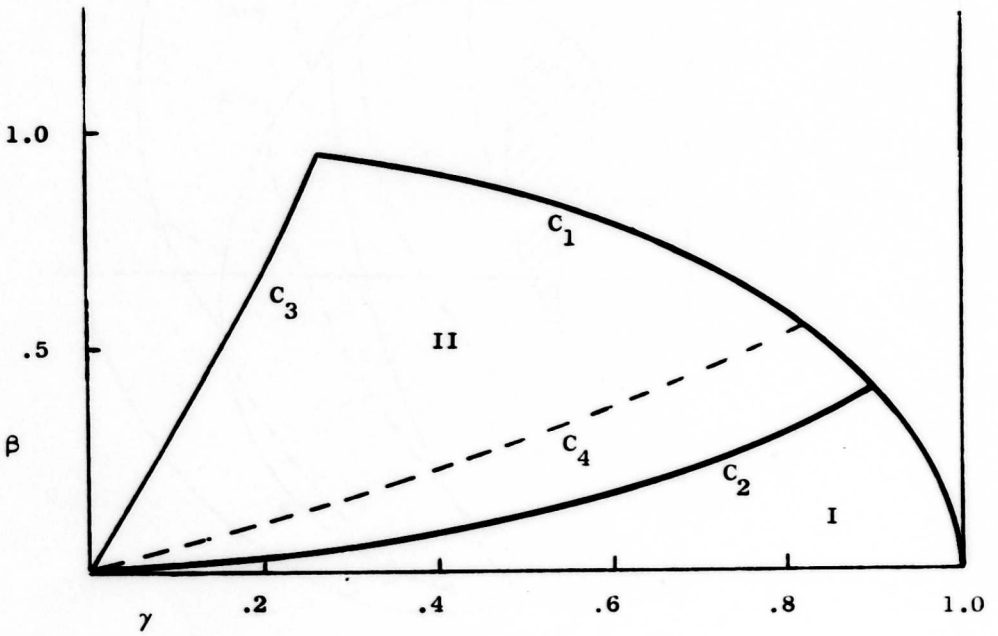

FIGURE 2.4. Regions in Parameter Space for the Classical Game

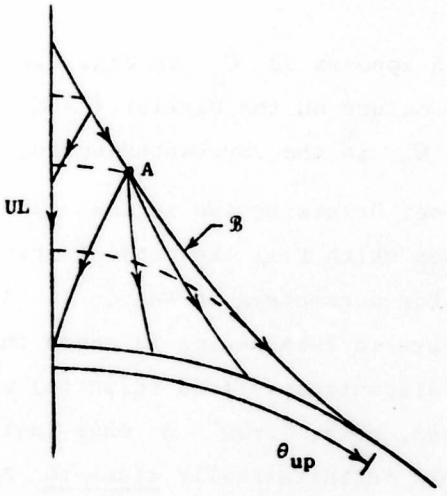

(a) Barriers Closed

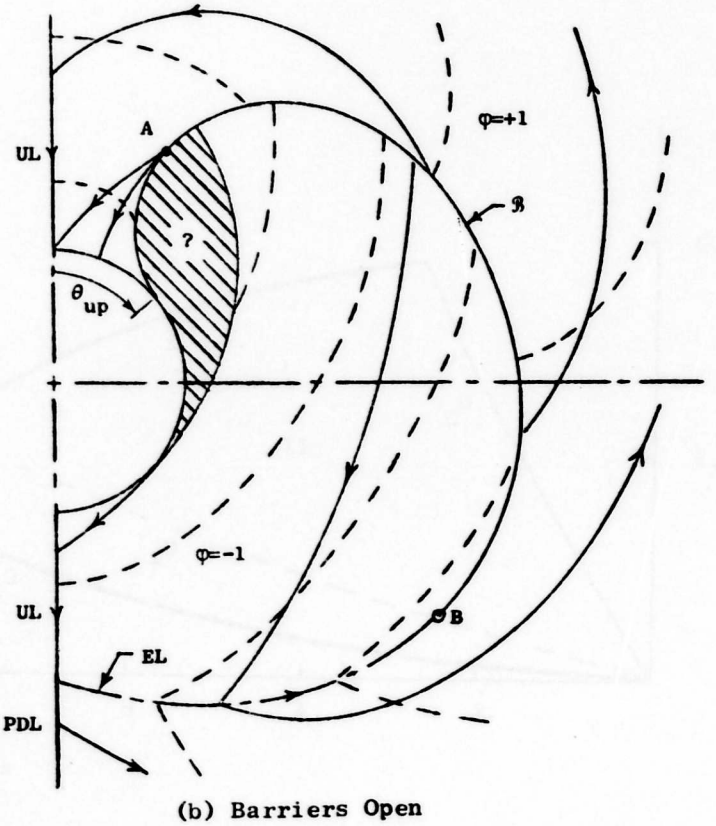

(b) Barriers Open

FIGURE 2.5. Trajectories and Isochrones in the Classical Game

barriers close, E follows the semipermeable barrier when possible, E preferring an early safe contact at θ_{up} to a later termination at $\theta = 0$. P, of course, turns toward E whatever E's strategy, because in this case, S has the sign of x, and P will reasonably prefer a safe contact to none at all. Thus, in this case we see that $\mathcal{B}$ is a locus of infinite discontinuity in the time-to-go, and it is an optimal path which ends tangentially at θ_{up}.

Contours of constant V can be easily calculated as the dashed lines in the figure. These isochrones are tangent to the barrier only below the point A. The discontinuity in E's strategy for initial conditions near $\mathcal{B}$ at the point A is the cause of this change in the isochrones.

The more complex diagram in Fig. 2.5(b) applies for parameters in Region II to the right of C_3, and this configuration is essentially as given in Ref. 1. Because the strategies are not known at <u>all</u> points, however, it may happen that some of the trajectories so far found are <u>not</u> optimal. In fact, this actually occurs for a small range of parameters, as will be shown in Chapter III. For present purposes, we may say that the trajectories of Fig. 2.5(b), though incomplete, are qualitatively representative, for all parameters right of C_3 and above C_4 in Region II. Of course, as (β,γ) change in Region II, the point A will be displaced along the barrier and the barrier's relative size will change, but this does not affect the <u>type</u> of solution. We will find, however, that the reverse-chase is absent for parameters close to the intersection of C_3 and C_1 in Region II.

The isochrones of Region II are more complex and interesting than those of Region I. The barrier appears as a discontinuity in the time-to-go, but this discontinuity decreases to zero at the end B of the barrier. The EL, which extends the barrier to the y-axis or to the capture circle, is a sharp minimum in V, in the sense that the time-to-go increases linearly in both directions normal to the EL. The normal to the local isochrone is thus indefinite on the EL, reflecting the fact that E can choose between two strategies on the EL.

Similarly we have found that when the barriers are open, the y-axis may be a UL or a PDL , depending on whether or not P's switch function is continuous across it. For the discontinuous (PDL) case, the normal to the isochrone is again double-valued, because the y-axis is here a sharp maximum in the time-to-go, V .

For initial conditions on the open barrier, P's strategy is a turn away ($\varphi = -1$) unless the parameters are below C_4 in Fig. 2.4. For these parameters, we will find that a range of positions on $\mathfrak{B}$ exists, for which $\varphi = +1$ is optimal on both sides of the barrier. Thus, $\mathfrak{B}$ is an optimal trajectory only in this case, and when the barriers close.

Chapter III

EXTENSIONS TO THE CLASSICAL RESULTS, $\beta^2+\gamma^2 \leq 1$

The parameter inequality in the chapter title holds whenever the barrier exists at θ_{up}. But when the right and left barriers do not intersect, strategies for $\underline{x}$ in the shaded area of Fig. 2.5(b) must be found. For parameters above C_4 (see Fig. 2.4), including those to the left of C_3, this extension is not difficult, though it entails treatment of "safe-contact" strategies. For parameters between C_2 and C_4 in Region II, however, two new exceptional lines are required to complete the solution. We begin by considering those trajectories which touch the capture circle at the lowest corner of the shaded area.

3.1 One-Dimensional Motion

We have seen in Fig. 2.5(b) that turn-away trajectories can arrive at the negative y-axis. The particular path which contacts the capture circle at the right edge of the shaded region is specified in terms of the intercept y_1 and the time from tangency to this intercept. The equations giving these two quantities are $r = \beta$, $\dot{r} = 0$, which require the use of the retrograde trajectories

$$\begin{aligned} x &= -1 + c\tau - (y_1-\gamma\tau)s\tau \\ y &= s\tau + (y_1-\gamma\tau)c\tau \ . \end{aligned} \tag{1}$$

The tangency condition is then expressed by the equations

$$\begin{aligned} 1 - c\tau + (y_1-\gamma\tau)s\tau + \tfrac{1}{2}[(y_1-\gamma\tau)^2 - \beta^2] &= 0 \\ (1-\gamma)s\tau + (y_1-\gamma\tau)(c\tau-\gamma) &= 0 \ . \end{aligned} \tag{2}$$

Eliminating y_1 gives a cubic in $c\tau$, which turns out to be the square of

$$\sqrt{1+\gamma^2-2\gamma c\tau}\ (1-c\tau) - \beta(c\tau-\gamma) = 0 \ . \tag{3}$$

This expression yields τ_1, the time from tangency to the negative y-

axis, in terms of which the intercept is

$$y_1 = \gamma\tau_1 + \frac{(1-\gamma)s\tau_1}{\gamma - c\tau_1} < -\beta \ . \tag{4}$$

The angle at which tangency occurs in given by (1) as

$$\tan\theta_m = \frac{x(y_1,\tau_1)}{y(y_1,\tau_1)} = \frac{\gamma c\tau_1 - 1}{\gamma s\tau_1} \ . \tag{5}$$

The supplement of this angle is <u>greater</u> than θ_{up} , as can be shown by using (3) and (4), together with the definition, $c\theta_{up} = \gamma$. That is, E is physically capable of maintaining safe-contact for angles greater than θ_m , but such a strategy is not optimal.

We consider next the conditions at tangency with the aim of extending the trajectories backwards from this point. The main equation in polar coordinates is

$$\min_{\varphi}\max_{\psi}[V_r\dot{r} + V_\theta\dot{\theta}] = -1 \ , \tag{6}$$

where the polar equations of motion are given in (11) of Sec. 2.3,

$$\dot{r} = -c\theta + \gamma c(\psi-\theta)$$

$$\dot{\theta} = -\varphi + \frac{1}{r}\left[s\theta + \gamma s(\psi-\theta)\right] \ .$$

The tangency condition $\dot{r} = 0$ relates ψ to θ (ambiguously), while (6) reduces to

$$\min_{\varphi} V_\theta\{-\varphi + \frac{1}{\beta}\left[s\theta + \gamma s(\psi-\theta)\right]\} = -1 \ , \tag{7}$$

where the angular adjoint is identical with P's switch function;

$$V_\theta = V_x y - V_y x \triangleq S \ . \tag{8}$$

The minimizing control of P is thus $\varphi = \text{sgn } S = -1$, and E's strategy must maximize $V_\theta\, s(\psi-\theta)$ while satisfying $\dot{r} = 0$. Since $V_\theta < 0$, at the point on the capture circle where safe contact ends, the ambiguity in E's control is resolved. Thus,

$$\psi = \theta - \cos^{-1}(c\theta/\gamma) \tag{9}$$

is E's safe-contact strategy when $\varphi = -1$. In one-dimensional (tangential) motion, we find that E's angular rate is

$$\dot{\theta} = 1 + (s\theta - \gamma\sqrt{1-c^2\theta/\gamma^2})/\beta \ , \tag{10}$$

and consequently,

$$V_\theta = -1/\dot{\theta} = -\frac{\beta}{\beta+s\theta-\gamma\sqrt{1-c^2\theta/\gamma^2}} \ . \tag{11}$$

We may now consider the trajectories which arrive at the capture circle, there to begin a safe-contact path which departs tangentially at the angle θ_m given in (5). Just prior to contact, the main equation for $\varphi = -1$ is written

$$\max_{\psi}[V_r\dot{r}^- + V_\theta\dot{\theta}^-] = -1 \ . \tag{12}$$

Since $r = \beta$ is the boundary of the regular region, the angular gradient on arrival is continuous. The maximization of (12) implies that

$$c(\psi^- - \theta) = \frac{V_r}{\sqrt{V_r^2+(V_\theta/\beta)^2}} \tag{13}$$

and therefore, using (11) for V_θ/β , (12) can be solved for

$$V_r = \frac{c\theta/\gamma}{\sqrt{1-c^2\theta/\gamma^2}\ (\beta+s\theta-\gamma\sqrt{1-c^2\theta/\gamma^2})} \ . \tag{14}$$

This finally permits (13) to be solved for $\psi^- = \theta - \cos^{-1}(c\theta/\gamma) = \psi^+$, and therefore $\dot{r}^- = \dot{r}^+ = 0$, so that trajectories and strategies are smooth on arrival at the capture circle. In fact, the continuity of ψ could have been anticipated from the fact that

$$\max_{\psi^-}(V_r\dot{r}^- + V_\theta\dot{\theta}^-) = \max_{\psi^+} V_\theta\dot{\theta}^+ = -1 \ ,$$

i.e., because E's vectogram is circular, H has a unique maximum relative to ψ , such that $\psi^- = \psi^+$. A typical safe-contact trajectory for $\varphi = -1$ is shown in Fig. 3.1.

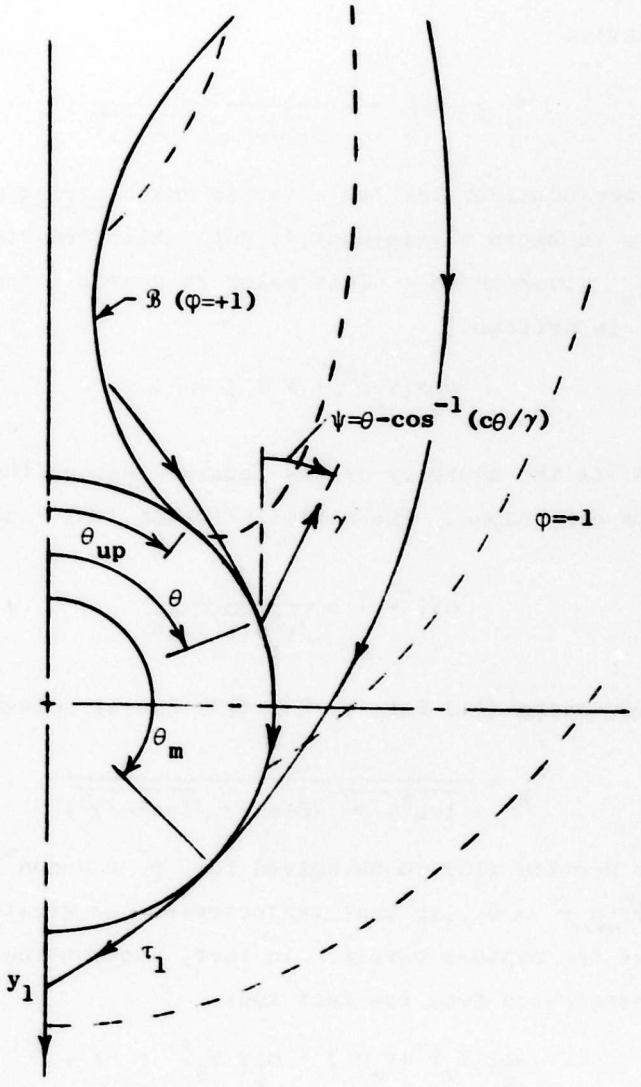

FIGURE 3.1. Safe Contact Arrival and Departure for φ = -1

3.2 Switch Line Replaces Equivocal Line

For parameters slightly to the left of C_3 in Fig. 2.4, the point A falls between the end B of the barrier and the negative y-axis. The points B and A are connected by a switch line (SL), on which S = 0, and A is connected to the capture circle or to the y-axis by an EL.

The disappearance of the EL occurs when the point A falls on the capture circle. This is easily derived as the locus

$$c(\beta/\gamma) = 1-\beta^2/2 \ , \tag{1}$$

which will be labelled C_5 in the parameter space drawing at the end of this chapter (Fig. 3.9). For parameters to the left of this line, retrogressive trajectories to A are interrupted by the capture circle, and the point B is connected to the capture circle by the SL.

The retrogressive switch time is determined as a function of arrival angle θ_o:

$$S = V_x y - V_y x = \frac{c\theta_o - c(\theta_o+\tau)}{c\theta_o - \gamma} = 0$$

or

$$\tau_s = 2(\pi-\theta_o) \ . \tag{2}$$

The arrival angle θ_1, as defined in Fig. 3.2, is given by equating $\tau_s = \tau_A = \beta/\gamma$, or $\theta_1 = \pi-\beta/2\gamma$. For all arrival angles between 0 and θ_1, A serves as a dispersal point for E, and it is interesting that in this case trajectories can <u>arrive</u> at A from two directions.

At the end of the barrier, the trajectory has the slope

$$\frac{dy}{dx} = \frac{1-x-\gamma c(\theta_o+\tau)}{y-\gamma s(\theta_o+\tau)} \ , \tag{3}$$

where the point B is evaluated using $c\theta_o = \gamma$ together with (1) to give, as in (14) of Sec. 2.3,

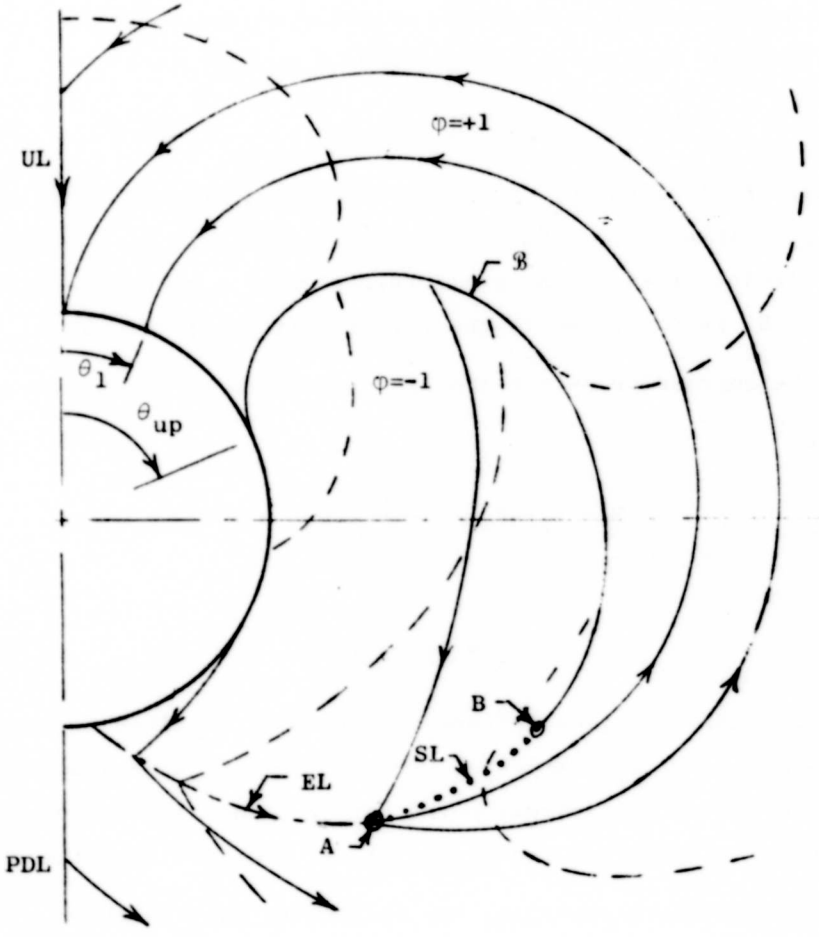

FIGURE 3.2. Trajectories for Parameters Between C_3 and C_5 in Region II

$$\left.\frac{dy}{dx}\right|_T = \frac{\sqrt{1-\gamma^2}}{\gamma} = -\frac{x}{y} \quad . \tag{4}$$

This implies that $dr/d\tau = 0$ at this point. The slope of the SL is

$$\left.\frac{dy}{dx}\right|_S = \frac{y_\theta + y_\tau (d\tau_s/d\theta_o)}{x_\theta + x_\tau (d\tau_s/d\theta_o)} \quad , \tag{5}$$

where $d\tau_s/d\theta_o = -2$, according to (2), and the partial derivatives follow immediately from the retrogressive equations for the trajectories. Substitution and simplification yield the result

$$\left.\frac{dy}{dx}\right|_S = \frac{\sqrt{1-\gamma^2}}{\gamma} \quad , \tag{6}$$

which with (4) proves that the SL is tangent to the trajectory at this point.

At the point A , however, where $\beta/\gamma = 2(\pi-\theta_1)$, the trajectory slope is found in terms of the arrival angle θ_1 ,

$$\left.\frac{dy}{dx}\right|_T = \frac{c2\theta_1 - \gamma c\theta_1}{-s2\theta_1 + \gamma s\theta_1} \quad . \tag{7}$$

This is the same result given for the slope of the SL at this point, as can easily be verified. The second extreme trajectory from A arrives at the capture circle at $\theta = 0$, and its slope at A is

$$\frac{dy}{dx} = \frac{c(\beta/\gamma)}{s(\beta/\gamma)} = \frac{c2\theta_1}{-s2\theta_1} \quad . \tag{8}$$

The EL slope at the point A requires use of the intermediate τ in the equations of motion, and the result is expressible as a function of γ and θ_1 . It has not been possible to derive analytical conclusions from the expression. However, numerical studies for a range of parameters left of C_3 in Region I show that the EL slope is not equal to either of the values (7) or (8).

The simplest way of expressing the SL is as a function of arrival

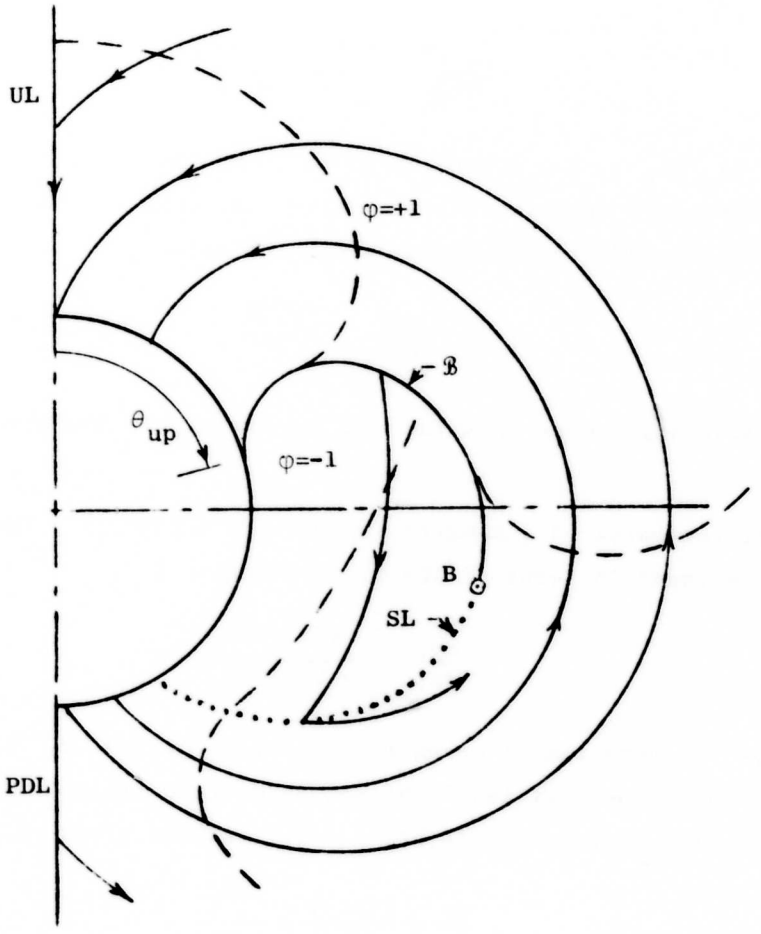

FIGURE 3.3. Trajectories for Parameters Left of C_5 in Region II

angle θ_o, by using the value $\tau = 2(\pi-\theta_o)$ in the retrogressive equations; i.e.,

$$\begin{aligned} x &= s\theta_o[2s\theta_o - \beta + 2\gamma(\pi-\theta_o)] \\ y &= -c\theta_o[2s\theta_o - \beta + 2\gamma(\pi-\theta_o)] \end{aligned} \tag{9}$$

where $0 \le \theta_o \le \cos^{-1}\gamma$ (cf. (14) of Sec. 2.3).

The qualitative appearance of the trajectories for parameters left of C_5, which is given by (1), is as shown in Fig. 3.3. Since S passes smoothly through zero for trajectories intersecting the SL, it follows that E is running toward P when the SL is crossed. Except for the absence of an EL, this configuration is very much like that of Fig. 3.2. We note that in both of these figures, a local maximum in the optimal time-to-go occurs at a point on the underside of the barrier roughly one-fourth of the way to the end of it. The loci of constant V can be regarded as elevation lines on a contour map of the playing space. This concept will be helpful in understanding some results to be found in the next section.

3.3 Switch Envelope and Pursuer's Dispersal Line

For parameters in the lower portion of Region II, it is found that $\mathfrak{B}$ is not necessarily a locus of discontinuity in P's strategy. That is, over a certain interval of $\mathfrak{B}$, the switch function is positive on both sides of it, such that when E is under the barrier here, P "lunges" toward him. The verb is appropriate because this is always a very brief maneuver, soon followed by a turn-away and subsequent safe-contact. As mentioned in Sec. 2.5, when φ changes sign across $\mathfrak{B}$, the barrier is not an optimal path but is only a locus of initial conditions for the turn-away maneuver. But, when parameters are such that the lunge region exists, we can expect P's switch line to lie to the right of $\mathfrak{B}$ (which now <u>is</u> an optimal path), somewhat as shown in Fig. 3.4. We consider a comparative test of the three retrograde paths shown in this figure.

At the point G_1, when the lowest path T_1 reaches the barrier, it is found that if P were to switch to $\varphi^- = +1$, thereby forcing E to switch to a strategy ψ^- perpendicular to $\mathcal{B}$, then for $\underline{x}$ on $\mathcal{B}$,

$$\nabla W^+ \cdot \dot{\underline{x}}^- > -1 \ . \tag{1}$$

The inequality implies that such a switch is to E's advantage and hence that $\varphi^- = +1$ is not optimal for such points. It may also happen, on the other hand, that at G_2 on a second path T_2, this double switch in strategies leads to the inequality

$$\nabla W^+ \cdot \dot{\underline{x}}^- < -1 \ , \tag{2}$$

which means that P can force E to cross the "+" contours <u>faster</u> than the optimal rate. Therefore, these contours are not correct at this point and E's strategy cannot be given by ∇W^+ in this region, where P lunges toward E.

If these inequalities hold, then at some intermediate point G of the barrier, we must find

$$\nabla W^+ \cdot \dot{\underline{x}}^- = V_x^+ \dot{x}^- + V_y^+ \dot{y}^- = -1 \ , \tag{3}$$

where the left side can be expressed as a function of θ_o, by using $\underline{x}^+ = \underline{x}^-$ to provide τ_b and τ_o in terms of θ_o. Specifically, we have

$$\begin{aligned} x^- &= 1 - c\tau_b + (\beta - \gamma\tau_b)s(\theta_{up} + \tau_b) \\ y^- &= s\tau_b + (\beta - \gamma\tau_b)c(\theta_{up} + \tau_b) \end{aligned} \tag{4}$$

$$\begin{aligned} x^+ &= -1 + c\tau_o + \beta s(\theta_o - \tau_o) - \gamma\tau_o s(\psi_o - \tau_o) \\ y^+ &= s\tau_o + \beta c(\theta_o - \tau_o) - \gamma\tau_o c(\psi_o - \tau_o) \ , \end{aligned} \tag{5}$$

where $\psi_o = \theta_o - \cos^{-1}(c\theta_o/\gamma)$ and $\theta_{up} = \cos^{-1}\gamma$. Finally, the adjoint components in (3) are easily found in terms of ψ_o and the retrogressive time from tangency, τ_o;

$$\begin{aligned} V_x^+ &= s(\psi_o - \tau_o)/D \\ V_y^+ &= c(\psi_o - \tau_o)/D \end{aligned} \tag{6}$$

$$D = \sqrt{1-c^2\theta_o/\gamma^2}\,(\beta+s\theta_o-\gamma\sqrt{1-c^2\theta_o/\gamma^2}) \ .$$

By numerical search methods, we determine the parameters θ_o , τ_o and τ_b which specify the endpoint G of the SE . Of course, when the condition (3) does not hold for <u>any</u> point on $\mathcal{B}$, the parameters (β,γ) are <u>above</u> the locus C_4 of Fig. 2.4. Since, whenever (3) holds, the barrier always has the qualitative form of Fig. 3.4, the point G is the lowest point of a "lunge" region. We then must find the switch line which begins at G and which separates this lunge region (φ = +1) from the turn-away region (φ = -1) .

To develop generating equations for this line, we first consider a group of trajectories parallel to, and right of, $\mathcal{B}$. At the point G ,

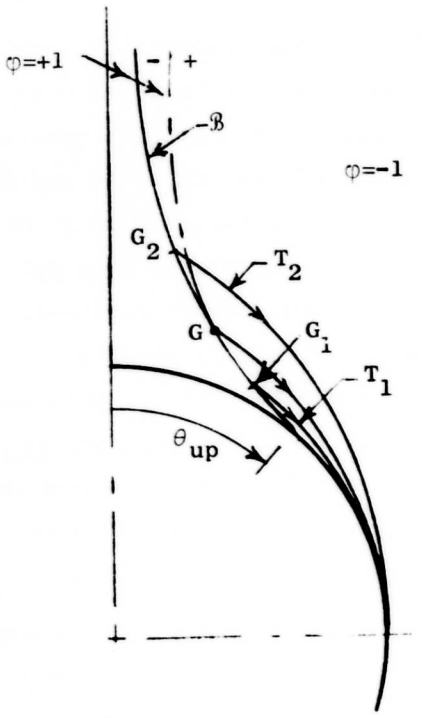

FIGURE 3.4. Detail Near Barrier When SE Exists

we have (3) together with the main equation on the prior side, $\nabla W^- \cdot \dot{\underline{x}}^- = -1$, which combine to give the slope of the switch line as a function of position,

$$\frac{dy}{dx} = - \frac{V_x^- - V_x^+}{V_y^- - V_y^+} . \qquad (7)$$

On $\mathcal{B}$, of course, $|\nabla W^-| \to \infty$, and so the slope of the switch line is the same as the slope of the local trajectory, $\mathcal{B}$. As the SL is followed away from $\mathcal{B}$, the incoming trajectories must continue to be tangential to it. This is so because, if they encountered this switch line at a non-zero angle, and if P chose to delay his turn-away, E would "chatter" between his strategies ψ^- and ψ^+ , thereby remaining on the line. Since E's vectogram is a circle, however, this chatter strategy would actually reduce his speed and hence would not yield $dV/dt = -1$, as did $\varphi = +1$ and $\psi = \psi^-$. Hence, the switch line is the envelope of the prior paths, and consequently it is called a "switch envelope" (SE).

While they are similar in some superficial respects, the SE differs in an important way from the EL described in Chapter II. The switch function goes smoothly to zero at the endpoint B of $\mathcal{B}$, which is then tangentially extended by the EL . It was found that $S^- = 0$ on the incoming paths to the EL , while $S^+ > 0$ on the departing trajectories. This meant that E could choose to <u>keep</u> $S = 0$ by running radially, which gave P's control as the intermediate value, $\breve{\varphi}$. By contrast, neither S^- nor S^+ is zero along the SE , but it is known that the component of ∇W along the SE is continuous, so that (3) holds along it. This implies that P's control <u>along</u> the SE is $\varphi^- = +1$, and hence E's arrival control is given by (3) in terms of θ_o and τ_o . The expression (7) for the SE slope is then solved for the derivative $d\theta_o/d\tau_o$.

As described in detail in Appendix A, the retrogressive integration of the SE is valid only so long as the curvature of the SE exceeds that of the incoming paths. This curvature condition is equivalent to a condition of derivatives of ψ^- . On the incoming paths, $\dot{\psi}^- = -1$, while on the SE , ψ^- is expressed as a function of θ_o and $\tau_o(\theta_o)$,

and its time rate of change is given in terms of these coordinates. In other words, $\dot{\psi}^-$ is discontinuous at tangency, except at the upper end of the SE .

At the coordinate θ_o , where these curvatures are equal, the SE is tangentially extended by a PDL . That this should be so is suggested by Fig. 3.5, where the cotangency of PDL , SE and trajectory at their meeting point is implied by a finite curvature condition on the trajectory at the junction.

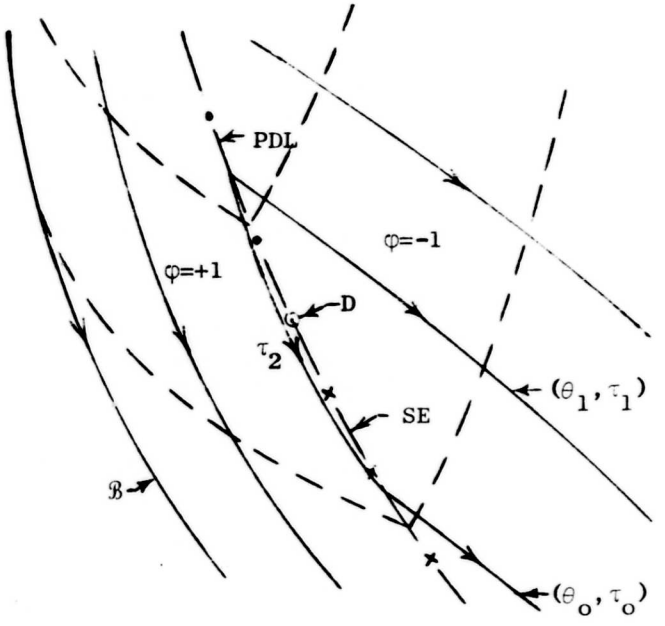

FIGURE 3.5. Detail Near Junction of SE and PDL

The PDL is simpler to construct than the SE , though the PDL is given in terms of SE coordinates, which must therefore be stored as they are computed. The retrogressive trajectories of either side must yield the same point on the PDL , and the time-to-go must be the same on the two paths. Denoting the side near the barrier by the superscript "+" (corresponding to the lunge strategy, $\varphi = +1$), we have

$$dx^+(\theta_o,\tau_2) = dx^-(\theta_1,\tau_1)$$

$$dy^+(\theta_o,\tau_2) = dy^-(\theta_1,\tau_1) \qquad (8)$$

$$dV^+(\theta_1,\tau_2,\theta_o) = dV^-(\tau_1) \ ,$$

where the various angles and times are as defined in Fig. 3.5. The appropriate differential equations required in generating the PDL are symbolically expressed using (8), with θ_o taken as a convenient independent variable (subscripts denote partial differentiation):

$$x^+_\theta + x^+_\tau \frac{d\tau_2}{d\theta_o} = x^-_\theta \frac{d\theta_1}{d\theta_o} + x^-_\tau \frac{d\tau_1}{d\theta_o}$$

$$y^+_\theta + y^+_\tau \frac{d\tau_2}{d\theta_o} = y^-_\theta \frac{d\theta_1}{d\theta_o} + y^-_\tau \frac{d\tau_1}{d\theta_o} \ . \qquad (9)$$

At given values of the dependent variables, the gradients ∇V^+ and ∇V^- are known for use in the slope equation, (7). This allows computation of

$$\frac{d\tau_2}{d\theta_o} = - \frac{y^+_\theta - x^+_\theta (dy/dx)}{y^+_\tau - x^+_\tau (dy/dx)} \ , \qquad (10)$$

and a straightforward inversion of (9) for the remaining two derivatives. Initial values at the point D are $\tau_2 = 0$, $\theta_1 = \theta_o$ and $\tau_1 = \tau_o$, the SE integration having provided θ_o and τ_o .

The upper end of the PDL occurs at the barrier, and these curves join here tangentially owing to the infinite magnitude of the gradient vector ∇V^+ at the barrier.* That is, the PDL slope, as given by (7), is

$$\frac{dy}{dx} = - \frac{V^-_x - V^+_x}{V^-_y - V^+_y} \to - \frac{V^+_x}{V^+_y} \ , \qquad (11)$$

*For some parameters near the lower edge of Region II, the PDL actually extends outside the shaded area of Fig. 2.5(b). This illustrates that unless the entire space is filled with trajectories, none of them can strictly be called "solutions."

which is equal to the slope of the adjacent barrier, as obtained using (2) of Sec. 2.3,

$$\frac{dy}{dx} = -\frac{v_x}{v_y} . \tag{12}$$

Since $\mathcal{B}$ is a trajectory on the "+" side of the PDL, the optimal time-to-go is a local maximum somewhere to the right of the tangential junction of PDL and $\mathcal{B}$, as will be shown in Fig. 3.7.

3.4. Focal Line

For parameters which are near the right corner of Region II, numerical generation of the SE shows that at some point below where the curvature condition denoting the start of the PDL is satisfied, the SE derivative vanishes, or $d\theta_o/d\tau_o = 0$. At this point on the SE, the velocities obtained by two sets of controls are identical; i.e., at a single point, incoming and outgoing velocities are equal, $\dot{\underline{x}}(\varphi^-,\psi^-) = \dot{\underline{x}}(\varphi^+,\psi^+)$. The point where this occurs is found to be the lower end of a "focal line" (FL), along which E runs regardless of P's strategy. Furthermore, the FL is an envelope of arrival paths on both sides. The incoming paths are tangential because, if P maintains his arrival strategy, E must do so as well, in order to keep $dV/dt = -1$. As in the case of the SE, both strategies are continuous when a path joins the FL, and therefore the paths themselves have continuous slopes and are tangential at the FL.

The FL is, like the SE, a local (sharp) maximum or crest in the time-to-go contours, and for <u>any</u> choice of φ, E can stay on this crest. Progress down the line will, however, be maximized if P chooses an extreme control, $\varphi = \pm 1$. As indicated in Fig. 3.6, the FL condition yields two equations in ψ^- and ψ^+, which are E's controls corresponding to $\varphi = -1$ and $+1$, respectively. Using the equations, then,

$$\begin{aligned} \dot{x} &= -y + \gamma s\psi^+ = y + \gamma s\psi^- \\ \dot{y} &= -1 + x + \gamma c\psi^+ = -1 - x + \gamma c\psi^- . \end{aligned} \tag{1}$$

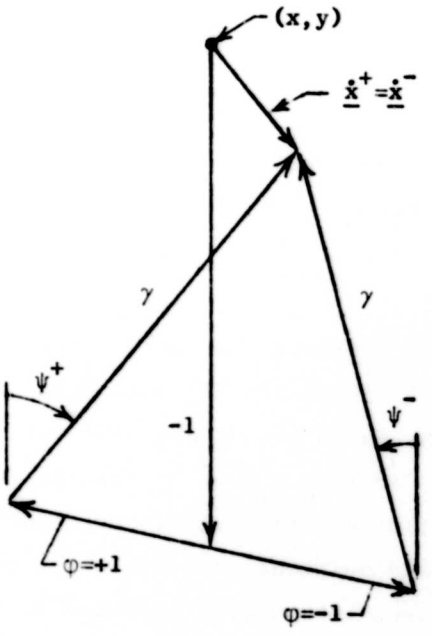

FIGURE 3.6. Focal Line Strategies

These give E's strategy as a function of both E's position on the FL and P's strategy ($\varphi = \pm 1$), as follows:

$$\begin{aligned} \gamma s\psi &= \varphi y + (x/r)\sqrt{\gamma^2 - r^2} \\ \gamma c\psi &= -\varphi x + (y/r)\sqrt{\gamma^2 - r^2} \ . \end{aligned} \tag{2}$$

Using these expressions in (1) gives the retrogressive differential equations for the FL as the simple pair,

$$\begin{aligned} \dot{x} &= -(x/r)\sqrt{\gamma^2 - r^2} \\ \dot{y} &= 1 - (y/r)\sqrt{\gamma^2 - r^2} \ . \end{aligned} \tag{3}$$

Neither strategy is explicit in (3), but $\varphi = \pm 1$ and $\psi(\varphi)$ is given by (2).

It is necessary to have the adjoints along the FL as well, since they are required in the subsequent integration of the SE . We know $s\psi/V_x = c\psi/V_y$ on both sides, for either choice of φ , and the main equation gives

$$V_x\dot{x} + V_y\dot{y} = (\dot{x}s\psi+\dot{y}c\psi)/D = -1 \ .$$

This can be solved for

$$D = \frac{1}{\gamma}[(y/r)\sqrt{\gamma^2-r^2} - \gamma^2 + r^2 - \varphi x]$$

and this denominator (the inverse of the gradient magnitude) is positive for $\underline{x}$ on the FL . The direction of the gradient vector on each side is parallel to E's strategy, (2).

The FL has features unlike those of any other type of exceptional curve found in this game. The equations (1) show that, to traverse the FL , P can choose either extreme rate of turn, and E's strategy depends on this choice, according to (2). Further, P can switch strategies ad libitum between $+1$ and -1 , all with no change in the relative trajectory, provided that E reacts immediately. Examination of the vector velocities in Fig. 3.6 shows that no intermediate turn rate can produce the same relative motion as $\varphi = \pm 1$. These comments are meant to emphasize the distinction between "chatter" on the EL , and "switching" on the FL . A further observation is that the switch function is never zero on the FL , while it remains at zero for motion along the EL .

The upper end of the FL occurs when its curvature is the same as that of an incoming path. This curvature criterion is simply written as a rate of change of ψ along the FL , or

$$\left.\frac{d\psi}{d\tau}\right|_f = \varphi \ . \tag{4}$$

If this equation is first satisfied for $\varphi = -1$, for example, the incoming trajectories to the <u>right</u> have the same curvature as the FL , and hence, as shown in Fig. 3.7, the FL is extended by an SE . When the time derivatives are written as in (3), we find the criterion as

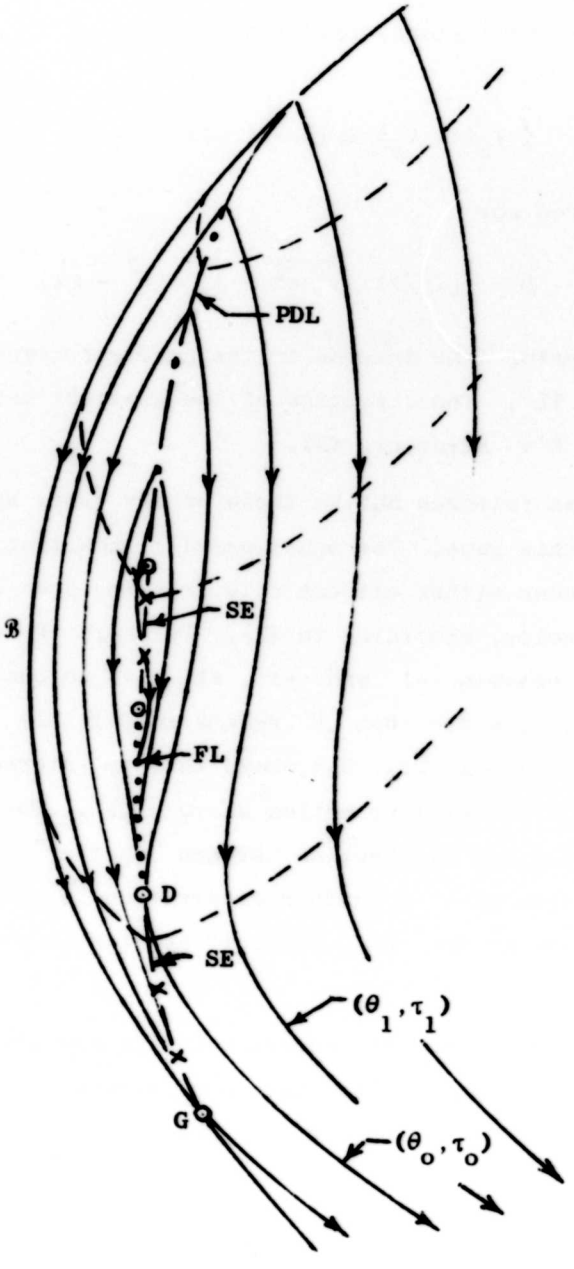

FIGURE 3.7. Trajectories Near the FL in Region II

$$ry - \sqrt{\gamma^2 - r^2}(2r^2 + \varphi x) = 0 \tag{5}$$

where $\varphi = \pm 1$. For the many cases of the focal line which have been analyzed numerically, (5) was first satisfied for $\varphi = -1$, so that the FL is extended by a SE . This means that a "reverse SE ," with trajectories tangent on the right, and for which (5) would be first satisfied for $\varphi = +1$, is apparently never realized.

Extension of the FL by an SE is straightforward except for the initial step in the integration. When $\tau_1 = 0$, using the notation of Fig. 3.8, the indeterminacy in the slope of the SE is evaluated by ex-

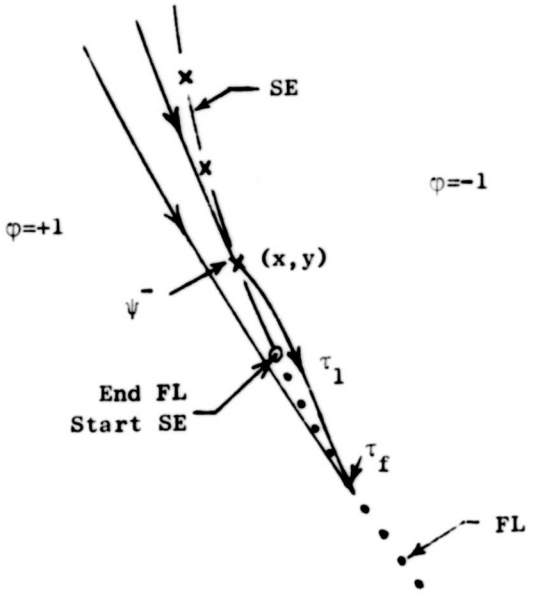

FIGURE 3.8. Detail Near Junction of SE and FL

pansion in series. Thus, the slope of the SE is

$$\frac{dy}{dx} = \frac{\dot{y}^-}{\dot{x}^-} = \frac{1 - x - \gamma c\psi^-}{y - \gamma s\psi^-} \tag{6}$$

where

$$c(\psi^- - \psi_f + \tau_1) = 1 + \frac{2}{\gamma}[c(\psi_f - \tau_1) - c\psi_f - r_f^2/\gamma] \ . \tag{7}$$

The expression (7) follows from the SE condition and the trajectories, which here are given as functions of (τ_f, τ_1) :

$$x = -1 + (x_f+1)c\tau_1 - y_f s\tau_1 - \gamma\tau_1 s(\psi_f-\tau_1)$$
$$y = y_f c\tau_1 + (x_f+1)s\tau_1 - \gamma\tau_1 c(\psi_f-\tau_1) \ . \tag{8}$$

The subscript f denotes a functional dependence on τ_f . Then the slope (6) is equated to the bilinear form,

$$\frac{dy}{dx} = \frac{y_{\tau_f}+y_\tau(d\tau_1/d\tau_f)}{x_{\tau_f}+x_\tau(d\tau_1/d\tau_f)} \ ,$$

which is inverted to yield

$$\frac{d\tau_1}{d\tau_f} = -\frac{x_{\tau_f}\dot{\bar{y}}-y_{\tau_f}\dot{\bar{x}}}{x_\tau\dot{\bar{y}}-y_\tau\dot{\bar{x}}} \triangleq \frac{A(\tau_1,\tau_f)}{B(\tau_1,\tau_f)} \ . \tag{9}$$

It is easy to see that $A = B = 0$ when $\tau_1 = 0$, since then all velocities are equal; e.g., $x_{\tau_f} = x_\tau = \dot{\bar{x}}$. With close attention to detail, it can also be shown that the first partial derivatives of A and B vanish at this time.* Consequently, (9) must be expressed as

$$\frac{d\tau_1}{d\tau_f} = -\frac{A_{\tau_1\tau_1}d\tau_1^2+2A_{\tau_1\tau_f}d\tau_1 d\tau_f+A_{\tau_f\tau_f}d\tau_f^2}{B_{\tau_1\tau_1}d\tau_1^2+2B_{\tau_1\tau_f}d\tau_1 d\tau_f+B_{\tau_f\tau_f}d\tau_f^2} \ . \tag{10}$$

It can then be shown that, at $\tau_1 = 0$, $A_{\tau_1\tau_f} = A_{\tau_f\tau_f} = B_{\tau_f\tau_f} = 0$, so that (10) becomes <u>linear</u>; the solution is

$$\frac{d\tau_1}{d\tau_f} = -\left.\frac{A_{\tau_1\tau_1}+2B_{\tau_1\tau_f}}{B_{\tau_1\tau_1}}\right|_{\tau_1=0} \ , \tag{11}$$

where

*The upper end of the FL is implied by (5) of Sec. 3.4, and this function is a factor of $dB/d\tau_1$.

$$A_{\tau_1\tau_1} = (A_1-A_2)(1-yv) + (B_1-B_2)xv$$

$$B_{\tau_1\tau_1} = (A_o-A_2)(1-yv) + (B_o-B_2)xv$$

$$2B_{\tau_1\tau_f} = (r^2-\gamma^2+x+yv)\left[\frac{x}{r^4}(2y-r^2v) + \frac{1}{r^2v}\left(\frac{y}{v} - \frac{y^2}{r^2v^2} - \frac{x^2}{r^2}\right)\right]$$

$$A_o = \frac{3}{2}\,xv - y$$

$$A_1 = y - \tfrac{1}{2}xv + (\gamma^2x^2-r^4)/r^4v$$

$$A_2 = \tfrac{1}{2}(xv+y)C_1^2 - (yv-x)C_2 + \tfrac{1}{2}y - xv$$

$$B_o = \frac{3}{2}\,yv + x - \tfrac{1}{2}$$

$$B_1 = -x + \tfrac{1}{2}(1-yv) + \gamma^2xy/r^4v$$

$$B_2 = \tfrac{1}{2}(yv-x)C_1^2 + (xv+y)C_2 + \tfrac{1}{2}(1-x) + yv$$

$$C_1 = 1 + x/r^2 - y/r^2v$$

$$C_2 = (y+x/v)/2r^2 - (\gamma^2-2r^2)(xv-y)^2/4r^6v^3$$

$$v = \sqrt{(\gamma^2/r^2)-1}\ ,$$

and x,y and $r = \sqrt{x^2+y^2}$ denote values at the junction of FL and SE.

The SE continues to extend upward until a curvature condition marks its tangency with a PDL, as in Sec. 3.3. The PDL is then found to continue until its tangency with $\mathcal{B}$. This final integration ends at the point where $\mathcal{B}$ is a trajectory connecting the top of the PDL with the bottom of the SE, as shown in Fig. 3.7. Also shown in that figure are the contours of constant V, and as mentioned earlier, a local maximum in time-to-go must exist at a point on $\mathcal{B}$ which is to the right of the PDL junction.

3.5 Parameter Space; Regions I and II

The current version of the parameter-space diagram is shown in Fig. 3.9. The locus C_4 is the line above which the SE and the attendant PDL are not present beneath the barrier. It is determined numerically, by seeking to satisfy (3) of Sec. 3.3 at a fixed γ, and for variable β. The curve C_5 represents parameters for which the dispersal point A occurs on the capture circle, and is easily found as (1) of Sec. 3.2. Finally, the small triangular zone bounded by C_2 and C_6 includes those parameters for which the SE is interrupted by the FL; the locus C_6 is also determined numerically.

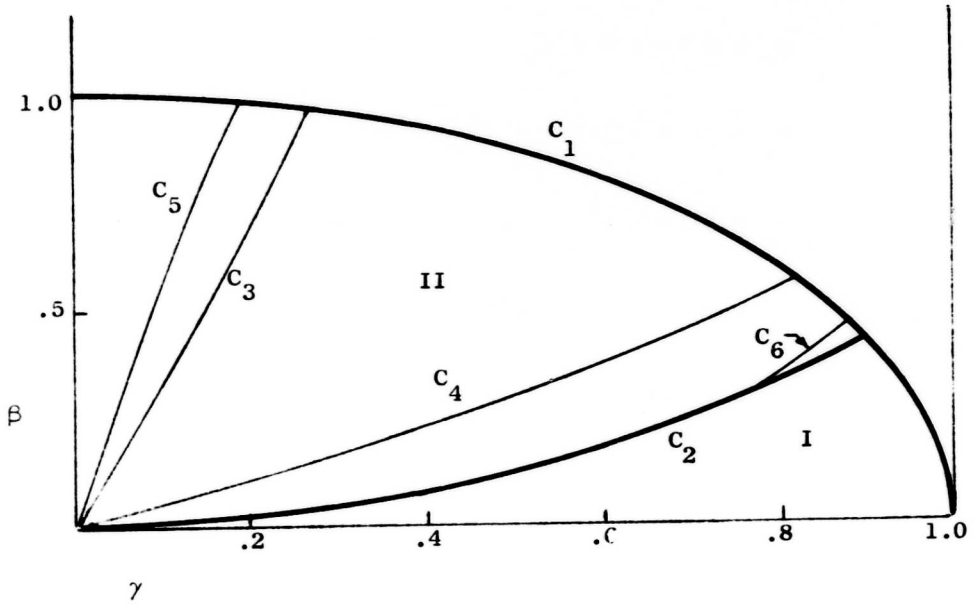

FIGURE 3.9. Regions in Parameter Space, $\beta^2 + \gamma^2 \leq 1$

In completing Region II of the parameter space, diagrams of optimal paths and isochrones have been given in Figs. 3.2 and 3.3, for parameters left of C_3. For parameters below C_4, the gross features of the trajectories in the area under the barrier, including the SE, FL and PDL, have been sketched in Figs. 3.4 through 3.8.

We note again that if the barriers do not intersect on the y-axis, the barrier is not an optimal path unless the SE exists. In this case (β,γ between C_2 and C_4), only that segment of $\mathfrak{B}$ between the SE and the PDL is an optimal path. The remainder of it is a locus (described with $\varphi = +1$) of initial conditions for which P's optimal strategy is a turn-away ($\varphi = -1$) .

Chapter IV

FURTHER EXTENSIONS, $\beta^2 + \gamma^2 > 1$

The classical results of the homicidal chauffeur game have been extended in Chapter III to all parameters satisfying the inequality $\beta^2 + \gamma^2 \leq 1$, and we have further subdivided this area into Regions I and II, according to whether or not the capture region is finite. The approach taken in this chapter is basically one of continuation of the loci in Fig. 3.9. Beginning the extension at the locus C_1, we will work upward in parameter space, introducing new complexities as required. In this way, previously defined loci are followed to their ends. Other loci will also enter the discussion, and it will be found convenient to separate the parameter space $\beta^2 + \gamma^2 > 1$ into three distinct regions.

4.1 A New Barrier

The equations describing the barrier in Region I were derived in Sec. 2.3, starting with the main equation in the terminal payoff form,

$$\min_{\varphi} \max_{\psi} [v_x \dot{x} + v_y \dot{y}] = 0 \ .$$

If this equation is considered to hold at $r = \beta$, but with $\beta^2 + \gamma^2 > 1$, we have seen in (12) of Sec. 2.3 that $\mathfrak{B}$ cannot end at θ_{up} with tangential velocity. Neither can both adjoints be zero. The remaining possibility, if this equation holds, is that an equilibrium point may exist where $\dot{x} = \dot{y} = 0$. For this static interpretation, the relative velocity equations are, with P turning toward E :

$$\begin{aligned} \beta c\theta - \gamma s\psi &= 0 \\ 1 - \beta s\theta - \gamma c\psi &= 0 \ . \end{aligned} \tag{1}$$

These can be solved for the equilibrium position and E's corresponding control,

$$\begin{aligned} s\theta_{eq} &= (1+\beta^2-\gamma^2)/2\beta \\ c\psi_{eq} &= (1-\beta^2+\gamma^2)/2\gamma \ . \end{aligned} \tag{2}$$

The first of these equations implies that $\beta \leq 1 + \gamma$ in order for the equilibrium to exist. But, we will see that a barrier is present for $\beta^2 + \gamma^2 \geq 1$ only when β is <u>much</u> less than $1 + \gamma$, so that the right and left barriers intersect ahead of P. An equilibrium strategy for P (for which the time-to-go is infinite) can be minimizing only if the capture region is bounded, since otherwise P could certainly choose a better strategy.

When the retrogressive equations are solved with the appropriate boundary conditions, the new barrier equations are

$$\begin{aligned} x &= 1 - c\tau + \beta s(\theta_{eq}+\tau) - \gamma\tau s(\psi_{eq}+\tau) \\ y &= s\tau + \beta c(\theta_{eq}+\tau) - \gamma\tau c(\psi_{eq}+\tau) \ . \end{aligned} \tag{3}$$

The parameters for which the right and left barriers intersect tangentially on the y-axis can be obtained as in Chapter II, by eliminating τ between the equations $x(\beta,\gamma,\tau) = 0$, and $\dot{x}(\beta,\gamma,\tau) = 0$. The result is $\beta(\gamma)$, the extension of C_2 lying to the right of C_1, which is given by the following rather unappetizing implicit function of the parameters:

$$1 + \beta c(\psi_{eq}-\theta_{eq}) - s\psi_{eq} - \gamma(\tfrac{\pi}{2} - \psi_{eq}) = 0 \ . \tag{4}$$

In this equation θ_{eq} and ψ_{eq} are first quadrant functions of (β,γ), defined in (2).

The switch function is

$$S = \gamma - c(\psi_{eq}+\tau) \ , \tag{5}$$

and since $\psi_{eq} > \theta_{eq} > \theta_{up} = \cos^{-1}\gamma$, this function is positive for all τ yielding $x \geq 0$ in (3). That is, the barriers never end before meeting on the y-axis when the parameters fall below the locus C_2 given by (4).

The trajectory given by (3) differs in three respects from the barrier trajectory given by (7) of Sec. 2.3:

i) The arrival velocity is zero in both radial and tangential directions, though the equilibrium point is reached from any point on the barrier in finite time;

ii) The new barrier is not tangential to the capture circle at arrival;

iii) The new barrier contacts the capture circle at the angle $\vartheta_{eq} > \vartheta_{up}$.

This new barrier is the outer edge of an angular interval of the capture circle on which safe-contact motion is optimal, with P turning toward E . Details of the relative motion, including the influence of an evader's "dispersal point" A , are given in the next section. The normalized gradient vector, which is parallel to E's optimal direction, is normal to the new barrier, as was the case in Region I. The gradient rotates at unit rate with motion of $\underline{x}$ down the barrier, until arrival at the equilibrium point.

4.2 Evader's Dispersal Point and Dispersal Line

When the parameters are outside the locus C_1 , but below C_2 , the point A (and its image across the y-axis) is inside rather than on the new barrier. This point is located by the same equations found in Chapter I,

$$x_A = 1 - c(\beta/\gamma)$$
$$y_A = s(\beta/\gamma) \ , \tag{1}$$

and trajectories from this evader's dispersal point are expressed as functions of the arrival angle $\theta \le \theta_o \le \theta_{up}$ and the retrogressive time, τ :

$$x = 1 - c\tau + (\beta-\gamma\tau)s(\theta+\tau)$$
$$y = s\tau + (\beta-\gamma\tau)c(\theta+\tau) \ . \tag{2}$$

The largest angle, ϑ_o , is given by solving the simultaneous equations $r(\vartheta_o,\tau_T) = \beta$, $\dot{r}(\vartheta_o,\tau_T) = 0$, as detailed in Appendix B-1, and as shown in Fig. 4.1.

This figure also shows that A is the near end of an evader's dispersal line (EDL) extending to the y-axis, there meeting the image EDL from the other dispersal point. This EDL is a locus of starting points for which E must choose between two equally optimal strategies, labelled "+" and "-" for reference purposes in Fig. 4.1. On the "-" side, E runs along the tangent to P's minimum turn circle, and the game ends as a straight-line chase. The other choice of strategy from

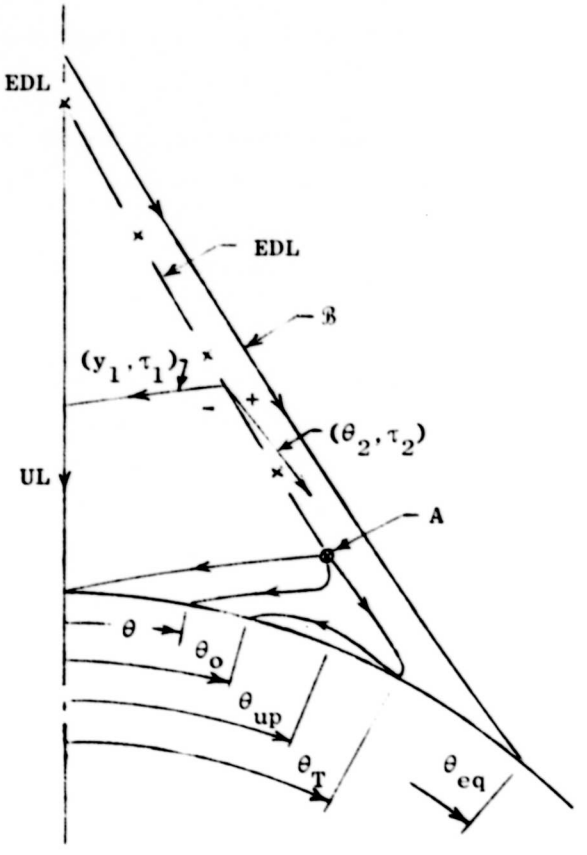

FIGURE 4.1. EDL from Point A in Region III

the EDL has E running straight until tangential arrival at the capture circle near the equilibrium point. Subsequent motion here is of the safe-contact type until θ decreases to θ_T, where E leaves the

circle for a short interval before termination at θ_o . It is easily shown that P's strategy is the same for either choice of E's (i.e., $S = V_x y - V_y x > 0$ if $x > 0$, for either $\bar{W}^-$ or $\bar{W}^+$). The "-" trajectories encounter the y-axis as in Chapter II, with P's switch function going smoothly to zero along this line. On the barrier side of the EDL , though, the switch function is positive as $\underline{x}$ approaches the brief y-axis segment of the EDL shown in Fig. 4.1. While it can be shown only numerically, there exists a discontinuity in both $\bar{W}$ and S across this line segment, such that P's strategy depends on E's choice.

Referring to Fig. B-1, the discontinuity in the gradient across the EDL gives an equation for the local slope as

$$\frac{dy}{dx} = - \frac{V_x^- - V_x^+}{V_y^- - V_y^+} . \tag{3}$$

Next, in equating $\underline{x}^+ = \underline{x}^-$, differential changes lead to relations between $d\theta_2, d\tau_2, dy_1, d\tau_1$. The appropriate independent variable is y_1 , since the other variables are either too nearly static or are not clearly monotonic. Thus, equating differential positions on either side, we derive simultaneous differential equations,

$$\begin{aligned} x_\theta^+ \frac{d\theta_2}{dy_1} + x_\tau^+ \frac{d\tau_2}{dy_1} &= x_{y_1}^- + x_\tau^- \frac{d\tau_1}{dy_1} \\ y_\theta^+ \frac{d\theta_2}{dy_1} + y_\tau^+ \frac{d\tau_2}{dy_1} &= y_{y_1}^- + y_\tau^- \frac{d\tau_1}{dy_1} . \end{aligned} \tag{4}$$

The required trajectories are given in terms of (y_1, τ_1) or (θ_2, τ_2) in Appendix B, as are the adjoints required in (3). The numerical integration of the coupled equations proceeds routinely in Region III of parameter space, as there are no unusual numerical problems. It is true that $d\theta_2/dy_1$ is nearly zero as θ_2 approaches θ_{eq} , but the determinant of the coefficient matrix of (4) is

$$x_\theta^+ y_\tau^+ - y_\theta^+ x_\tau^+ = \tau_2 [(\gamma \sqrt{1-c^2\theta_2/\gamma^2} + s\theta_2)^2 - \beta s\theta_2] > 0 ,$$

which means that there are no indeterminacies in the integration of (3) and (4).

The gradient vector ∇V in Region III varies smoothly with position except across the EDL, and all of the contours of constant V intersect the capture circle outside the usable part. Note in particular that as the new barrier is approached, the time-to-go approaches infinity continuously, while in Region I, the time-to-go is discontinuous at $\mathcal{B}$.

The safe-contact trajectories which follow the tangential arrival at θ_2 (see Fig. B-1) are described in polar coordinates as

$$\begin{aligned} \dot{r} &= -c\theta + \gamma c(\psi-\theta) = 0 \\ \dot{\theta} &= -1 + (s\theta+\gamma\sqrt{1-c^2\theta/\gamma^2})/\beta \ , \end{aligned} \tag{5}$$

where $r = \beta$ has been used in the angular equation and where $\theta_T \leq \theta < \theta_{eq}$. The radial equation gives E's control for this motion as (cf. (9) of Sec. 3.1):

$$\psi = \theta + \cos^{-1}(c\theta/\gamma) \ , \tag{6}$$

and, as expected, E's tangential angular velocity decreases from zero as θ decreases from θ_{eq}. All tangential paths depart the capture circle at $\theta = \theta_T$, which has been calculated as the initial value of θ_2 in the EDL integration. This last portion of the "+" paths (see Fig. 4.1) has E running in a straight path in real space, after tangential departure and before termination at $\theta = \theta_o$.

4.3 Conjugate Point Replaces Dispersal Point

As the speed ratio is increased for parameters above C_1, two extreme trajectories from A coalesce to a single curve, which is point-tangential at $\theta_T > \theta_{up}$ and which ends at the arrival angle $\theta = 0$. For larger γ, such that the y-axis is included in the point-tangential trajectory, the retrogressive equations from the y-intercept are

$$\begin{aligned} x &= 1 - c\tau_1 + (y_1-\gamma\tau_1)s\tau_1 \\ y &= s\tau_1 + (y_1-\gamma\tau_1)c\tau_1 \ . \end{aligned} \tag{1}$$

A conjugate point, C , is located on the lowest such trajectory by the condition $y_1 - \gamma\tau_1 = 0$. Here it is easily seen that the conjugate point condition is met; i.e., when $\tau_1 = y_1/\gamma$, the Jacobian determinant is, using (1):

$$\frac{\partial(x,y)}{\partial(y_1,\tau_1)} = \begin{vmatrix} s\tau_1 & (1-\gamma)s\tau_1 \\ c\tau_1 & (1-\gamma)c\tau_1 \end{vmatrix} = 0 \ . \qquad (2)$$

An EDL emanating from C marks the right end of trajectories to the y-axis, and the time along these trajectories is $\tau_1 < y_1/\gamma$ for those above the point-tangential trajectory. A trajectory-slope discontinuity occurs across the EDL , this discontinuity decreasing to zero at the point C . The tangency of the point-tangential trajectory and the EDL at C implies that an indeterminacy exists in the expressions for the derivatives at this point. This indeterminacy is evaluated in Appendix B.

The parameter-space locus for which the dispersal point A becomes the conjugate point C is found by requiring $r(\beta,\gamma,\tau_1) = \beta$, $\dot{r}(\beta,\gamma,\tau_1) = 0$, where $\tau_1 \searrow \tau_c = \beta/\gamma$, using (1) with $y_1 = \beta$. Considering these as two equations in β and τ_1 , we determine τ_T as the smallest root to

$$(1-c\tau_1-\tfrac{1}{2}\gamma^2\tau_1^2)(\gamma-c\tau_1) + (1-\gamma)s\tau_1(s\tau_1-\gamma\tau_1) = 0 \ . \qquad (3)$$

When this is solved numerically for $\tau_T(\gamma)$, the corresponding parameter is

$$\beta(\gamma) = \gamma\tau_T + (1-\gamma)s\tau_T/(\gamma-c\tau_T) \ , \qquad (4)$$

and a parameter locus is generated for all τ_T in the interval 0 to π . This curve will be denoted as C_7 in the parameter space drawing to be shown as Fig. 4.10 in Sec. 4.6.

The last point on C_7 has the coordinates $\beta = 2$, $\gamma = 2/\pi \cong .635$, and here C is at the right edge of the capture circle, with the trajectory departing tangentially upward. This means that $1 - c(y_1/\gamma) = \beta^2/2$, and $s(y_1/\gamma) = 0$. Together these conditions imply that $y_1 = \pi\gamma$

and that the conjugate point region is bounded from above by the line, $\beta = 2$, this locus to be denoted as C_9 in Fig. 4.10.

For parameters in Region III, the effect of crossing the locus C_7 is shown in Fig. 4.2. The EDL calculation is discussed in more detail in Appendix B, but here it is noted that the initial values of y_1 and $\tau_2 = y_1/\gamma - \tau_T$ derive from expanding $r(y_1, \tau_T) = \beta$, $\dot{r}(y_1, \tau_T) = 0$. Eliminating y_1 leads to a cubic in $c\tau_T$,

$$2\gamma c^3\tau_T + (1+4\gamma+\gamma^2-\beta^2)c^2\tau_T - 2[1+\gamma^2+\gamma(1-\beta^2)]c\tau_T + \gamma^2(1-\beta^2) + 1 = 0 , \quad (5)$$

and the corresponding ordinate is

$$y_1 = \gamma\tau_T + (1-\gamma)s\tau_T/(\gamma-c\tau_T) . \quad (6)$$

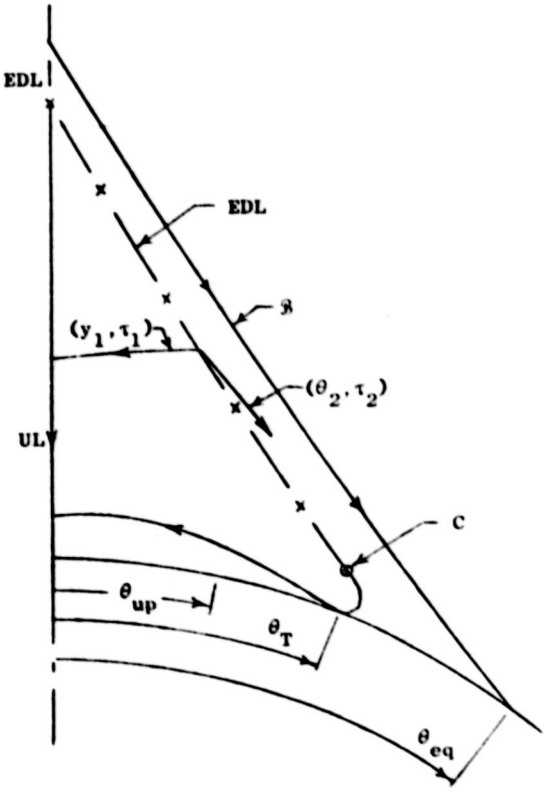

FIGURE 4.2. EDL from Point C in Region III

Comparing Fig. 4.1 with Fig. 4.2 illustrates the difference between trajectories for parameters in Region III, on either side of the locus given by (4).

4.4 Pursuer's Dispersal Line Replaces Open Barrier

We recall that in Region II, P's strategy when $r = \beta$ was $\varphi = +1$ with $\theta < \theta_{up}$ and $\varphi = -1$ otherwise. The barrier intersection with the capture circle thus marked a discontinuity in P's strategy. For $\beta^2 + \gamma^2 > 1$, however, we have seen in Sec. 4.1 that safe-contact motion is possible for $\varphi = +1$, $\theta > \theta_{up}$. When parameters pass from Region III to IV, the equilibrium point exists as long as $\beta < 1 + \gamma$, but the barrier from this point will be open, since the parameters will then fall above the locus given by (4) of Sec. 4.1. This barrier starts on the capture circle at θ_{eq}, and when $\varphi = +1$, the relative inward motion will be very slow when E is located on the capture circle just ahead of θ_{eq}. Indeed, the time-to-go will approach infinity, so that P should obviously turn away ($\varphi = -1$) when E is close to this equilibrium point. Accordingly, there must be a dispersal line for P starting on the capture circle slightly in front of the open barrier, which then loses its significance.

Hence, when the barrier from θ_{eq} is open, capture in a finite time is possible from all initial conditions, and we may think of this barrier as being "replaced" by the PDL. We note that the gradient and P's switch function are discontinuous across this line, and when the equilibrium point exists (i.e., $\sqrt{1-\gamma^2} < \beta < 1 + \gamma$), the PDL begins at an angle θ_p very slightly less than θ_{eq} as given by (2) of Sec. 4.1. When $\beta > 1 + \gamma$, so that θ_{eq} no longer exists, the PDL may begin on the capture circle at an angle $\theta_p > \pi/2$, or on the negative y-axis, or even on the equivocal line, as will be shown. The variety of possible configurations of PDL makes its numerical computation difficult, as is further implied by the following possibilities:

i) The trajectory for $\varphi = +1$ can depart tangentially from the PDL, indicating that the SE is present for these para-

meters. That is, the extension above Region II of C_4 (see Fig. 3.9) is required.

ii) The SE, in turn, may be interrupted by the FL; i.e., we must locate the extension of C_6 of Fig. 3.9.

iii) The dispersal point A is replaced by the conjugate point C for parameters to the right of C_7, as discussed in Sec. 4.3.

iv) The point A may separate the SL from the EL, or may fall inside the capture circle, the EDL no longer existing. That is, C_3 and C_5 of Fig. 3.9 must be extended upward out of Region II.

These considerations have an obvious significance in the computation of the PDL, but for the present we restrict attention to the equations which describe it, and to the determination of those parameters for which it exists.

For parameters slightly above C_1 such that the PDL exists, the configuration of exceptional lines will resemble that shown in Fig. 4.3(a). This configuration is representative of parameters in the neighborhood of $\beta \cong 1.4$, $\gamma \cong .6$, such that the PDL is not interrupted by the SE as mentioned above. The turn-away region resembles that which exists for parameters in Region II, and when parameters are close to the locus C_1, the EDL and PDL are nearly coincident, so that they can be thought of as "replacing" the barrier which exists in Region II.

In (b) of the figure is shown a configuration for parameters near the values $\beta \cong 1.82$, $\gamma \cong .8$, so that θ_{eq} does not exist, and such that the point A has been supplanted by the conjugate point C. For these parameters, the two dispersal lines are more widely separated, and the turn-away region is proportionately smaller.

The equations which specify the PDL are similar to those described in Sec. 3.3. That is, the position is the same for two different retrograde paths, and the main equation holds for either of P's strategies. Using the notation of Fig. 4.3(a), for example, the PDL would be found

by simultaneous solution of the three equations,

$$x_\theta^+ \frac{d\theta_1}{d\theta_2} + x_\tau^+ \frac{d\tau_1}{d\theta_2} = x_\theta^- + x_\tau^- \frac{d\tau_2}{d\theta_2}$$

$$y_\theta^+ \frac{d\theta_1}{d\theta_2} + y_\tau^+ \frac{d\tau_1}{d\theta_2} = y_\theta^- + y_\tau^- \frac{d\tau_2}{d\theta_2} \qquad (1)$$

$$\frac{dy}{dx} = - \frac{V_x^- - V_x^+}{V_y^- - V_y^+} .$$

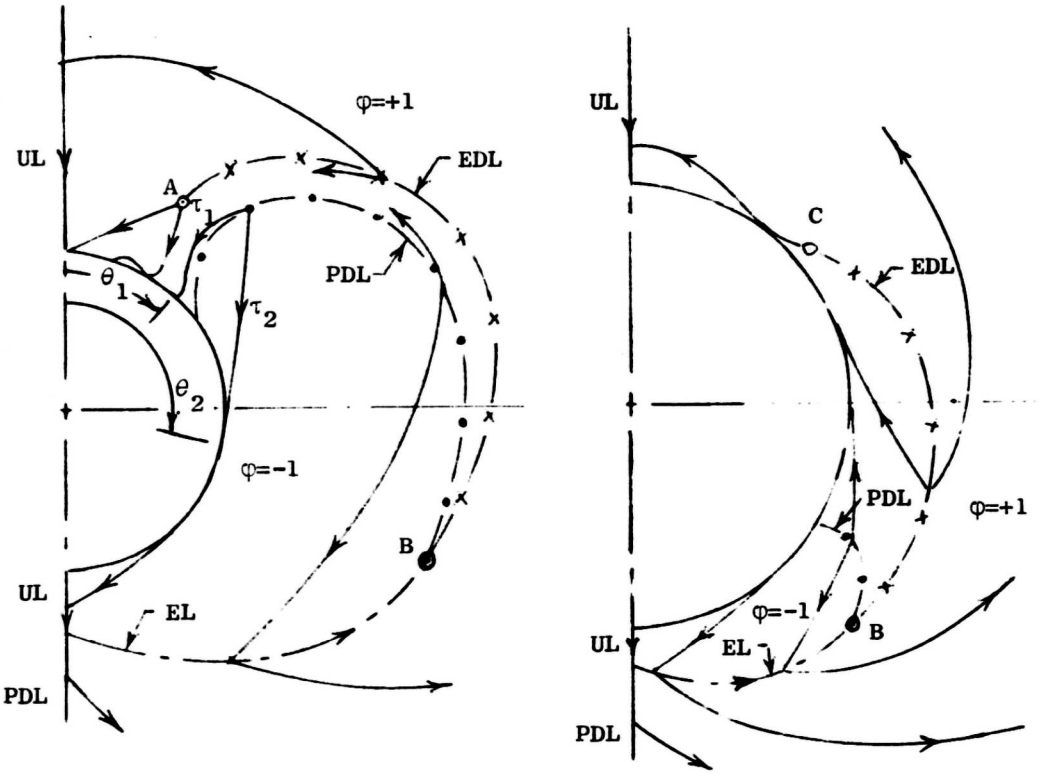

(a) $\beta < 1+\gamma$ (b) $\beta > 1+\gamma$

FIGURE 4.3. EDL and PDL in Region IV

At any point $\underline{x}^{+}(\theta_1, \tau_1) = \underline{x}^{-}(\theta_2, \tau_2)$, these equations can be solved for the indicated derivatives, θ_2 having been taken as the independent variable. The superscripts in (1) are chosen to agree with the sign of the switch function. Hence, providing the configuration actually is as shown in the figure, it remains only to find a set of "initial" conditions in order for the PDL to be numerically calculable.

The first few attempts to integrate the PDL were carried out for parameters only slightly above C_1 , so that the relevant initial conditions were those at the near end of the PDL , slightly inward of θ_{eq} . Initial conditions could be found only after numerical integration of the EDL , the EL and the safe-contact equations of retrograde motion back to θ_{eq} . The initial conditions required for the PDL integration would then be $\tau_1 = \tau_2 = 0$ and $\theta_1 = \theta_2 = \theta_p$, and hence only θ_p needed to be determined numerically, as described in Appendix B. This procedure was followed by a subsequent PDL integration, which continued until the switch function equalled zero on the "+" side of it. It was found that the end point of the PDL was "close" to the end point of the EDL , as pictured in Ref. 2. Subsequent numerical studies showed, however, that these endpoints are actually coincident, and that the two dispersal lines join the EL at a common point, labelled B as in the barrier case of Region II. This means that for configurations similar to that shown in Fig. 4.3(b), the PDL can be profitably integrated <u>inward</u> from the far end, simultaneously with the EL . This has important numerical advantages, particularly when $\beta > 1 + \gamma$, such that the approximate location of the near end of the PDL is unknown.

In determining the parameters for which the PDL exists, we consider the changes in its appearance due to changes in β , for a fixed value of γ , this fixed value lying between 0 and 1 . The largest value β for which it can exist will be found, and this locus $\beta(\gamma)$ will be denoted C_8 , for reference purposes.

When γ is sufficiently small, the point A is not a dispersal point, because the retrogressive switch time is

$$\tau_s \triangleq 2(\pi - \theta_o) < \beta/\gamma \triangleq \tau_A .$$

Also, when the point-contact trajectory is tangent to the capture-circle at the angle $\theta_T = \pi/2$, the retrogressive equations are

$$\begin{aligned} x &= 1 - c\tau + (\beta-\gamma\tau)s(\theta_o+\tau) = \beta \\ y &= s\tau + (\beta-\gamma\tau)c(\theta_o+\tau) = 0 \ . \end{aligned} \tag{2}$$

But, at this point we know E's optimal direction must be tangential, $\psi = \theta_o + \tau = \pi$, so (2) yields

$$x = \beta = 1 - c\tau_T \ , \tag{3}$$

where τ_T is the least positive root to the equation,

$$s\tau_T + c\tau_T + \gamma\tau_T - 1 = 0 \ . \tag{4}$$

While this analysis appears unmotivated, it may be observed that, when the independent variable is changed to $\tau' = \tau - \tau_T$, the trajectory (2) is obviously <u>symmetric</u> with respect to the x-axis. That is, with time τ' measured from tangency at $\theta_o = \pi/2$, and $\psi_o = \pi$, the trajectory is given by

$$\begin{aligned} x &= 1 + (\beta-1)c\tau' + \gamma\tau' s\tau' \\ y &= -(\beta-1)s\tau' + \gamma\tau' c\tau' \ . \end{aligned} \tag{5}$$

This means that the switch function is also symmetric and is therefore equal to zero at <u>both</u> ends of the tangential trajectory indicated in Fig. 4.4(a). This finally means that parameters are such that the PDL is of zero length, having just vanished into the capture circle. Hence, our sought function in parameter space is obtained by eliminating τ_T from (3) and (4). In a relatively useful form, the result is

$$\gamma = \frac{\beta - \sqrt{2\beta-\beta^2}}{\cos^{-1}(1-\beta)} \tag{6}$$

This function denotes the left end of the locus C_8 (to be shown in Fig. 4.10), and it is appropriate until γ is so large that A appears on the capture circle. The criterion for this circumstance is

$$\tau_A = 2\tau_T = \beta/\gamma$$

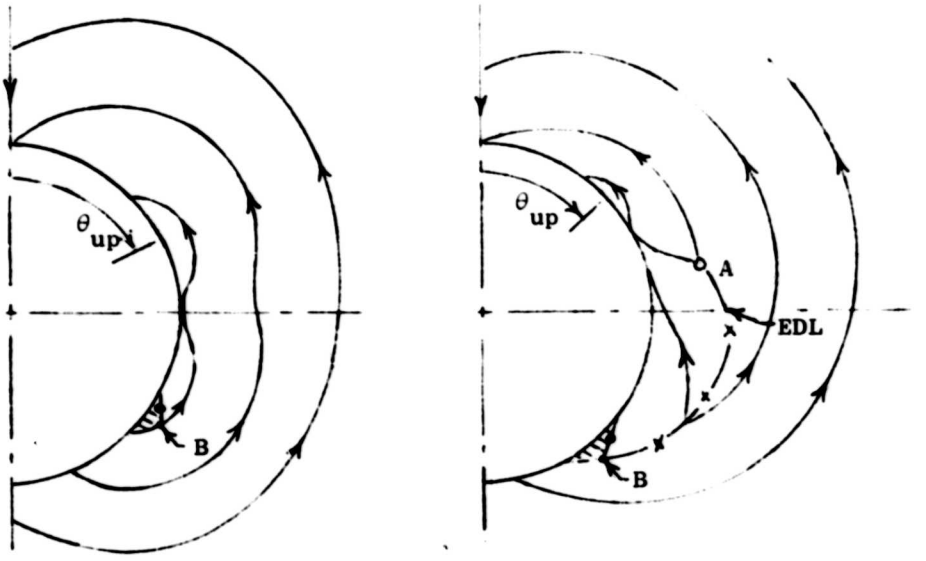

(a) $\gamma < .362$

(b) $.362 < \gamma < .78$

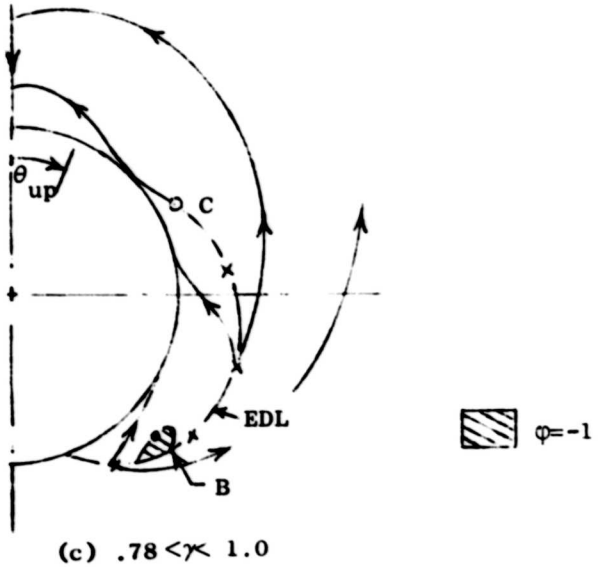

(c) $.78 < \gamma < 1.0$

FIGURE 4.4. Trajectories for Parameters Just Under C_8

which, with (3) and (4), implies that $\tau_T = \cos^{-1}(-3/5) \cong 2.21$. It follows that the last point on the locus (6) is

$$\gamma = 4/5\tau_T \cong .362$$
$$\beta = 8/5 = 1.6 \quad . \tag{7}$$

When (6) yields a value of $\gamma > .362$, the point A is outside the capture circle, and is the start of an EDL. The condition (6) must be replaced by another, when $\gamma > .362$, such that $S = 0$ on the inner side of the EDL when $r = \beta$. That is, if $S = 0$ while $r > \beta$, a PDL exists between this point and the capture circle.

The conditions described above are not subject to analytic treatment, since the EDL equations must be integrated numerically. This implies that β is to be adjusted, at a fixed γ, until the point B at the junction of EDL and PDL occurs at $r = \beta$. The qualitative appearance of the relevant curves for β just below C_8 is shown in Fig. 4.4(b). This procedure is sufficient as γ increases until the dispersal point A is supplanted by the conjugate point, at $\gamma \cong .78$, when C_8 is crossed by C_7. For larger γ, the calculations relate to the point C, and the conditions for the vanishing of the PDL are slightly changed. For γ greater than about .7, the left end of the PDL shrinks toward its right end at the point B, as shown in Fig. 4.4(c). As the speed ratio approaches unity, it is found that the configuration near B is very sensitive to parameter changes, and consequently the precise location of C_8 is difficult to assess in this region. The locus appears to pass through the point $\beta = 2$, $\gamma = 1$ in parameter space, but this observation has only a numerical basis.

We have discussed safe-contact motion in Region II for $\varphi = -1$, when P turns away from E. Likewise, tangential relative motion appears for $\varphi = +1$, when E is inboard of the equilibrium point, for parameters in Region III. For parameters below $\beta = 1 + \gamma$ in Region IV, moreover, safe-contact motion can occur for <u>both</u> of P's turn directions. As β approaches C_8, however, particularly for large γ, the turn-away region does not necessary border the capture circle, so that tangential motion can occur only for $\varphi = +1$. In this case,

tangential motion appears whenever a point-tangential trajectory joins the point A , or the point C , to the capture circle. These trajectories can be expressed in terms of the arrival angle θ_o , and the retrogressive time-to-tangency τ_T , by expanding $r = \beta$, $\dot{r} = 0$, as two equations in (β, γ) .

If the parameters are in the region above C_8 , P never turns away from E , and tangential motion can occur only for $\varphi = +1$. The maximum angle on the capture circle for which tangential motion is possible is found by equating the radial acceleration to zero in unconstrained motion, with $r = \beta$ and $\dot{r} = 0$. Rearranging the result yields an equation satisfied by this $\theta_m > 90°$,

$$r\ddot{r} = \beta s\theta_m - (s\theta_m + \gamma\sqrt{1-c^2\theta_m/\gamma^2})^2 = 0 \ . \qquad (8)$$

For parameters below C_8 , the PDL exists, and the maximum angle at which tangential motion occurs for $\varphi = -1$ depends on the subsequent trajectory. We have determined one such relation in (5) of Sec. 3.1 for the case when the departing trajectory encounters the negative y-axis. In Region IV, the "last" tangential path for $\varphi = -1$ may encounter the EL or it may not exist at all. That is, all paths departing the circle with $\varphi = -1$ may do so non-tangentially, as shown in (a) of Fig. 4.5.

When the speed ratio is high and $\beta > 1 + \gamma$, the shape of the PDL is extremely sensitive to parameter changes. Typical trajectory variations for $\gamma = .9$ are shown in Fig. 4.5 for three slightly different values of β .

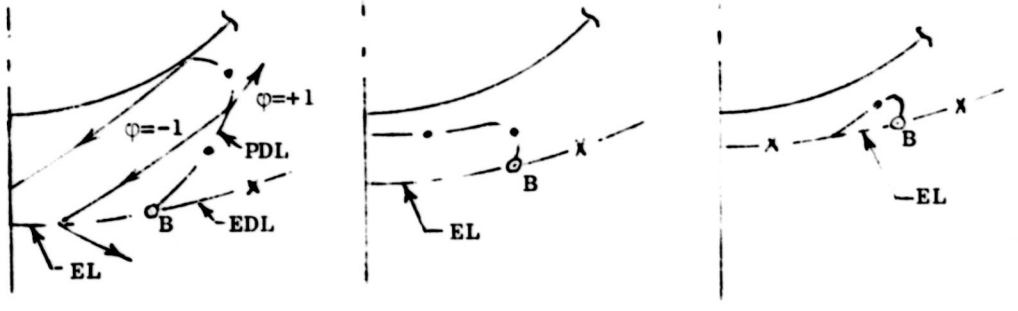

(a) β=1.914 (b) β=1.916 (c) β=1.918

FIGURE 4.5. PDL Variations with β for $\gamma = .9$

4.5 Other Loci and Trajectories in Regions IV and V

The condition for the disappearance of the EDL (the extension above Region II of locus C_3) is that the switch function vanish at the point A on the point-tangential trajectory. Using the solution for this trajectory, the condition requires satisfaction of the equality

$$\tau_A = \beta/\gamma = \tau_s = 2(\pi-\theta_o) \ , \qquad (1)$$

where θ_o and τ_T are coupled through $r = \beta$, $\dot{r} = 0$, as given in (1) of Appendix B-1.

The result of eliminating θ_o and τ_T to give $\beta(\gamma)$ is the segment of C_3 lying between C_1 and C_8, as will be shown in Fig. 4.10. In Fig. 4.6 is shown the nature of the switch lines and trajectories for

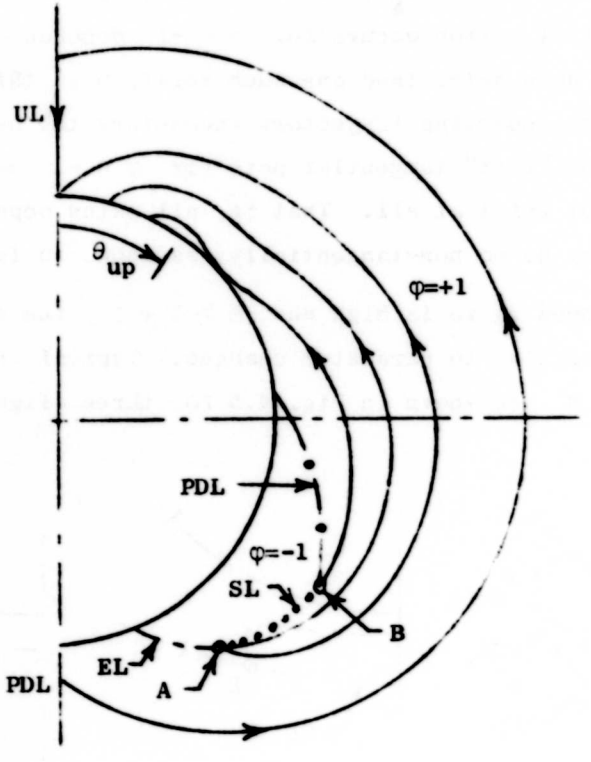

FIGURE 4.6. Trajectories for Parameters Between C_3 and C_5 in Region IV

parameters slightly to the left of this portion of C_3 . Extending C_5 above C_1 is accomplished simply by requiring the dispersal point A to fall on the capture circle, using (1) of Sec. 3.2 for $\beta \leq 2$. For (β, γ) left of C_5 , but below C_8 , the EL is absent and the configuration is as shown in Fig. 4.7.

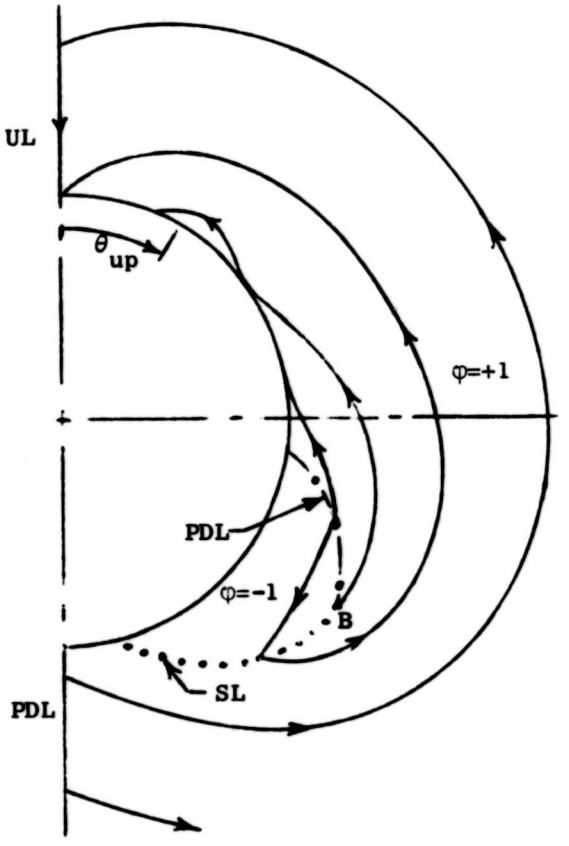

FIGURE 4.7. Trajectories for Parameters Left of C_5 in Region IV

For parameters in Region V above C_8 , the disappearance of the EDL again results when A is on the capture circle. This is the same function as mentioned above, and it extends from $\beta = \gamma = 0$ to the point $\beta = 2$, $\gamma = 2/\pi \cong .635$. It will be seen in Fig. 4.10 that C_3 and C_5 intersect C_8 at the same point (where $\theta_T = \pi/2$).

The locus C_4 denotes the upper border of an area in which the SE exists, and it is found by fixing γ and determining the largest β for which the required cotangency condition holds. A test of a given pair of parameters thus requires the retrogressive integration of the EDL, EL and safe-contact equations, until θ_p is found at the base of the PDL on the capture circle. (See Appendix B.) Integration of the PDL then determines if the SE is present by the condition $d\theta_1/d\tau_1 = 0$. If this equation is not satisfied at any point on the PDL, the corresponding parameters are <u>above</u> the locus C_4.

Similarly, the locus C_6 bounds an area of Region IV for which the SE is interrupted by a FL, and this locus is found as in Sec. 3.4, by integrating the SE until the FL condition is satisfied or not. This again is a straightforward but tedious numerical trial and error procedure.

In Fig. 4.8 is shown a qualitative sketch of the switch line and trajectories resulting for a pair of parameters just above locus C_2 in Region IV. Here it is seen that the EDL meets the y-axis while the PDL, SE and FL do not. This combination of parameters generates the most complex structure believed to exist in the game. As many as 15 stages are possible for certain initial conditions, and for these parameters a chase can include every qualitative feature of the homicidal chauffeur game except the barrier and the switch line.

A brief discussion of the 15-stage chase may be instructive. From an initial position on the PDL, as shown in Fig. 4.8, P chooses $\varphi = +1$ until just after the forward portion of the SE is encountered. The turn-away ($\varphi = -1$) leads E down to the FL, on which any number of switches by P can be performed. This leads <u>x</u> again onto the SE, for which $\varphi = +1$, until the PDL is met again, where P now chooses to turn away. Safe-contact with $\varphi = -1$ is followed by a reverse chase, which is continued along the EL until the point B is reached. Here E chooses the UL strategy of the y-axis and therefore $\varphi = +1$ until this singular arc is reached, when $\varphi = 0$. This leads <u>x</u> down to the

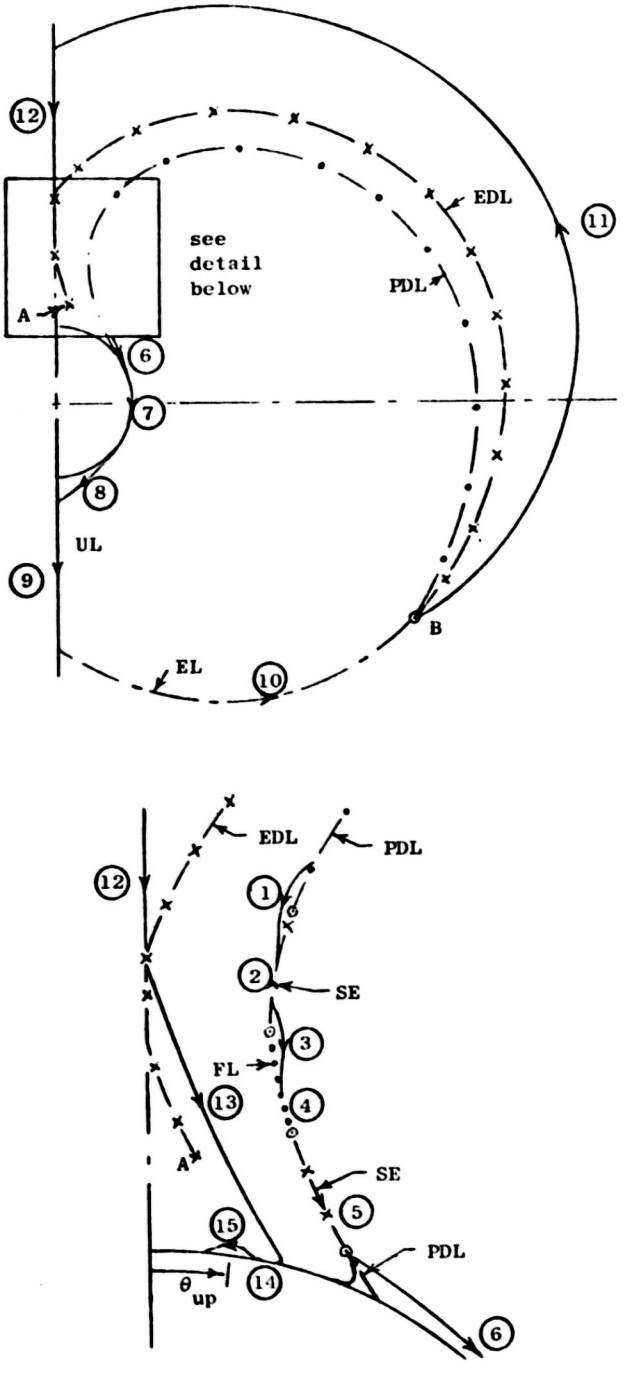

FIGURE 4.8. A Fifteen-Stage Game in Region IV

EDL again, where E chooses to run toward the right equilibrium point, thus forcing P to take $\varphi = +1$. The final stages include a second brief safe-contact episode.

Continuing our discussion of the parameter space loci in Regions IV and V, the locus C_7 continues to $\beta = 2$, and denotes the border of a zone in which a conjugate point exists. The array of dispersal and equivocal lines when the point C exists, for (β,γ) below C_8 and to the right of C_7, has been shown in Fig. 4.3(b).

The left-hand portion of C_8 ($\gamma < .362$), above which the PDL does not exist, is given by (6) of Sec. 4.4. This can also be considered as the locus of tangential contact at $\theta_T = 90°$, and it can be extended upward to $\beta = 2$, as in Fig. B-2, where it provides a convenient reference line for visualizing the point-tangent trajectories.

We can also find a parameter locus above which optimal tangential motion does not occur for $\varphi = +1$. When $\gamma < .503$, this locus is given by simultaneous solution of three equations in θ_o, τ_T and β (γ being a fixed parameter). The equations are $r = \beta$, $\dot{r} = 0$, and (8) of Sec. 4.4, which is equivalent to $\dot{V} = 0$ in two-dimensional motion. This locus will be labelled C_{10} in the parameter space drawing of Fig. 4.10. For $\gamma > .503$, this curve is extended by C_5, for which A is on the capture circle, with $\tau_T = \tau_A$. Typical trajectory configurations in Region V are shown in Fig. 4.9. Here it is seen that P never turns away from E, but that safe-contact and the EDL are still possibilities. For sufficiently large β, as in (d) of this figure, only the y-axis remains as an exceptional line.

4.6 Parameter Space, Regions III, IV and V

In completing our study of the parameter space for the game, it has been convenient to define three new regions. These are bounded by the heavy lines in Fig. 4.10. Region III features a closed barrier and an EDL, IV is characterized by both PDL and EDL, and for parameters in V the situation becomes relatively simple again, the evader's dispersal line and safe-contact trajectories disappearing one by one as this region is traversed.

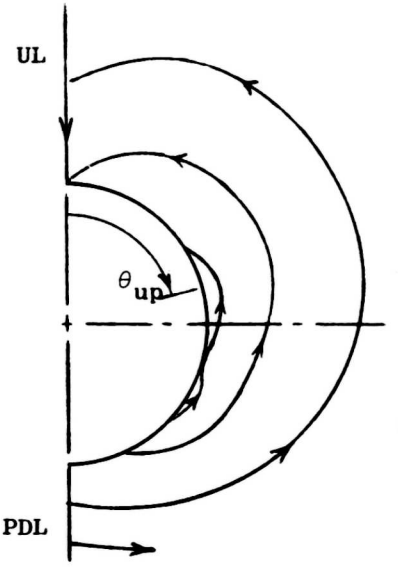

(a) Parameters Between C_8 and C_{10}

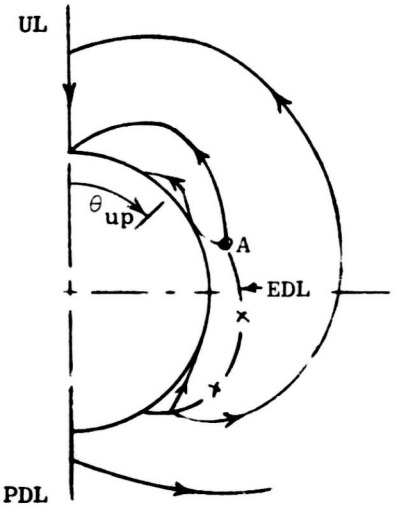

(b) Parameters Between C_8 and C_7

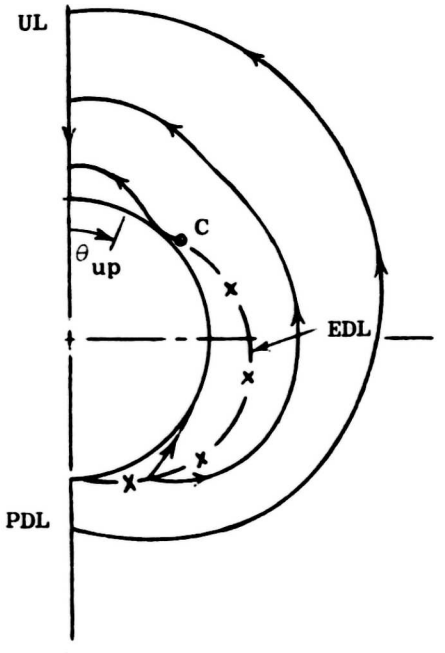

(c) Parameters Between C_8 and C_9

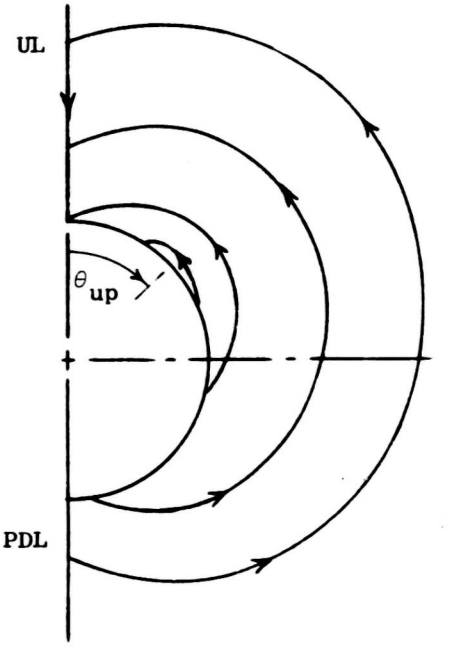

(d) Parameters Above C_9 and C_{10}

FIGURE 4.9. Trajectories for Parameters in Region V

Parameter curve C_2 is continued to $\gamma = 1$, defining the closed barrier parameters of Region III. Here the new barrier contacts the capture circle at an equilibrium point, and in the capture region there exists an EDL which starts at a dispersal point, or at a conjugate point, this distinction being specified by a parameter locus C_7.

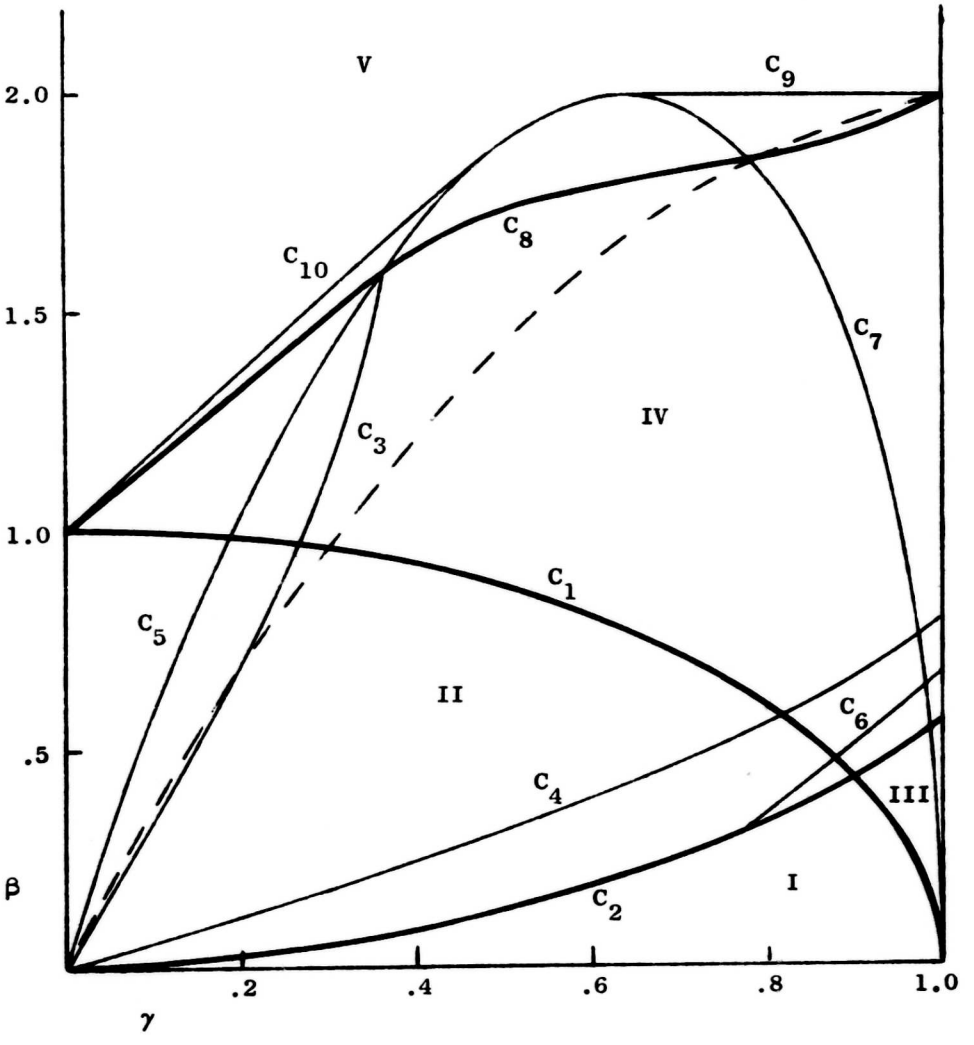

FIGURE 4.10. Regions in Parameter Space

In Region IV very complex games are possible, as the barrier is replaced by the EDL-PDL combination. The upper boundary to this region, C_8, specifies the disappearance of P's turn-away strategy, and the other curves in this region are extensions of loci first defined for Regions II and III. In particular, the possibility exists for both the SE and FL in Region IV, and safe-contact is optimal for both extreme strategies of P.

The loci of Region V are continuations of those in IV, except for C_9, above which the conjugate point disappears, and C_{10}, above which safe-contact for $\varphi = +1$ disappears. The high maneuverability of P, when β is above C_9 or C_{10}, means that an optimal game is simply played by both players, P's strategy being at most a sharp turn followed by a straight chase, and E's path being straight throughout.

The parameter chart of Fig. 4.10 also includes an unlabelled dashed line which passes diagonally through the space. This locus corresponds to a configuration in which the EL (or EDL) passes behind P and to the point $x = 0$, $y = -\beta$. While not an important locus in the sense of denoting the presence or absence of switch lines, dispersal lines, etc., it does assist in the sketching of qualitative features of a specific game.

Chapter V

CONCLUSIONS

It has been shown that the type of solution to the homicidal chauffeur game is determined by the values of two independent parameters. The speed ratio and P's maneuverability ratio are the two parameters of the game, and the form of the solution is believed to be known for all combinations of these parameters. An optimally played game can consist of from one to fifteen stages, depending upon the parameters and the initial relative position.

The exceptional lines which arise in the game border the regular regions in the relative space, and the exceptional lines themselves may or may not be trajectories. In Table I are given the distinguishing characteristics of the exceptional lines which can occur in the solution to the game.

The barrier is an optimal path when it is closed, such that the capture region is finite. When the barriers are open, a range of parameters exists for which a segment of the barrier is an optimal path, along which P lunges toward E . The remaining portion is a locus of initial conditions for which P's strategy is a turn-away. The universal line, or singular arc, corresponds to straight-line motion of both players, and is found to occur for all values of the parameters.

Dispersal lines for P are found to exist both as a straight line directly behind P and as curved lines to the right and left of P . For initial conditions on these lines, P must choose between a hard left and a hard right turn, and E's strategy depends on this choice. Similarly, a dispersal line for E is found as a locus of initial conditions for which E chooses from two equivalent strategies. For most parameters, P's strategy does not depend on E's choice. However, when a segment of E's dispersal line falls directly ahead of the pursuer, P's strategy does depend on E's choice.

Safe contact motion, for which E follows a curved path in real space, is found to occur for both extreme turn directions of P .

TABLE I

EXCEPTIONAL LINES AND THEIR CHARACTERISTICS

Line	Definition and Characteristics
$\mathfrak{B}$	Barrier, across which ∇W is discontinuous. It may be open (Region II), in which case it is an optimal path only if S has the same sign on either side of it. It may also be closed (Regions I and III) and it denotes a discontinuity in V in Regions I and II.
UL	Universal line, a portion of the y-axis which is a path corresponding to straight line motion of both players, across which ∇W is continuous, and along which $S = \dot{S} = 0$.
PDL_y	A portion of the negative y-axis which is a pursuer's dispersal line, on which P must choose between hard left and hard right turns. Both ∇W and S are discontinuous across this line.
PDL	Pursuer's dispersal line for $x \neq 0$, which is found by numerical integration. Both ∇W and S are discontinuous, and S changes sign, across this line.
EDL_a	Evader's dispersal line emanating from a dispersal point A and across which ∇W and S are discontinuous, but S retains its sign across it.
EDL_c	Evader's dispersal line emanating from a conjugate point C .
$1D^+$	Safe contact motion ($r = \beta$, $\dot{r} = 0$) for which P turns toward E , who follows a curved path in real space while maintaining safe contact.
$1D^-$	Safe contact motion for which P turns away from E .
EL	Equivocal line, along which $S = 0$ and E has a choice of two strategies, one of which keeps $\underline{x}$ on the EL . ∇W and S are discontinuous across this line.
SL	Switch line, along which $S = 0$ and across which P's strategy switches. E's strategy across the SL is continuous, since ∇W and S are smooth across it.
SE	Switch envelope, across which ∇W and S are discontinuous, and which is a trajectory or not, according to P's choice.
FL	Focal line, across which ∇W and S are discontinuous, and which is a trajectory requiring <u>either</u> $\varphi = +1$ or $\varphi = -1$, according to P's choice.

Other exceptional lines which can also be optimal trajectories include the equivocal line, the switch envelope, and the focal line. While these lines are more difficult to explain or justify on physical grounds, their appearance in the solution adds interest to the problem. In fact, a general conclusion of the study is that a more complete understanding of the theory often follows from attempting a solution to a particular application. Thus, for example, it is unlikely that the switch envelope phenomenon could have been predicted from a purely analytical attack on the problem.

As to the parameters for which each type of exceptional line occurs, Fig. 5.1 labels twenty significant subregions of the parameter space, and Table II summarizes by listing the exceptional lines which exist in each subregion, using the notation given in Table I.

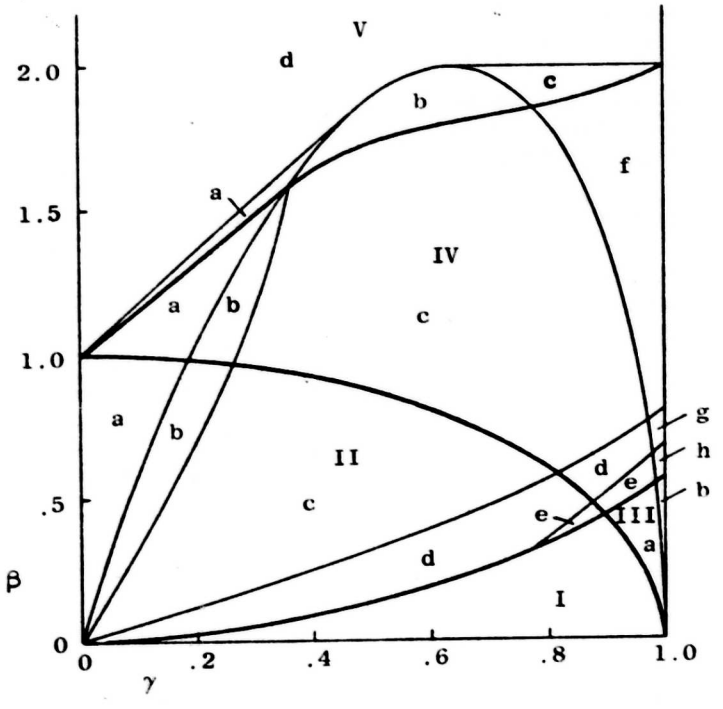

FIGURE 5.1. Definitions of Subregions

TABLE II

DISTRIBUTION OF EXCEPTIONAL LINES

Region	Sub-region	Exceptional Lines Present in Each Subregion											
		$\mathcal{P}$	UL	PDL_y	PDL	EDL_a	EDL_c	$1D^+$	$1D^-$	EL	SL	SE	FL
I		x	x										
II	a	x	x	x					x		x		
	b	x	x	x					x	x	x		
	c	x	x	x					x	x			
	d	x	x	x					x	x		x	
	e	x	x	x					x	x		x	x
III	a	x	x			x		x					
	b	x	x				x	x					
IV	a		x	x	x			x	x		x		
	b		x	x	x			x	x	x	x		
	c		x	x	x	x		x	x	x			
	d		x	x	x	x		x	x	x		x	
	e		x	x	x	x		x	x	x		x	x
	f		x	x	x		x	x	x	x			
	g		x	x	x		x	x	x	x		x	
	h		x	x	x		x	x	x	x		x	x
V	a		x	x				x					
	b		x	x		x		x					
	c		x	x			x	x					
	d		x	x									

The loci C_1, C_2 and C_8 which separate the five regions of the parameter space are particularly significant because

i) for (β,γ) above C_1, the barrier through $\dot{\varepsilon}_{up}$ no longer exists, and the time-to-go is everywhere continuous;

ii) for (β,γ) below C_2, the capture region is finite;

iii) for (β,γ) above C_8, P never turns away from E.

It is to be noted that minor changes in the configuration can occur even in a specific subregion of parameter space. Thus, for example, the configuration of Fig. 4.8 occurs only for parameters in a minute strip at the lower edge of subregion IVe. Similarly, near the upper edge of

subregion IVf, the PDL may or may not contact the capture circle. The loci separating these various possibilities, however, are not considered important enough to be calculated, particularly since this would entail very lengthy trial and error methods.

APPENDIX A

SWITCH ENVELOPE

The SE appears for parameters near the lower boundary of Regions II and IV. In Region II, it is specified as beginning on the barrier at the lower bound of points for which P saves time by turning toward E. The criterion for this occurrence is

$$V_x^+ \overset{\circ}{x}^- + V_y^+ \overset{\circ}{y}^- = 1, \tag{1}$$

where

$$\begin{aligned} V_x^+ &= s(\psi_o - \tau_o)/D \\ V_y^+ &= c(\psi_o - \tau_o)/D \\ \psi_o &= \theta_o - \cos^{-1}(c\theta_o/\gamma) \\ D &= \sqrt{1-c^2\theta_o/\gamma^2}\ (\beta + s\theta_o - \sqrt{1-c^2\theta_o/\gamma^2}) , \end{aligned} \tag{2}$$

and where

$$\begin{aligned} \overset{\circ}{x}^- &= y - \gamma s(\theta_{up} + \tau_b) \\ \overset{\circ}{y}^- &= 1 - x - \gamma c(\theta_{up} + \tau_b) . \end{aligned} \tag{3}$$

Retrogressive trajectories needed in this study are the barrier, constructed with $\varphi = +1$,

$$\begin{aligned} x^- &= 1 - c\tau_b + (\beta - \gamma\tau_b)s(\theta_{up} + \tau_b) \\ y^- &= s\tau_b + (\beta - \gamma\tau_b)c(\theta_{up} + \tau_b) , \end{aligned} \tag{4}$$

and the turn-away paths ($\varphi = -1$) which encounter the capture circle tangentially,

$$\begin{aligned} x^+ &= -1 + c\tau_o + \beta s(\theta_o - \tau_o) - \gamma\tau_o s(\psi_o - \tau_o) \\ y^+ &= s\tau_o + \beta c(\theta_o - \tau_o) - \gamma\tau_o c(\psi_o - \tau_o) . \end{aligned} \tag{5}$$

The SE exists if and only if (1) holds at some point, τ_b, on the barrier. To find such a point, a barrier time $\tau_b > 0$ is chosen, and the resulting (x,y) are solved for the parameters (θ_o,τ_o) using (5). These are then used in (2) and (3) so that the left side of (1) can be evaluated. The time τ_b is adjusted until this left side equals 1, or until it is found that the left side is always less than 1, for all $\tau_b \leq 2(\pi - \theta_{up})$. For parameters between C_2 and C_4, the results of the iteration are initial values of θ_o, τ_o and $\bar{\psi} = \theta_{up} + \tau_b$, which are then used as initial conditions in the retrogressive SE integration.

The local slope of the SE is then expressed as a bilinear function of the unknown $d\theta_o/d\tau_o$,

$$\frac{dy}{dx} = \frac{y_\tau + y_\theta(d\theta_o/d\tau_o)}{x_\tau + x_\theta(d\theta_o/d\tau_o)} \quad , \tag{6}$$

and (1) is used with the incoming velocity on the SE,

$$\dot{x}^- = y - \gamma s\bar{\psi}$$

$$\dot{y}^- = 1 - x - \gamma c\bar{\psi} \quad ,$$

to give an equation for E's prior control, $\bar{\psi}$. Following some simplification, this equation is*

$$c(\bar{\psi}-\psi_o+\tau_o) = R(\theta_o,\tau_o) = 1 + \frac{2}{\gamma}\left\{c(\psi_o-\tau_o)-c\psi_o-\beta\sqrt{1-c^2\theta_o/\gamma^2}\right\} \quad . \tag{7}$$

The prior control then permits calculation of the SE slope in terms of (θ_o,τ_o):

$$\frac{dy}{dx} = \frac{1 - x - \gamma c\bar{\psi}}{y - \gamma s\bar{\psi}} \quad . \tag{8}$$

*While multiple-valued, the inverse-cosine operation is trouble-free if it is recalled that $\bar{\psi}$ remains practically normal to the barrier as the SE is integrated away from it.

Finally, (6) gives

$$\frac{d\theta_o}{d\tau_o} = -\frac{y_\tau - x_\tau(dy/dx)}{y_\theta - x_\theta(dy/dx)} \quad , \tag{9}$$

and numerical integration of (9) for a small change in the independent variable (here taken as τ_o) is followed by updated values for $\underline{x}$ on the SE. The derivative in (9) is never indeterminate. This retrogressive integration proceeds until either of two geometric circumstances arises;

i) the curvature of the incoming path equals that of the SE, implying that the SE is here tangentially extended by a PDL, or

ii) the derivative (9) equals zero, implying that the departing trajectory is tangential to the SE, which in this case is tangentially joined to an FL.

The first case is equivalent to a requirement on the time-derivative of $\bar{\psi}$ for motion along the SE, in that the integration proceeds only while $d\bar{\psi}/d\tau_s < 1$. This derivative is expressed more conveniently as

$$\frac{d\bar{\psi}}{d\tau_s} = \frac{d\bar{\psi}/d\theta_o}{dy/d\theta_o}\frac{dy}{d\tau_s} \quad , \tag{10}$$

where, using (7),

$$\frac{d\bar{\psi}}{d\theta_o} = \frac{d\psi_o}{d\theta_o} - \frac{R_\theta}{s(\bar{\psi}-\psi_o+\tau_o)} - \left[1 + \frac{R_\tau}{s(\bar{\psi}-\psi_o+\tau_o)}\right]\frac{d\tau_o}{d\theta_o}$$

$$\frac{dy}{d\theta_o} = y_\theta + y_\tau\,(d\tau_o/d\theta_o)$$

$$\frac{dy}{d\tau_s} = 1 - x - \gamma c\bar{\psi} \quad .$$

When $d\bar{\psi}/d\tau_s = 1$, a PDL starts, as shown in Fig. 3.5, and it is necessary to have the adjoints on the prior side, which are:

$$V_x^- = s\psi^-/D^-$$

$$V_y^- = c\psi^-/D^- \quad . \tag{11}$$

The denominator in (11) is expressed in terms of the current position on the SE, using the main equation on the prior side to give

$$D^- = (1-x)c\psi^- + ys\psi^- - \gamma \quad . \tag{12}$$

Because the SE is tangential at the barrier, this function vanishes, and the adjoints are infinite, at this lowest point of the SE.

The integration of the SE when parameters are in Region IV is much the same, except that the barrier no longer exists. The lower end of the SE is instead coincident and cotangential with the upper end of a PDL and with a trajectory for $\varphi = +1$, as shown in Fig. 4.8. The condition denoting this point on the PDL is $d\theta_1/d\tau_1 = 0$ (or its equivalent, $d\zeta/d\tau_1 = 0$). The prior trajectory thus takes the place of the barrier in the analysis above, and the integration of the SE then proceeds, with no indeterminacies, by calculating the derivative according to (9).

APPENDIX B

COMPUTATION OF DISPERSAL LINES

B-1 Evader's Dispersal Line

In the simplest case, which serves to illustrate the steps involved, we may consider the configuration of Fig. B-1, for which the parameters fall in Regions III or IV, to the left of locus C_7. The equations which determine the EDL are three, in the four variables indicated.

For a given pair (β,γ) it is first necessary to calculate the initial values θ_T, τ_2 for the point-tangential trajectory leaving the point A farthest to the right in the Figure. This trajectory is readily expressed in terms of θ_o and the retrogressive time to tangency τ_T such that $r(\theta_o,\tau_T) = \beta$ and $\dot{r}(\theta_o,\tau_T) = 0$, or

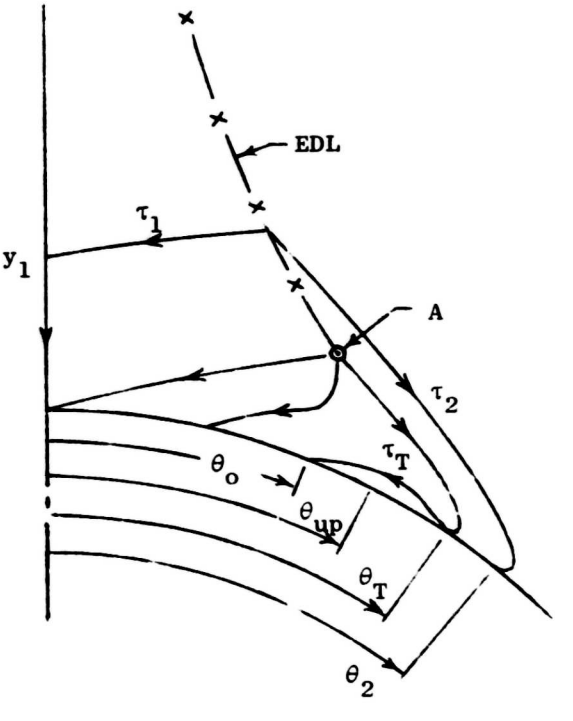

FIGURE B-1. Notation Near Dispersal Point A

$$1 - c\tau_T + (\beta-\gamma\tau_T)[s(\theta_o+\tau_T)-s\theta_o] - \beta\gamma\tau_T + \tfrac{1}{2}\gamma^2\tau_T^2 = 0$$

$$s\tau_T + (\beta-\gamma\tau_T)[c(\theta_o+\tau_T)-\gamma] - \gamma[s(\theta_o+\tau_T)-s\theta_o] = 0 \ . \qquad (1)$$

Fixing θ_o and τ_T at convenient values permits calculation of the corresponding β,γ shown in Fig. B-2, to the left of the locus C_7. The initial value of the time variable shown in Fig. B-1 is $\tau_2 = \beta/\gamma-\tau_T$. When the conjugate point C is present (β,γ right of C_7), the equations take the form

$$1 - c\tau_T + (y_1-\gamma\tau_T)s\tau_T + \tfrac{1}{2}[(y_1-\gamma\tau_T)^2 - \beta^2] = 0$$

$$(1-\gamma)s\tau_T + (y_1-\gamma\tau_T)(c\tau_T - \gamma) = 0 \ , \qquad (2)$$

which can then be solved for the parameters, given convenient levels of y_1 and τ_T. These functions of (β,γ) are also shown in Fig. B-2, to the right of locus C_7. The points of special interest in this Figure are:

i) The tangency angle is $\theta_T = 90°$ along the diagonal dashed locus, and in general can be found by

$$\beta c\theta_T = s\tau_T + (\beta-\gamma\tau_T)c(\theta_o+\tau_T),$$

where θ_o and τ_T are read from the Figure.

ii) The arrival angle θ_o approaches 90° as γ approaches 0.

iii) The locus C_{10} denotes the parameters above which tangential motion does not occur. For $\gamma < .503$, C_{10} is determined by the requirement that in free motion, $\ddot{r} = 0$ at tangency, and for $.503 < \gamma < .632$, it is determined by having A fall on the capture circle. The locus is completed with the straight line $\beta = 2$, along which $\tau_T = \pi$.

In developing the EDL by numerical integration, it is necessary only to express the positions and adjoints as functions of the parameters (y_1,τ_1) or (θ_2,τ_2). Referring to the general solutions of Chap. I and to Fig. B-1, these are:

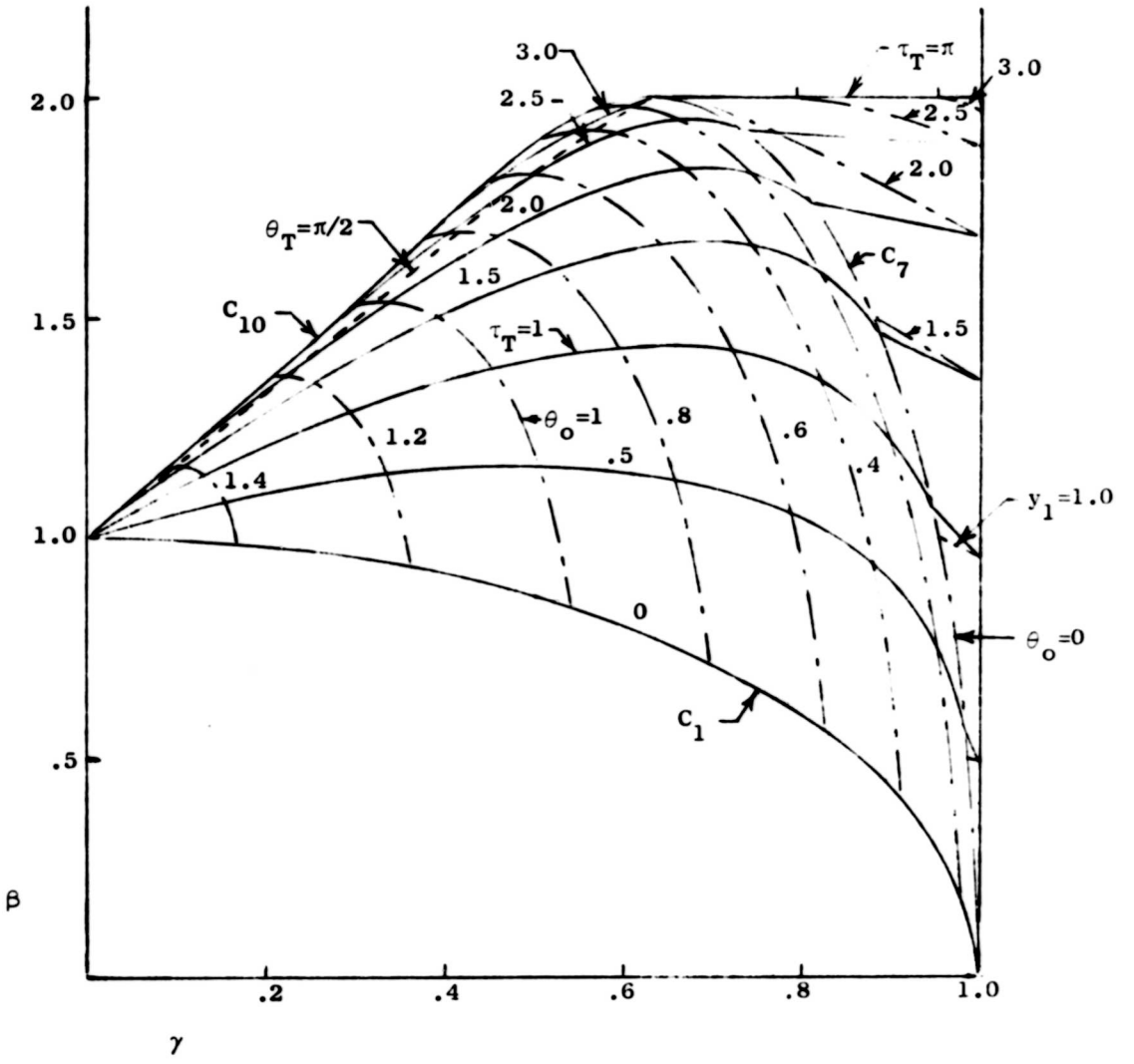

FIGURE B-2. Parametric Solutions for Points A and C

$$x^+ = 1 - c\tau_2 + \beta s(\theta_2+\tau_2) - \gamma\tau_2 s(\psi_2+\tau_2)$$

$$y^+ = s\tau_2 + \beta c(\theta_2+\tau_2) - \gamma\tau_2 c(\psi_2+\tau_2) \qquad (3)$$

$$x^- = 1 - c\tau_1 + (y_1-\gamma\tau_1)s\tau_1$$

$$y^- = s\tau_1 + (y_1-\gamma\tau_1)c\tau_1 \qquad (4)$$

$$V_x^+ = s(\psi_2+\tau_2)/D$$

$$V_y^+ = c(\psi_2+\tau_2)/D \qquad (5)$$

$$D = \sqrt{1-c^2\theta_2/\gamma^2}\ (\beta - s\theta_2 - \gamma\sqrt{1-c^2\theta_2/\gamma^2})$$

$$V_x^- = s\tau_1/(1-\gamma)$$

$$V_y^- = c\tau_1/(1-\gamma)\ . \qquad (6)$$

These functions and their derivatives are used in (3) and (4) of Sec. 4.2, which are then solved for the derivatives $d\tau_1/dy_1$, $d\theta_2/dy_1$ and $d\tau_2/dy_1$.

For parameters in the range $\sqrt{1-\gamma^2} < \beta < 1+\gamma$, the equilibrium point θ_{eq} exists, and as the EDL is integrated outward toward the point B (where it meets the PDL), the angle θ_2 is very nearly equal to θ_{eq}. For numerical reasons, therefore, a more suitable variable is ζ, defined by $e^{-\zeta} = \theta_{eq} - \theta_2$, as will be discussed in App. B-2.

In terms of this variable, the slope of the EDL is then expressible as

$$\frac{dy}{dx} = -\frac{D\,s\tau_1 - (1-\gamma)s(\psi_2+\tau_2)}{D\,c\tau_1 - (1-\gamma)c(\psi_2+\tau_2)} \cong -\frac{s(\psi_{eq}+\tau_2)}{c(\psi_{eq}+\tau_2)}$$

since

$$D \cong e^{-\zeta}\, \beta\, c\theta_{eq}/\gamma$$

$$\psi_2 \cong \psi_{eq} \ ,$$

and further substitution permits cancellation of $e^{-\zeta}$ from numerator and denominator of the derivatives; the results are:

$$\frac{d\tau_1}{dy_1} = -\frac{c(\psi_{eq}+\tau_2-\tau_1)}{\gamma[1 - c(\psi_{eq}+\tau_2-\tau_1)]}$$

$$\frac{d\zeta}{dy_1} = \frac{(y_1 - \gamma\tau_1)c\theta_{eq}}{\gamma(1-\gamma)\tau_2(\beta - s\theta_{eq})} \qquad (7)$$

$$\frac{d\tau_2}{dy_1} = \frac{y_1 - \gamma\tau_1}{\gamma^2\tau_2[1 - c(\psi_{eq}+\tau_2-\tau_1)]} \ .$$

The initial values of the four parameters are easily computed ($y_1=\beta$, $\tau_1=\beta/\gamma$, τ_2 and θ_2 from Fig. B-2), and the equations (7) are integrated simultaneously until the switch function vanishes on the inner side (this occurs long before $S = 0$ on the outer side) of the EDL, or when

$$S = V_x^+ y - V_y^+ x = c\psi_{eq} - \beta s(\psi_{eq}-\theta_{eq}) - c(\psi_{eq}+\tau_2) = 0 \ .$$

For parameters right of C_7, the conjugate point C marks the near end of the EDL, and because the trajectories on either side reduce to the same path at C, the necessary derivatives are indeterminate. Referring to Fig. B-3, the two paths give, at the point C,

$$x_c = 1 - c\tau_1 = 1 - c\tau_2 + \beta s(\theta_2+\tau_2) - \gamma\tau_2 s(\psi_2+\tau_2)$$

$$y_c = s\tau_1 = s\tau_2 + \beta c(\theta_2+\tau_2) - \gamma\tau_2 c(\psi_2+\tau_2) \ ,$$

and equating adjoints provides two more equations,

$$\tau_1 = \psi_2 + \tau_2$$

$$1 - \gamma = \sqrt{1-c^2\theta_2/\gamma^2}(\beta - s\theta_2 - \gamma\sqrt{1-c^2\theta_2/\gamma^2})$$

The last equation is solved for $\theta_2 = \theta_T$, in terms of the parameters, and then the preceding equations give initial values for

$$\tau_2 = \frac{(1-\gamma)c\theta_2}{\gamma^2\sqrt{1-c^2\theta_2/\gamma^2}}$$

$$\tau_1 = \tau_2 + \theta_2 + \cos^{-1}(c\theta_2/\gamma) \qquad (8)$$

$$y_1 = \gamma\tau_1 \ .$$

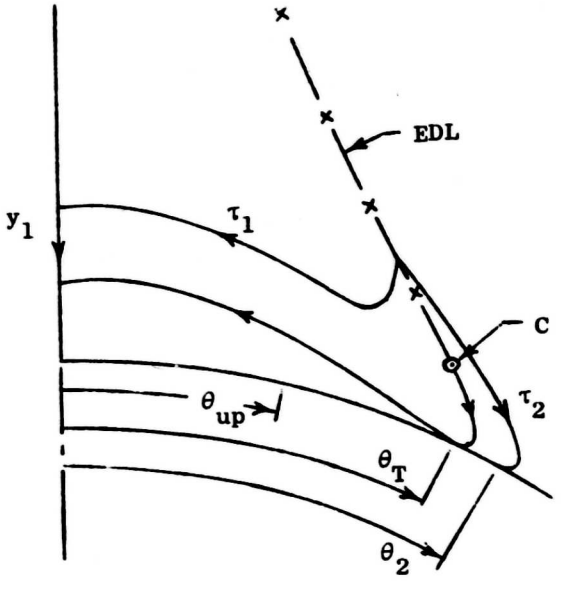

FIGURE B-3. Notation Near Conjugate Point C

The indeterminacy at C requires that second-order expressions for the derivatives be found. The slope of the EDL is

$$\frac{dy}{dx} = \cot \tau_1 = - \frac{V_x^- - V_x^+}{V_y^- - V_y^+} ,$$

and when expanded to second order in $\Delta\tau_1$, $\Delta\tau_2$, $\Delta\theta_2$, we find

$$\Delta\tau_1^2 - \Delta\tau_2^2 = \frac{2D_\theta}{1 - \gamma} \Delta\theta_2 ,$$

where $D_\theta = \partial D/\partial\theta_2$, as given by (5). Likewise, expressing changes in x and y to second-order yields, after some effort,

$$\Delta y_1 \Delta\tau_1 + \tfrac{1}{2}(1-2\gamma)(\Delta\tau_1^2 - \Delta\tau_2^2) = (\beta c\theta_2/\gamma - \gamma\tau_2\Psi_\theta)\Delta\theta_2$$

$$\Delta y_1 + (1-\gamma)(\Delta\tau_1 - \Delta\tau_2) = 0.$$

Eliminating $\Delta\theta_2$ and $\Delta\tau_2$ gives a large quadratic in $\Delta\tau_1/\Delta y_1$, but when the identity

$$\beta c\theta_2/\gamma - \gamma\tau_2\Psi_\theta = D_\theta$$

is used, the quadratic becomes the very simple linear expression,

$$\frac{\Delta\tau_1}{\Delta y_1} = \frac{2-3\gamma}{2(1-\gamma)(2\gamma-1)} . \qquad (9)$$

The other two derivatives then follow as

$$\frac{\Delta\tau_2}{\Delta y_1} = \frac{\gamma}{2(1-\gamma)(2\gamma-1)} \qquad (10)$$

$$\frac{\Delta\theta_2}{\Delta y_1^2} = \frac{\gamma}{2(2\gamma-1)c\theta_2\left[s\theta_2 + \gamma\sqrt{1-c^2\theta_2/\gamma^2} - \dfrac{(1-\gamma)s\theta_2}{\gamma(1-c^2\theta_2/\gamma^2)}\right]} . \qquad (11)$$

These expressions are useful only for the first step of the integration, after which it can proceed normally, the indeterminacy no longer existing.

B-2 Pursuer's Dispersal Line

We first discuss the near indeterminacy in the construction of the PDL which exists just under the barrier for parameters near C_6 in Region II. For these parameters, it may happen that (9) of Sec. 3.3 is "numerically" indeterminate, as it is based on differencing nearly equal numbers. A straightforward means of overcoming this problem consists of finding a point on the PDL which is "far away" from the indeterminacy. That is, an intelligent guess is made as to the parameters $(\theta_1, \tau_1, \tau_2)$ which correspond to a convenient value of θ_o. This value θ_o is known from the integration of the SE and is taken back from the <u>end</u> of the SE, where $\tau_2 = 0$ and $\theta_1 = \theta_o$. The PDL conditions are written at this estimated point as

$$\begin{aligned} x^+(\theta_o, \tau_2) &= x^-(\theta_1, \tau_1) \\ y^+(\theta_o, \tau_2) &= y^-(\theta_1, \tau_2) \\ V^+(\theta_1, \theta_o, \tau_2) &= V^-(\tau_1) \end{aligned} \tag{1}$$

where initially only θ_o is known. The initial estimates of the other variables allow calculation of the six indicated quantities, though, and linearization gives

$$\begin{aligned} x^-_\theta \, \delta\theta_1 + x^-_\tau \, \delta\tau_1 - x^+_\tau \, \delta\tau_2 &\cong x^+ - x^- = \Delta x \\ y^-_\theta \, \delta\theta_1 + y^-_\tau \, \delta\tau_1 - y^+_\tau \, \delta\tau_2 &\cong y^+ - y^- = \Delta y \\ -V^+_\theta \, \delta\theta_1 + V^-_\tau \, \delta\tau_1 - V^+_\tau \, \delta\tau_2 &\cong V^+ - V^- = \Delta V, \end{aligned} \tag{2}$$

where the 3×3 matrix of partial derivatives is evaluated using the

current estimates of the sought quantities. Inverting the matrix gives corrections to the previous estimates as

$$\begin{bmatrix} \delta\theta_1 \\ \delta\tau_1 \\ \delta\tau_2 \end{bmatrix} = \begin{bmatrix} x_\theta^- & x_\tau^- & -x_\tau^+ \\ y_\theta^- & y_\tau^- & -y_\tau^+ \\ -V_\theta^+ & 1 & -1 \end{bmatrix}^{-1} \begin{bmatrix} \Delta x \\ \Delta y \\ \Delta V \end{bmatrix} \qquad (3)$$

and the steps are then repeated until the calculated errors are negligibly small. The result of the process just described is a set of variables $(\theta_1, \tau_1, \tau_2)$ and a corresponding point (x,y) on the PDL. The numerical integration of the PDL can then proceed in either direction; i.e., toward or away from the numerical indeterminacy. In a typical case, integration toward the indeterminacy is carried out only until the computed values of, say, τ_2 become noisy as the point D of the SE is approached from above.

We next consider the numerical problems associated with the generation of the PDL which exists for (β,γ) in Region IV. For parameters in the lower portion of this region, the equilibrium point θ_{eq} is defined on the capture circle, and the near end of the PDL begins just above the possible equilibrium as in Fig. 4.3(a). When the parameters are closer to the upper edge of Region IV, θ_{eq} is no longer defined (according to (2) of Sec. 4.1) and the PDL may resemble the locus of Fig. 4.3(b).

For the type of configuration shown in (a) of this Figure, it is qualitatively clear that the safe-contact motion is very slow at positions between θ_p and θ_T, because the time on this brief segment is practically equal to the time required for the "long way around", via the EL and the positive y-axis, say. Hence, θ_p may be nearly equal to θ_{eq} (where $\dot{\theta} = 0$ for $\varphi = +1$) in which case an appropriate dependent variable is ζ, as defined in Section B-1. In the region of parameter space between $\beta = \sqrt{1-\gamma^2}$ and $\beta = 1+\gamma$, the smallest value of this variable, ζ, is found to be in the range 2 to 5, corresponding to angles between point-tangency and equilibrium of from .4° to 8°, virtually at the near end of the EDL. At the other extreme, the largest value of

occurs in measuring the very small angle between the PDL and the equilibrium point. A typical value encountered, for parameters near locus C_1, is $\zeta = 1000$, which corresponds to an angular separation of 10^{-435} radians*. These facts imply that ζ is a necessary type of variable for use in numerically integrating the PDL, when $\beta < 1+\gamma$.

The solutions to be used for at least the beginning of the PDL are

$$x^+ = 1 - c\tau_1 + \beta s(\theta_1+\tau_1) - \gamma\tau_1 s(\psi_1+\tau_1)$$
$$y^+ = s\tau_1 + \beta c(\theta_1+\tau_1) - \gamma\tau_1 c(\psi_1+\tau_1) \qquad (4)$$

and

$$x^- = -1 + c\tau_2 + \beta s(\theta_2-\tau_2) - \gamma\tau_2 s(\psi_2-\tau_2)$$
$$y^- = s\tau_2 + \beta c(\theta_2-\tau_2) - \gamma\tau_2 c(\psi_2-\tau_2) \qquad (5)$$

where

$$\psi_1 = \theta_1 + \cos^{-1}(c\theta_1/\gamma)$$
$$\psi_2 = \theta_2 - \cos^{-1}(c\theta_2/\gamma)$$

The set (5) may require replacement by equations describing motion to the negative y-axis, or to the EL, as suggested by Fig. 4.3.

According to the definition of the PDL, we first locate the angular coordinate θ_p at its near end, such that the total time to termination is the same by two paths. For parameters below $\beta = 1+\gamma$, the configuration is as shown in Fig. B-4.

---

* The angle subtended by an electron at a radial distance of one light-year is about 10^{-30} radians.

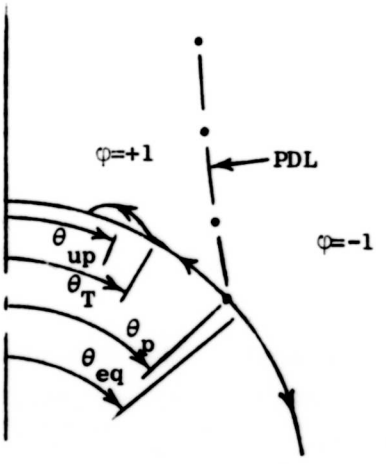

FIGURE B-4. Detail of PDL Near Capture Circle

The integral for the elapsed time during safe-contact with $\varphi=+1$ is

$$\tau_1 = \int_{\theta_T}^{\theta_p} \frac{\beta \, d\theta}{\beta - s\theta - \gamma\sqrt{1-c^2\theta/\gamma^2}} \tag{6}$$

where the denominator is zero just outside the upper limit of integration, at $\theta_{eq} = \theta_p + e^{-\zeta}$. An accurate evaluation of the integral is accomplished by expressing the integrand as

$$\frac{1}{D(\theta)} = \frac{1}{D(\theta)} - \frac{1}{D_\theta(\theta_{eq})(\theta-\theta_{eq})} + \frac{1}{D_\theta(\theta_{eq})(\theta-\theta_{eq})}$$

By adding and subtracting the linear term in a Taylor series, the difference of the first two terms remains small as θ approaches θ_{eq}, while the last term is integrable as a logarithmic factor, using

$$D_\theta(\theta_{eq}) = -c\theta_{eq}\left[1 + \frac{s\theta_{eq}}{\gamma\sqrt{1-c^2\theta_{eq}/\gamma^2}}\right]$$

Approximating the upper limit of integration in (6) by θ_{eq} then gives

$$\zeta = -\ell n(\theta_{eq}-\theta_p) \cong -\ell n(\theta_{eq}-\theta_T) - D_\theta(\theta_{eq})(\tau_e-\tau_T-\tau_i) , \qquad (7)$$

where

$$\tau_i = \int_{\theta_T}^{\theta_{eq}} \left(\frac{1}{D(\theta)} - \frac{1}{D_\theta(\theta_{eq})(\theta-\theta_{eq})} \right) d\theta \qquad (8)$$

has been determined numerically. This procedure results in initial values of ζ, $\tau_1 = \tau_2 = 0$, and $\theta_2 = \theta_p$, as required for the integration of the coupled PDL equations.

Because the initial values of ζ are quite large (in contrast to their values at θ_T), it is essential to express both numerator and denominator of the derivatives as factors of $e^{-\zeta}$. Following cancellation of this term, we find

$$\frac{d\zeta}{d\tau_1} = \frac{D_\theta \gamma \sqrt{1-c^2\theta_{eq}/\gamma^2}\sqrt{1-c^2\theta_2/\gamma^2}\; s(\psi_{eq}+\tau_1) + \frac{\partial y^+}{\partial \tau_1}\, s(\psi_2-\tau_2-\psi_{eq}-\tau_1)}{\beta\gamma\sqrt{1-c^2\theta_{eq}/\gamma^2}\sqrt{1-c^2\theta_2/\gamma^2}\;(\beta + s\theta_2 - \gamma\sqrt{1-c^2\theta_2/\gamma^2})s(\psi_{eq}+\tau_1)} , \qquad (9)$$

where

$$\frac{\partial y^+}{\partial \tau_1} = c\tau_1 - \beta s(\theta_{eq}+\tau_1) - \gamma[c(\psi_{eq}+\tau_1) - \tau_p s(\psi_{eq}+\tau_1)] .$$

In terms of this derivative, the remaining two are written

$$\frac{d\theta_2}{d\tau_1} = \frac{R_y \bar{x_\tau} - R_x \bar{y_\tau}}{\bar{x_\tau}\bar{y_\theta} - \bar{y_\tau}\bar{x_\theta}} \qquad (10)$$

$$\frac{d\tau_2}{d\tau_1} = \frac{R_x \bar{y_\theta} - R_y \bar{x_\theta}}{\bar{x_\tau}\bar{y_\theta} - \bar{y_\tau}\bar{x_\theta}} . \qquad (11)$$

Digital integration of (9)-(11) then generates the PDL until one of two things occurs:

i) The derivative $d\zeta/d\tau_1$ vanishes, implying that $d\theta_1/d\tau_1 = 0$, so the PDL condition becomes

$$\frac{dy}{dx} = \frac{y_\tau^+ + y_\theta^+(d\theta_1/d\tau_1)}{x_\tau^+ + x_\theta^+(d\theta_1/d\tau_1)} = \frac{y_\tau^+}{x_\tau^+} = -\frac{V_x^- - V_x^+}{V_y^- - V_y^+} \quad .$$

Together with the main equation, $\nabla V^+ \cdot \dot{\underline{x}}^+ = -1$, this implies the SE condition, $\nabla V^- \cdot \dot{\underline{x}}^+ = -1$. Hence, when $d\zeta/d\tau_1 = 0$, a switch envelope begins. This occurs for parameters below C_4 in Region IV.

ii) The PDL meets the EDL at the point B, where the switch function $S = 0$. In this case, for parameters above C_4, it is often more convenient to perform the integration of the PDL from the point B inward, rather than from the capture circle outward.

In the first case, the SE is generated as described in App. A, while in the second case, a different set of equations is required to generate the PDL. Referring to Fig. B-5, we have a relation between θ_1 and τ_1 from the switch function equation, $S = V_x^+ y - V_y^+ x = 0$, which yields

$$c(\psi_1+\tau_1) = \gamma + \sqrt{1-c^2\theta_1/\gamma^2}\ (\beta - s\theta_1 - \gamma\sqrt{1-c^2\theta_1/\gamma^2}) \quad . \quad (12)$$

The object of the following analysis is a set of differential equations relating τ_e, τ_2, τ_1, and θ_1, thus permitting simultaneous generation of both EL and PDL. Taking τ_e as the independent variable, the PDL equations give

$$\begin{aligned} x_\theta^+ \frac{d\theta_1}{d\tau_e} + x_\tau^+ \frac{d\tau_1}{d\tau_e} &= x_{\tau_e}^- + x_{\tau_2}^- \frac{d\tau_2}{d\tau_e} \\ y_\theta^+ \frac{d\theta_1}{d\tau_e} + y_\tau^+ \frac{d\tau_1}{d\tau_e} &= y_{\tau_e}^- + y_{\tau_2}^- \frac{d\tau_2}{d\tau_e} \end{aligned} \quad (13)$$

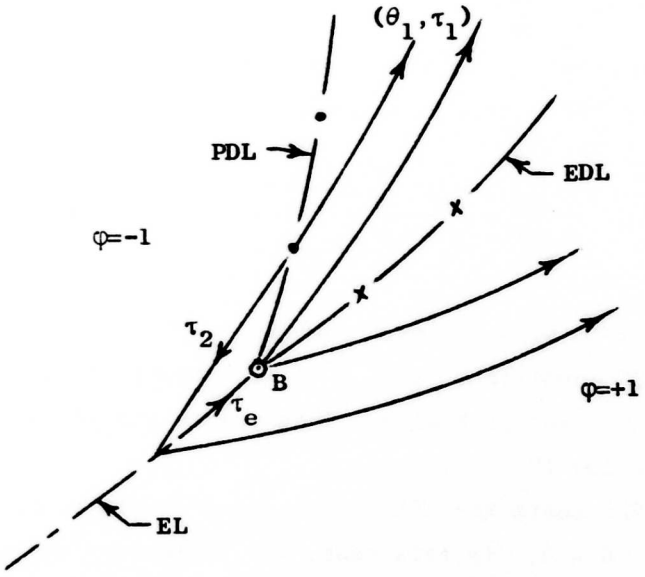

FIGURE B-5. Detail Near Junction of PDL and EDL

and

$$\frac{dy}{dx} = \frac{y^-_{\tau_e} + y^-_{\tau_2}(d\tau_2/d\tau_e)}{x^-_{\tau_e} + x^-_{\tau_2}(d\tau_2/d\tau_e)} = -\frac{V_x^- - V_x^+}{V_y^- - V_y^+} , \qquad (14)$$

where

$$V_x^- = s(\psi_e - \tau_2)/D_1(x,y)$$

$$V_y^- = c(\psi_e - \tau_2)/D_1(x,y)$$

$$V_x^+ = s(\psi_1 + \tau_1)/D(\theta_1)$$

$$V_y^+ = c(\psi_1 + \tau_1)/D(\theta_1) .$$

At the point B, of course, $\nabla V^- = \nabla V^+$, because $\tau_e = \tau_2 = 0$; hence $\psi_1 + \tau_1 = \psi_e = \tan^{-1}(x_B/y_B)$, and

$$D_1 = - y/r - \gamma = D = \sqrt{1-c^2\theta_1/\gamma^2}(\beta + s\theta_1 - \gamma\sqrt{1-c^2\theta_1/\gamma^2}).$$

The indeterminacy of (14) can then be evaluated by l'Hôpital's rule. After cross-multiplying, we find

$$\begin{aligned}(y\bar{}_{\tau_e} + y\bar{}_{\tau_2}\frac{d\tau_2}{d\tau_e})[(D_\theta y + Dx\psi_\theta)\frac{d\theta_1}{d\tau_e} + Dx(\frac{d\tau_2}{d\tau_e} + \frac{d\tau_1}{d\tau_e}) + \gamma x(\breve{\varphi}-x/r^2)] \\ + (x\bar{}_{\tau_e} + x\bar{}_{\tau_2}\frac{d\tau_2}{d\tau_e})[(D_\theta x - Dy\psi_\theta)\frac{d\theta_1}{d\tau_e} - Dy(\frac{d\tau_2}{d\tau_e} + \frac{d\tau_1}{d\tau_e}) - (r+\gamma y)(\breve{\varphi}-x/r^2)] = 0\end{aligned} \tag{15}$$

where the subscript θ is an abbreviation for the partial derivative, $\partial/\partial\theta_1$. The pair of equations (13) is then solved for

$$\begin{aligned}\frac{d\theta_1}{d\tau_e} &= A_1 + A_2(d\tau_2/d\tau_e) \\ \frac{d\tau_1}{d\tau_e} &= A_3 + A_4(d\tau_2/d\tau_e)\ ,\end{aligned} \tag{16}$$

where

$$A_1 = (y+\gamma r)(\breve{\varphi}-1)/\Delta$$

$$A_2 = - 2(y+\gamma r)/\Delta$$

$$A_3 = [(\gamma^2\tau_1\psi_\theta - \beta c\theta_1)(1+y/\gamma r) + \beta r\sqrt{1-c^2\theta_1/\gamma^2}(\breve{\varphi}-x/r^2)]/\Delta$$

$$A_4 = [(\gamma^2\tau_1\psi_\theta - \beta c\theta_1)(1+y/\gamma r) - \beta r\sqrt{1-c^2\theta_1/\gamma^2}(1+x/r^2)]/\Delta$$

$$\Delta = \tau_1[(s\theta_1 + \gamma\sqrt{1-c^2\theta_1/\gamma^2})^2 - \beta s\theta_1]$$

and

$$\breve{\varphi} = 1 - \gamma\frac{r^2-x+r\sqrt{r^2-2x}}{r(r-y)}$$

Substitution into (15) yields a quadratic with intimidating coefficients,

$$A\left(\frac{d\tau_2}{d\tau_e}\right)^2 + B\,\frac{d\tau_2}{d\tau_e} + C = 0 \qquad (17)$$

where

$$A = y_{\tau_2}^{-}[(D_\theta y+Dx\psi_\theta)A_2 + Dx(A_4+1)] + x_{\tau_2}^{-}[(D_\theta x-Dy\psi_\theta)A_2-Dy(A_4+1)]$$

$$B = y_{\tau_e}^{-}[(D_\theta y+Dx\psi_\theta)A_2 + Dx(A_4+1)]$$

$$+ y_{\tau_2}^{-}[(D_\theta y+Dx\psi_\theta)A_1 + DxA_3 + \gamma x(\breve{\phi}-x/r^2)]$$

$$+ x_{\tau_e}^{-}[(D_\theta x-Dy\psi_\theta)A_2 - Dy(A_4+1)]$$

$$+ x_{\tau_2}^{-}[(D_\theta x-Dy\psi_\theta)A_1 - DyA_3 - (r+\gamma y)(\breve{\phi}-x/r^2)]$$

and

$$C = y_{\tau_e}^{-}[(D_\theta y+Dx\psi_\theta)A_1 + DxA_3 + \gamma x(\breve{\phi}-x/r^2)]$$

$$+ x_{\tau_e}^{-}[(D_\theta x-Dy\psi_\theta)A_1 - DyA_3 - (r+\gamma y)(\breve{\phi}-x/r^2)]$$

The positive root to (17) is then given by

$$d\tau_2/d\tau_e = (-B - \sqrt{B^2 - 4AC})/2A, \qquad (18)$$

which permits calculation of the remaining derivatives by (16), and the local slope of the PDL by (14).

APPENDIX C

TRAJECTORIES IN REAL SPACE

It is interesting and instructive to determine the motion of P and E in the fixed coordinate system, using (1) and (2) of Sec. 1.2. The integration is simple to carry out, requiring only $\varphi(t)$ and $\psi(t)$ for any initial condition, so that

$$\begin{aligned} x_p(t) &= x_{p_o} + \int_o^t s\theta_p(\xi)\, d\xi \\ y_p(t) &= y_{p_o} + \int_o^t c\theta_p(\xi)\, d\xi \end{aligned} \tag{1}$$

where

$$\theta_p(t) = \theta_{p_o} + \int_o^t \varphi(\xi)\, d\xi \ ,$$

and

$$\begin{aligned} x_e(t) &= x_{e_o} + \gamma \int_o^t s[\psi(\xi)+\theta_p(\xi)]\, d\xi \\ y_e(t) &= y_{e_o} + \gamma \int_o^t c[\psi(\xi)+\theta_p(\xi)]\, d\xi \end{aligned} \tag{2}$$

In these equations, of course, $\varphi(t)$ and $\psi(t)$ have been determined by retrogressive integration of the equations of relative motion, and either control or both may be discontinuous when an exceptional line is crossed. Because the relative trajectory has been computed for discrete time intervals, it is obviously important to choose a "proper" step size, such that the intermediate switch times can be accurately estimated, and yet so that the total computer time required is not excessive.

In real space, E's motion is often a sequence of straight lines, as might be expected intuitively. In portions of the game, however, E follows a curved path, as in safe-contact motion, and along the EL, the SE and the FL.

Motion along the EL (Ref. 1) has E following a gradually curved pursuit path in real space, while P turns at an intermediate rate. Both

paths can be interrupted whenever E chooses to flee along the tangent to P's minimum-turn circle, whereupon P turns at maximum rate.

The FL trajectories also present interesting real space characteristics. If P so chooses, his path can be a series of brief tangential circular arcs, while E's corresponding motion is an equal number of nearly straight jagged segments having a sawtooth appearance. On the other hand, the SE trajectory for P is a sharp right turn, while E's strategy thereon is a transcendental function of the relative position which amounts to a gentle curve in real space. When P finally turns away, causing E to leave the SE, E's strategy is again discontinuous.

The equilibrium point in Region III corresponds to the following real space trajectory: As E traverses the barrier towards the equilibrium point, he is following a straight path in real space. After arrival at the capture circle, however, with zero relative velocity, E's path is a circle of radius γ, P's path in real space being a concentric unit circle, described at the same angular rate.

For initial conditions slightly inward of the barrier, E's path during safe-contact motion is "nearly" circular. That is, P's motion is circular and E is moving very slowly tangentially inward to the usable part. The same characteristics hold for parameters in Region IV, if E's path brings him to the capture circle at an angle between θ_T and θ_p.

In the course of this research, brief animated films were prepared of multi-stage chases for three sets of parameters, using the computing and plotting facilities of the Stanford Computation Center. In the films, the chauffeur was represented by the capture circle, and the pedestrian by a small square. The pursuer was typically drawn in six successive positions during the time required to traverse one diameter of the capture circle, and each drawing was photographed four times, the standard 16mm projector speed being 24 frames/sec. A representative 100-second film of a chase, shown in both relative and real coordinate systems, required some 400 simple drawings of P and E, together with a few coordinate lines. The Calcomp plotting facility at the Stanford Computation Center was used

for this task, and subsequent camera work was ably executed by animation specialists at the Stanford Film Workshop.

REFERENCES

1. Isaacs, R., Differential Games, John Wiley and Sons, New York, 1965.

2. Breakwell, J. V., and Merz, A. W., "Toward a Complete Solution of the Homicidal Chauffeur Game," Proc. of the First Int'l. Conf. on the Theory and Appl. of Diff. Games, Amherst, Mass., Oct. 1969, pp. III-1 to III-5.